ORNL/Sub/94-SS112/06

# SUPPORT SERVICES FOR CERAMIC FIBER- CERAMIC MATRIX COMPOSITES

Final Annual Technical Progress Report

September 28, 2001

Report Prepared by
John P. Hurley and Charlene R. Crocker
Energy & Environmental Research Center
University of North Dakota
PO Box 9018
Grand Forks, North Dakota 58202-9018
under
Subcontract No. 19X-SS 112V

for

OAK RIDGE NATIONAL LABORATORY
Oak Ridge, Tennessee 3783 1
Managed by
UT-BATTELLE, LLC
for the
U.S. DEPARTMENT OF ENERGY
under contract DE-AC05-96OR22464

ORNL/Sub/94-SS112/06

# SUPPORT SERVICES FOR CERAMIC FIBER- CERAMIC MATRIX COMPOSITES

Final Annual Technical Progress Report

September 28, 2001

Research sponsored by the U.S. Department of Energy
Office of Fossil Energy
Advanced Research Materials Program
DOE/FE AA 15 10 10 0
Work Breakdown Structure Element UNDEERC-4

Report Prepared by
John P. Hurley and Charlene R. Crocker
Energy & Environmental Research Center
University of North Dakota
PO Box 9018
Grand Forks, North Dakota 58202-9018
under
Subcontract No. 19X-SS 112V

for

OAK RIDGE NATIONAL LABORATORY
Oak Ridge, Tennessee 3783 1
Managed by
UT-BATTELLE, LLC
for the
U.S. DEPARTMENT OF ENERGY
under contract DE-AC05-96OR22464

## TABLE OF CONTENTS



Continued . . .

## TABLE OF CONTENTS (continued)

## LIST OF FIGURES



Continued . . .

## LIST OF FIGURES (continued)



Continued . . .

## LIST OF FIGURES (continued)



Continued . . .

## LIST OF FIGURES (continued)



Continued . . .

## LIST OF FIGURES (continued)



Continued . . .

## LIST OF FIGURES (continued)



Continued . . .

## LIST OF FIGURES (continued)

## LIST OF TABLES

# SUPPORT SERVICES FOR CERAMIC FIBER-CERAMIC MATRIX COMPOSITES

Research sponsored by the U.S. Department of Energy, Fossil Energy Advanced Research Materials Program, DOE/FE AA 15 10 10 0, Work Breakdown Structure Element UNDEERC-4

## INTRODUCTION

To increase national energy self-sufficiency for the near future, power systems will be required to fire low-grade fuels more efficiently than is currently possible. The typical coal-fired steam cycle used at present is limited to a maximum steam temperature of 540°C and a conversion efficiency of 35%. Higher working-fluid temperatures are required to boost efficiency, exposing subsystems to very damaging conditions. Issues of special concern to materials developers are corrosion and warping of hot-gas particulate filters and corrosion and erosion of high-temperature heat exchangers.

The University of North Dakota Energy & Environmental Research Center (EERC) is working with the National Energy Technology Laboratory in conjunction with NCC Engineering, Inc., to provide technical assistance and coal by-products to the Fossil Energy Materials Advanced Research and Technology Development Materials Program investigating materials failure in fossil energy systems. The main activities of the EERC are to assemble coal slag and hot-gas filter ash samples for use by materials researchers, to assist in providing opportunities for realistic tests of advanced materials in pilot-scale fossil energy systems, and to provide analytical support in determining corrosion mechanisms of the exposed materials.

In this final report for the project year of September 2000 through August 2001, the facilities at the EERC that can be used by researchers for realistic testing of materials are described. Researchers can include sample coupons in each of these facilities at no cost since they are being operated under separate funding. In addition, two pilot-scale coal combustion tests are described in which material sample coupons were included from researchers involved in the development of fossil energy materials. The results of scanning electron microscopy (SEM) energy dispersive x-ray analyses of the corrosion products and interactions between the surface scales of the coupons and the products of coal combustion found on the coupons exposed during those tests are reported. Finally, a relative comparison of ceramic and alloy material performance based on the SEM results is presented.

## DESCRIPTIONS OF EERC PILOT-SCALE EQUIPMENT

### The Slagging Furnace System

Figure 1 is a simplified illustration of the pilot-scale slagging furnace system (SFS). It was constructed with funding from the U.S. Department of Energy Combustion 2000 Program through a subcontract to the United Technologies Research Center to support testing and development of subsystems to be used in a high-temperature advanced furnace. It consists of

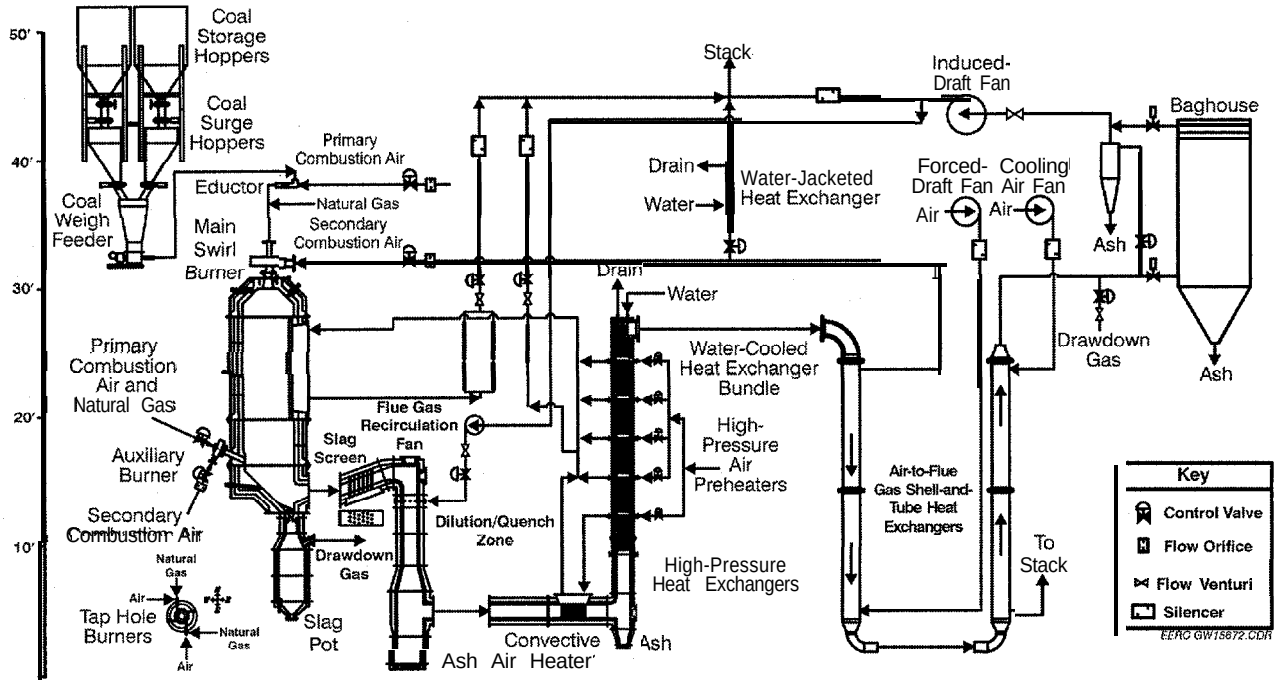


Figure 1. The EERC SFS.

eight main components: 1) slagging furnace, 2) slag screen/slag tap, 3) dilution-quench zone, 4) process air preheaters, 5) convective air heater (CAH) section, 6) radiant air heater (RAH) panel, 7) tube-and-shell heat exchangers, and 8) pulse-jet baghouse. The SFS design is intended to be as fuel-flexible as possible, with maximum furnace exit temperatures of 1480" to 1590°C to maintain the desired heat transfer to the RAH panel and slag flow. The furnace has a nominal firing rate of 2.6 x $10^6$ kJ/hr and a range of 2.1 to 3.2 x $10^6$ kJ/hr using a single burner. The furnace design was based on Illinois No. 6 bituminous coal (25,800 kJ/kg) and a nominal furnace residence time of 3.5 s. The EERC oriented the furnace vertically (downfired) so that slag would not interfere with the operation of the burner. Internal dimensions are 119 cm in diameter by roughly 4.9 m in total length. It is lined with three layers of refractory totaling 30 cm thick to minimize heat loss. This insulation keeps the wall surface temperature near that of the gas stream. The inner layer is composed of an alumina castable, developed by the EERC in cooperation with the Plibrico Company, that has been shown in bench and pilot tests to be extremely resistant to slag corrosion at the high wall temperatures.

Material sample coupons can be inserted into the system either through ports in the main combustor, in the slag screen, or on racks in the convective pass downstream of the CAH. Most samples were included downstream of the CAH. Near that subsystem, gas temperatures are maintained at 980°C, but they drop further back in the system to approximately 175°C as the gas enters the exit stack. To be included in SFS tests, materials coupons should be no more than 5 cm wide and able to be slipped onto a 1.2-cm-thick Inconel support rod.

## The Transport Reactor Development Unit

In addition to exposure to combustion conditions in the SFS, materials coupons can also be exposed to gasification gas and dust in the hot-gas filter vessel (HGFV) of the transport reactor development unit (TRDU). The TRDU is a 2.6 x $10^6$-kJ/hr pressurized circulating fluid-bed gasifier similar to the gasifier being tested at the Southern Company Services Wilsonville, Alabama, facility. The system is illustrated in Figure 2. It has an exit gas temperature of up to 980°C, a nominal gas flow rate of 510 $m^3$/hr, and an operating pressure of 0.93-1.1 MPa. The TRDU system can be divided into three sections: the coal feed section, the TRDU, and the product recovery section. The TRDU proper consists of a riser reactor with an expanded mixing zone at the bottom, a disengager, and a primary cyclone and standpipe. All of the components in the system are refractory-lined and designed mechanically for 1.1 MPa and an internal temperature of 1090 ° C.

The premixed coal and limestone fed to the transport reactor can be admitted through one of three nozzles, which are at varying elevations. Oxidant is fed to the reactor through two pairs of nozzles at varying elevations within the mixing zone. For the combustion mode of operation, additional nozzles are provided in the riser for feeding secondary air. Hot solids from the standpipe are circulated into the mixing zone where they come into contact with the oxidant and the steam, which is injected into the J-leg. This feature enables spent char to contact oxidant and steam prior to the fresh coal feed. Gasification or combustion and desulfurization reactions are carried out in the riser, as coal, sorbent, and oxidant (with steam for gasification) flow up the riser. The solids circulation into the mixing zone is controlled by the solids level in the standpipe. The bulk of entrained solids leaving the riser is separated from the gas stream in the disengager and circulated back to the riser via the standpipe. A solids stream is withdrawn from the standpipe via an auger to maintain the system's solids inventory at an appropriate level. Gas exiting the disengager enters a primary cyclone that has been modified to provide variable particulate collection performance. Solids from the dipleg of the primary cyclone are collected in a lock hopper. Gas exiting this cyclone enters a jacketed-pipe heat exchanger before entering the HGFV. The cleaned gases leaving the HGFV enter a quench system before being depressurized and vented to a flare.

This vessel is designed to handle all of the gas flow from the TRDU at its expected operating conditions. The vessel is approximately 1.2 m inner diameter (i.d.) and 4.7 m long and is designed to handle gas flows of approximately 550 $m^3$/hr at temperatures up to 980°C and 0.99 MPa. The refractory has a 0.7 l-m i.d. with a shroud diameter of approximately 0.56 m. The vessel is sized such that it could handle candle filters up to 1.5 m long; however, 1.0-m candles are being used in the initial 540°C gasification tests. Candle filters are 60 mm outer diameter with 10-cm center line-to-center line spacing. The total number of candles that can be mounted in the current geometry of the HGFV tube sheet is 19.

Standard TRDU tests consist of 200 hours of operation under gasification conditions with the HGFV operating at temperatures of 540°–650°C, 0.93 MPa. Materials coupons are exposed in the system by sliding them over 1.3-cm-diameter stainless steel rods in the free space below the candle filters. Samples up to 5.1 cm wide can be included. The composition of the gas to

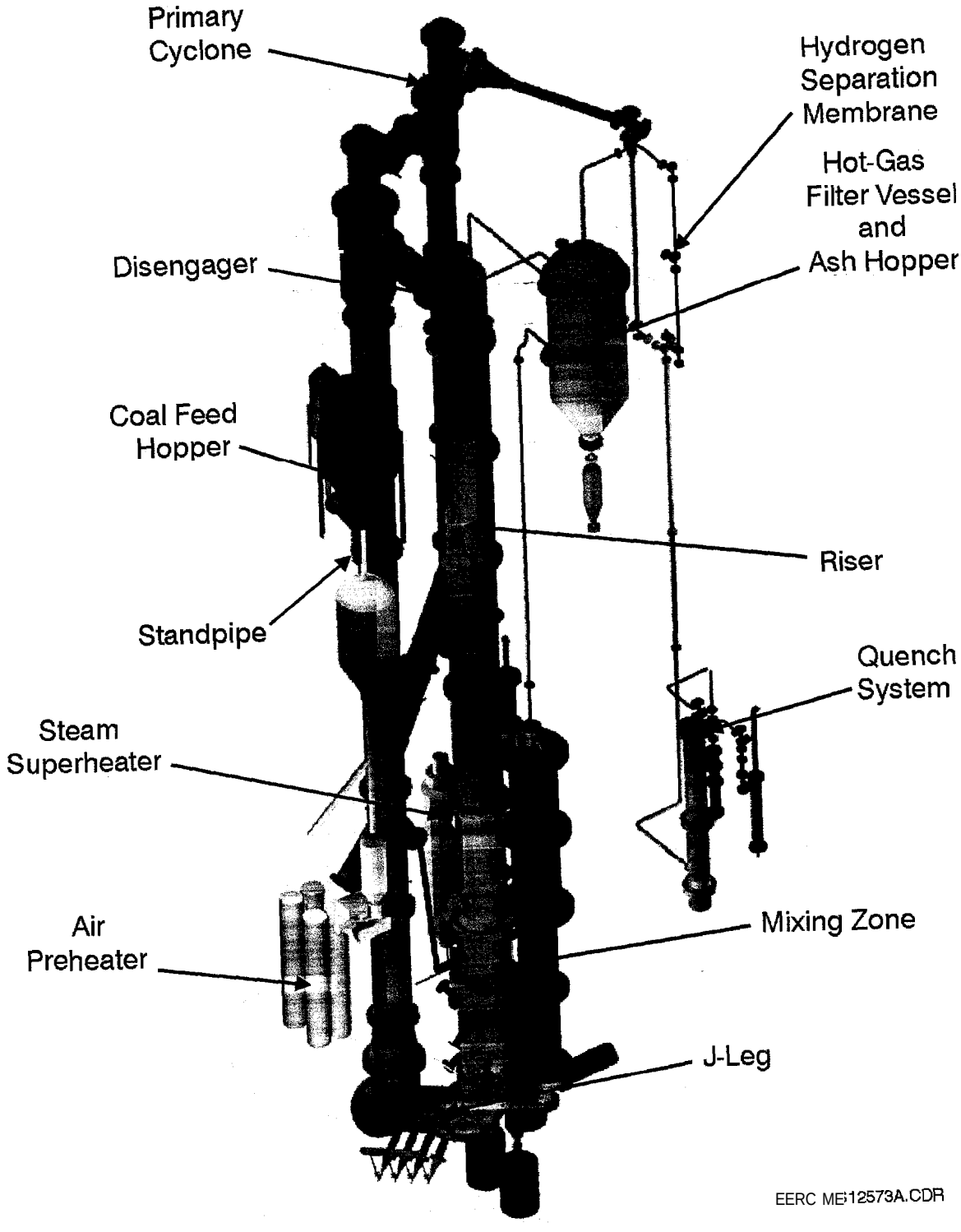


Figure 2. TRDU and HGFV in the EERC gasification tower.

which the materials coupons would be exposed in the HGFV is approximately 8%-14% $H_2O$, 6%-9% each of CO and H,, 8%-10% CO,, and l.O%-2.5% $CH_4$, with the balance being $N_2$ and other trace constituents.

## RESULTS AND DISCUSSION OF THE COUPON TESTING

The EERC performed two 200-hour tests in the SFS, one in March and one in June of 2000, during which ceramic and alloy samples were exposed to coal combustion conditions. In addition, 15 samples were installed in the filter vessel of the TRDU in July 2000 for a 200-hour oxygen-enriched gasification test. The samples included eight mullite rings from Oak Ridge National Laboratory (ORNL), four SiC/SiC rings from Honeywell Advanced Composites, Inc., and three alloys from Special Metals Corporation (SMC). The test, originally scheduled for October, was finally was performed in January 2001. During the test, the samples were exposed to 125 hours of coal utilization by-products, of which 109 hours were during coal gasification mode. Two coals, Prater Creek Kentucky bituminous and Navajo New Mexico subbituminous, were gasified for roughly two days each. The approximate temperature in the filter vessel was 450°C. After consultation with the coupon providers, it was decided to leave the coupons in place for additional gasification tests in March and June 2001. During the March test, the samples were exposed to 137 hours of coal utilizing by-products, of which 121 hours were in gasification mode. The three coals gasified for roughly two days each were the Navajo New Mexico and Wyodak Wyoming subbituminous and Illinois No. 6 Baldwin bituminous coals. During the June 2001 test, total exposure was 191 hours, with 176 hours during coal gasification. Three North Dakota lignite coals were gasified for the Center, Falkirk, and Freedom Mines. As of July 2001, the samples have been exposed to 453 hours of coal feed, of which 406 hours were during oxygen-enriched gasification. These samples have not been removed from the filter vessel, so discussion of their appearance or analyses of the coupons will not be included in this document.

### Samples Exposed in the March 2000 SFS Test

ORNL provided ceramic rings and alloy coupons to be exposed in either the SFS or the TRDU. Ten pure mullite ceramic rings were installed in the convective pass of the SFS for the March test. Several of the samples were analyzed after the test, and several others were left in the system for the June test. The rings included five samples that were light grey because of contamination during processing. In addition, eight white ceramic rings with a composition of $2Al_2O_3$–$3SiO_2$ (mullite) were installed in the HGFV of the TRDU in July. All rings were approximately 2.5 cm high and 6.3 cm in diameter, with a wall thickness of 0.8 cm. Eight metal coupons were also installed in the SFS for the March test. They were duplicate samples of four metal alloys reportedly composed of iron (Fe) with chromium (Cr) and silicon (Si), Fe with aluminum (Al), Fe with nickel (Ni) and Cr, or Ni with molybdenum (MO) and Cr. The samples were 3.7 cm square and 1.3 cm thick.

Honeywell Advanced Composites, Inc., provided eight ceramic rings to be exposed in the SFS during both the March and June tests. Four were white ceramic rings composed of the trade

material PRD-66 which contained mullite, alumina, and cordierite. The other four were charcoal gray rings of enhanced silicon carbide fibers in a silicon carbide matrix (SiC–SiC). The PRD-66 rings were similar in dimensions to the ceramic rings received from ORNL. Three of the SiC–SiC rings were 6.0 cm in diameter, and the fourth was 5.4 cm. All four SiC–SiC rings were 2.5 cm high and had a wall thickness of 0.3 cm.

### March Test Conditions

The metal alloys and the 18 ceramic samples were placed on a three-tiered Iconite rack and installed in the convective pass of the SFS 13 in. beyond the CAH. Figure 3 shows- the samples from the upstream side in position prior to the system being sealed for the March test. After gradual heating of the system, the samples were exposed to 200 hours of flue gas generated by combustion of a Powder River Basin subbituminous coal from the Cordero Rojo Mine. The average flue gas flow rate through the convective pass was 940 scfm. The composition of the gas (on a dry basis) to which the coupons were exposed was 300 ppm SO,, 530 ppm NO,, 30 ppm CO, 4.9% 0,, and 13.4% CO,, with $N_2$ as the remainder. The average temperature was 965°C. Measurements during subsequent runs indicate that temperature variation across the duct is no more than 2°C. Figure 4 shows a profile of the flue gas temperature just downstream of the sample rack during the run. The temperature ranged from about 949°–982°C. The six vertical lines on the chart indicate when coal feed stopped and started during the run. Excess slag buildup at the tap forced coal feed shutdown twice during the run. As the graph indicates, temperature was relatively stable during this process.

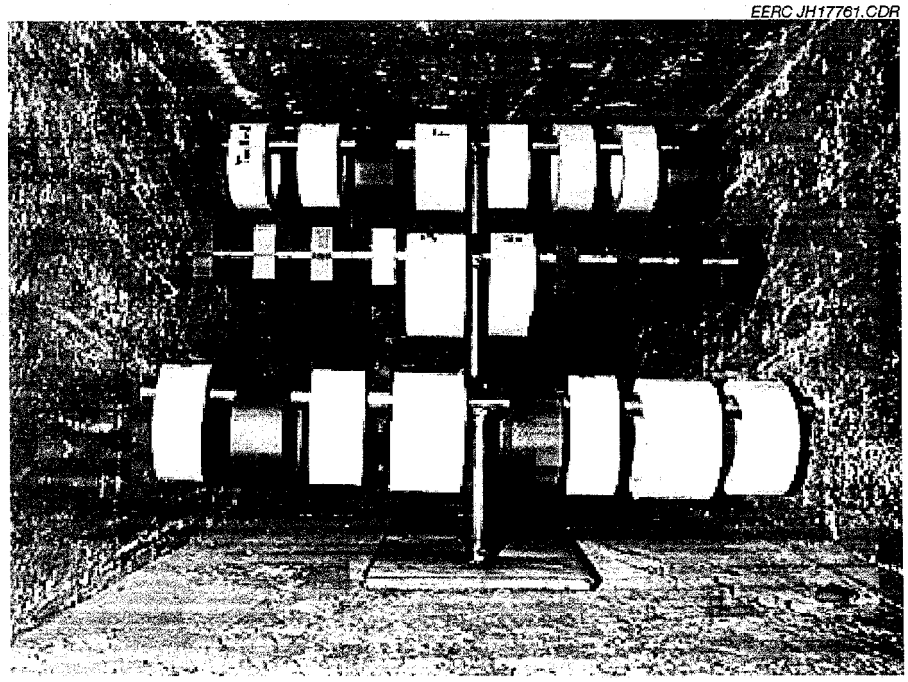


Figure 3. Upstream view of samples installed in the SFS convective pass.

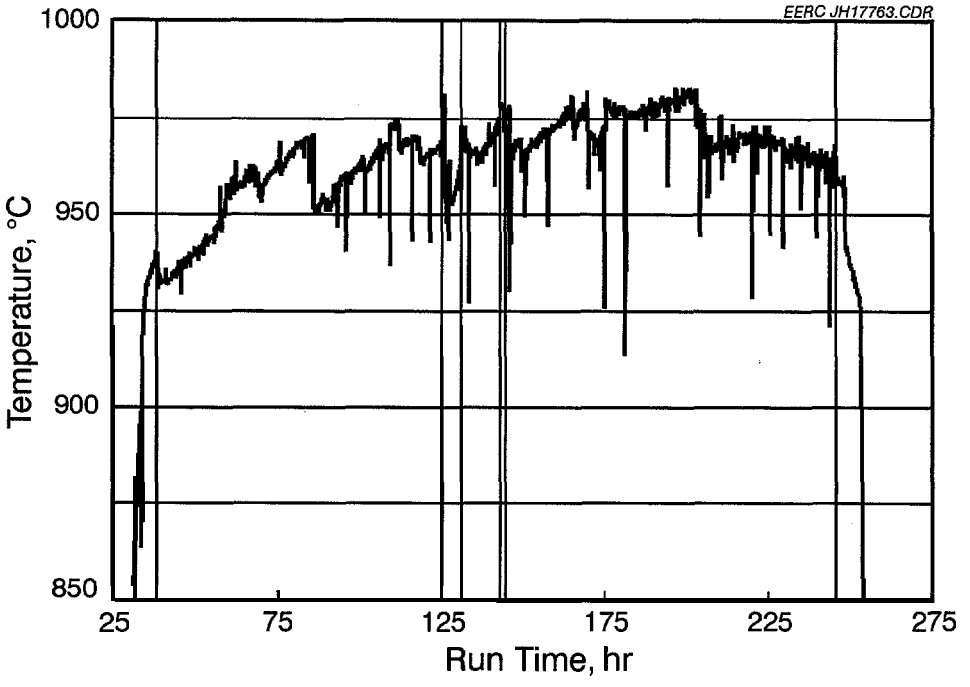


Figure 4. Temperature profile downstream of the samples.

Two activities that did affect temperature in the convective pass were quench zone cleaning and cleaning of the CAH (sootblowing). Cleaning of the quench zone (just upstream of the convective pass) was performed as needed, approximately every 6 hours. A port must be opened during cleaning, with the result that the flue gas temperature drops and the gas velocity increases.

Also, sootblowing of the front tubes on the CAH occurred every 8 hours with pressurized room temperature N,. This caused temporary temperature decreases and higher concentrations of ash blown against the coupons.

During the run, the samples were observed via site ports located throughout the SFS convective pass. The samples, which initially swung in the force of the flue gas, became cemented in place by the ash deposits by Day 4 of the 9-day test. Figure 5 shows the extent of ash deposition on the upstream surfaces of samples at the end of the test. In addition, ash filled the open areas in the center of each ceramic ring. Downstream deposition on the samples, shown in Figure 6, was lighter.

After the combustion test, the sample rack was carefully removed from the SFS. The coupons were separated from each other and the rack, maintaining as much ash on the samples as possible. Each sample was examined and photographed, with care being taken not to dissociate the ash from the coupon. Visual inspection of the rings revealed no changes because of the exposure. Some rings were subjected to SEM analysis to determine corrosion and erosion effects not visible to the eye. The remainder of the samples were returned to the submitter or cleaned and reinstalled in the SFS for further high-temperature exposure during the June test run.

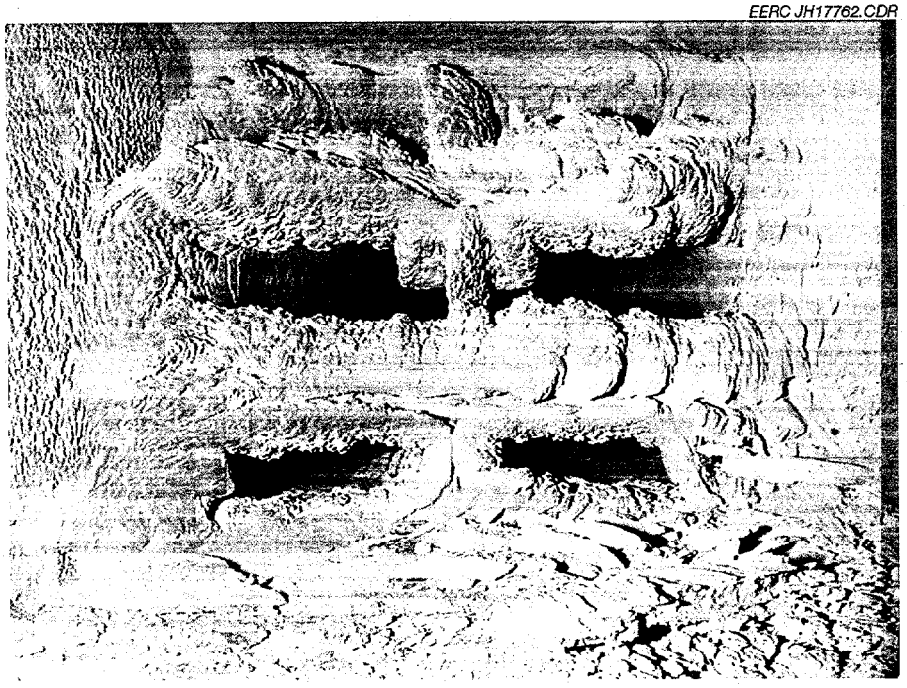


Figure 5. Upstream view of samples with ash deposition.

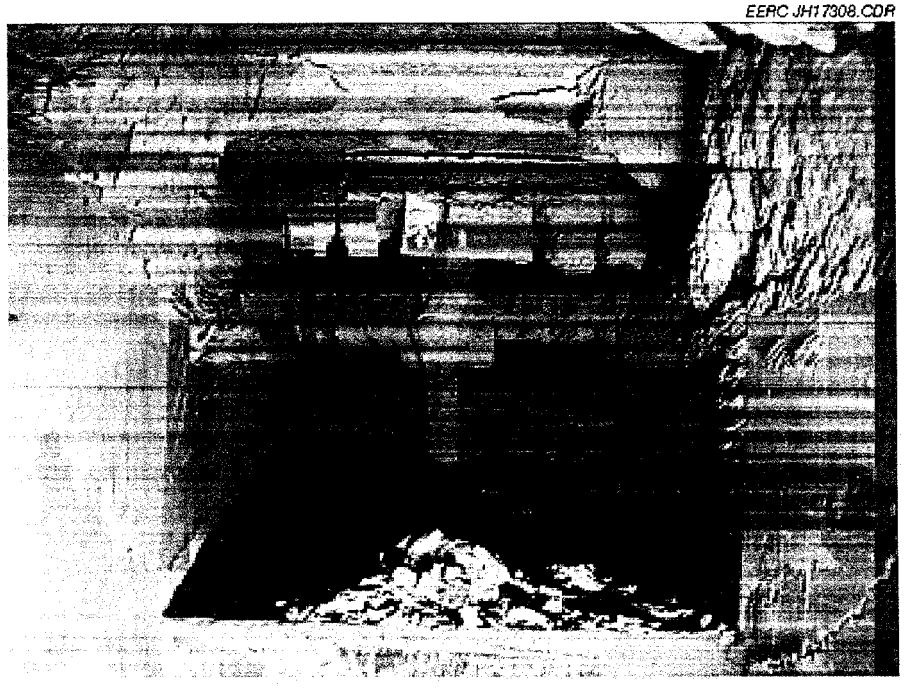


Figure 6. Downstream view of samples with ash deposition.

In contrast to the ceramic rings, the metal coupons exhibited effects of both corrosion and erosion. Visual inspection showed discoloration of all metal sample surfaces. Four sample surfaces included blotchy white patches. Two samples were severely corroded, turning green, and flecking off layers of material. These samples are visible on the center right of Figure 6. One sample from each pair and the two green samples were analyzed by SEM. The results of the analyses follow.

Samples of bulk coal ash and ash deposits formed in the convective pass were analyzed by wavelength-dispersive x-ray fluorescence and SEM point count (SEMPC), respectively. As shown in Table 1, the compositions of the deposits that formed in the convective pass on the SFS coupons contained much less Si and much more calcium than the bulk coal ash. Computer-controlled scanning electron microscope analyses of the minerals in the coal indicate that the mineral matter in the coal is composed primarily of silica-rich clays. Approximately half of the mass of the clay is composed of particles with diameters over 10 μm. These particles would be expected to be collected with relatively high efficiency in the slag screen upstream of the convective pass, leaving the ash particles reaching the sample coupons relatively deficient in silica. In contrast, only small amounts of calcium-rich minerals are found in the coal, even though the coal ash contains over 30% calcium on a sulfur-free oxide basis. This implies that the

TABLE 1

Composition of the Bulk Cordero Rojo Coal Ash and the Convective Pass Deposits (normalized sulfur-free oxide basis)

| Oxides, wt % | Cordero Rojo Coal ASH | Convective Pass Ash Deposit |
|---|---|---|
| $SiO_2$ | 29.5 | 20.7 |
| $Al_2O_3$ | 19.1 | 20.2 |
| $Fe_2O_3$ | 6.9 | 8.9 |
| $TiO_2$ | 1.9 | 2.1 |
| $P_2O_5$ | 1.0 | 2.1 |
| CaO | 33.3 | 38.5 |
| MgO | 6.6 | 5.9 |
| $Na_2O$ | 1.2 | 1.3 |
| $K_2O$ | 0.5 | 0.3 |
| $SO_3$[1] | 15.2 | 5.9 |

[1] Normalized with other oxides.

calcium occurs in the coal primarily as the salt of an organic acid, highly dispersed and able to form micron-sized calcium-rich ash particles upon combustion of the coal. This size range of particle is inefficiently captured in the SFS slag screen, leaving the ash reaching the materials coupons relatively enriched in calcium. SEMPC analyses indicate that the calcium in the deposits primarily occurs as calcium oxide, much of which is partially sulfated, and calcium aluminosilicates, a portion of which is also partially sulfated.

### SEM Analyses of Coupons Exposed During the March 2000 Test

SEM analysis of the coupons prior to exposure was not performed.

#### *NMARL Sample 00-0571 Submitted by Honeywell, HACI #0257-01-001-2-5*

**Sample description:** Charcoal gray SiC/SiC ring 25 mm high by 54 mm diameter, with a wall thickness of 3 mm.

**Postexposure appearance:** Figure 7 shows the sample removed from the sample holder after the March test run. Ash deposit obscures much of the sample surface. No material degradation was observed. Cross-sectioned sample set in epoxy remains very dark gray.

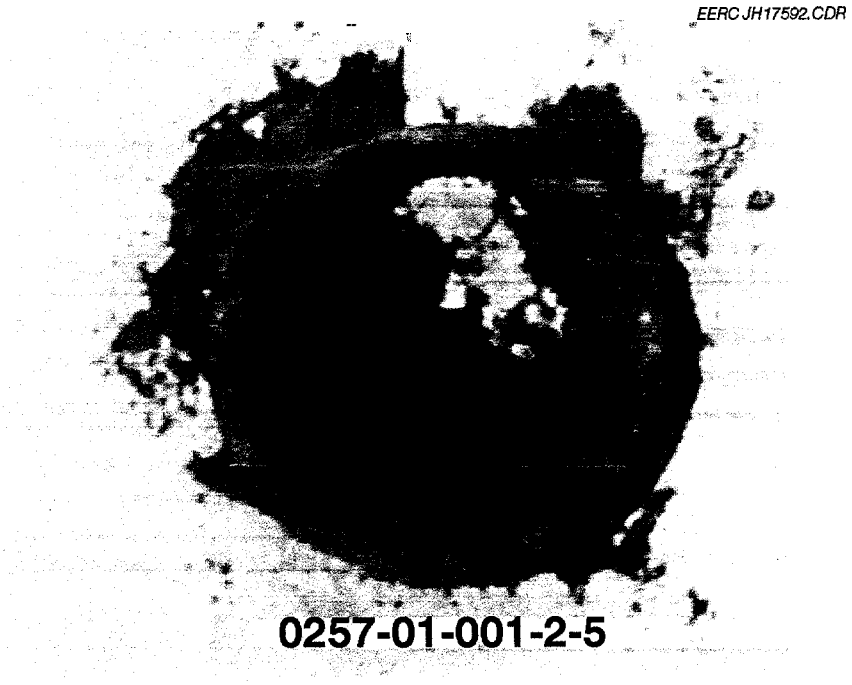


Figure 7. Honeywell SiC–SiC sample removed from the sample holder after the March test run (HACI #0257-01-001-2-5).

SEM Morphology

The sample was described by the submitter as SiC fibers in a SiC matrix. It was prepared for SEM analysis according to the submitter's instructions. Figure 8 is a backscattered electron image of the sample material and ash deposit at 100× magnification. It shows a cross section of weave of lengthwise and crosswise fibers, amorphous bundles and voids, amorphous binder at the surface, and a light layer of ash. The darkest areas are mounting epoxy.

No subsurface corrosion was observed in the cross section. The material-ash interface appears limited to the surface of the ring. The depth of the ash deposit ranged from less than 1 μm to greater than 70 μm. Figure 9 includes a natural divot in the surface (left of center in the photo) that filled with ash. It did not penetrate or otherwise degrade the material. Composition of the deposited ash layer was consistent with that of the convective pass ash deposit described in Table 1. No signs of corrosion or erosion were indicated throughout the sample cross section, although a thin surface layer less than 5 μm thick was rich in calcium and silicon which may indicate very limited attack.

### *NMARL Sample 00-0570 Submitted by Virginie Vaubert, ORNL #Jan 11-l*

**Sample description:** White mullite ring 33 mm high by 62 mm diameter, with a wall thickness of 7 mm.

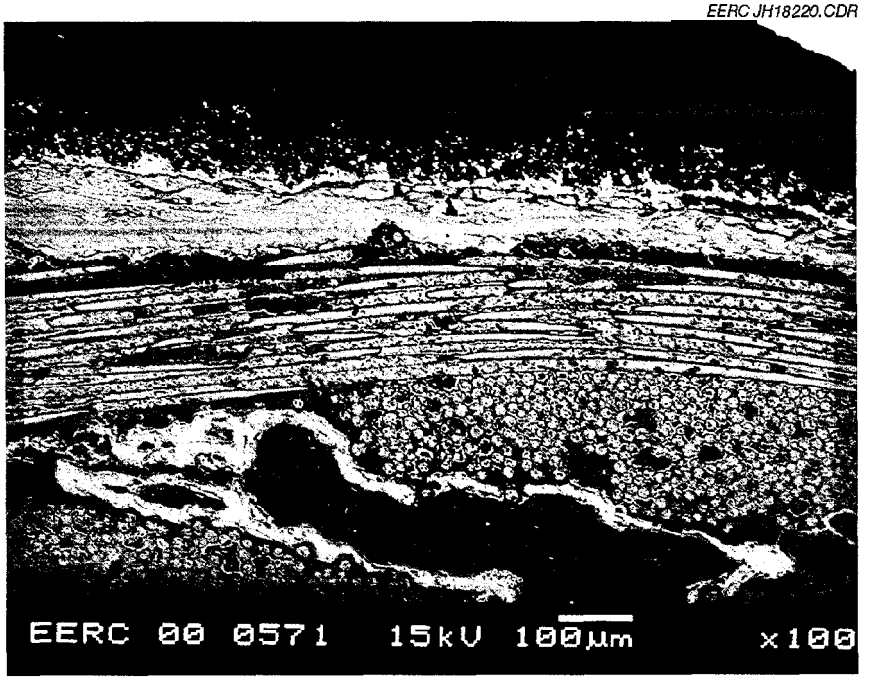


Figure 8. Honeywell SiC–SiC material and ash deposit at 100× magnification (HACI #0257-01-001-2-5).

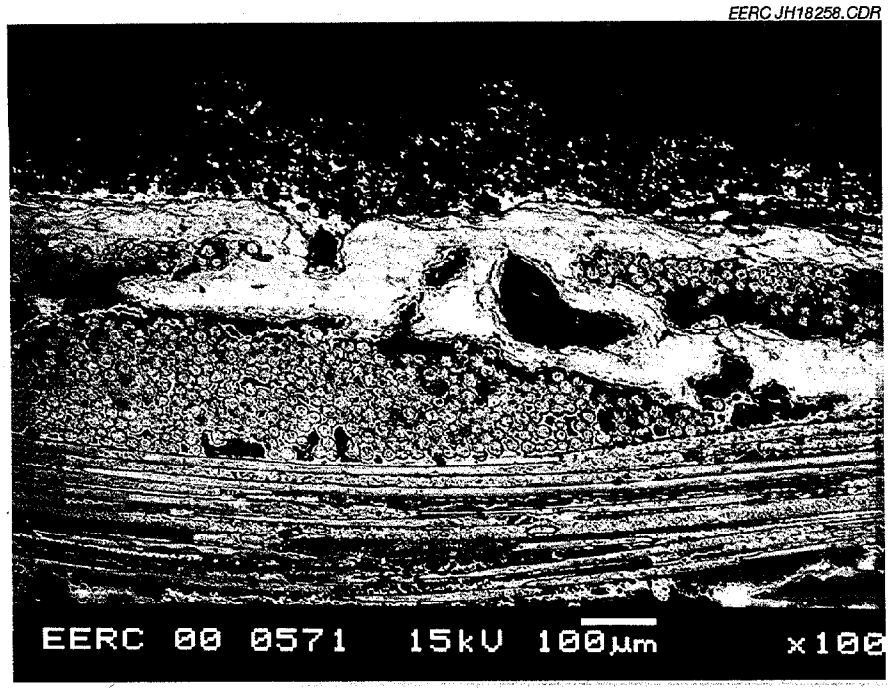


Figure 9. Honeywell SiC–SiC material and ash deposit at 100× magnification. Divot in sample surface (HACI #0257-0 l-001 -2-5).

**Postexposure appearance:** Figure 10 shows the sample removed from the sample holder after the March test run. Ash deposit obscures much of the surface. No degradation was observed. The cross-sectioned sample set in epoxy looks dirty white from inclusion of black ash particles. The depth of the ash deposit ranged from 100 µm to greater than 70 mm.

SEM Morphology

The sample was described as being composed of mullite. Figure 11 shows a representative example of the material and deposited ash at 100× magnification. SEM analysis of the bulk material indicated a composition of 49 wt% Al, 37 wt% 0, and 13 wt% Si.

Ash penetration was minimal, but there was no gas flow through the material. No subsurface corrosion was observed in the cross section. Ash filled the voids between the mullite grains at the surface to a depth of 180 µm as shown in the figure. It otherwise did not penetrate or degrade the sample.

Composition of the deposited ash layer was consistent with that of the convective pass ash deposit described in Table 1. Evidence of surface corrosion may be indicated by a thin, discontinuous layer (<5 µm thick) of apparent corrosion product at the sample-ash interface. This layer is rich in calcium, aluminum, and silicon.

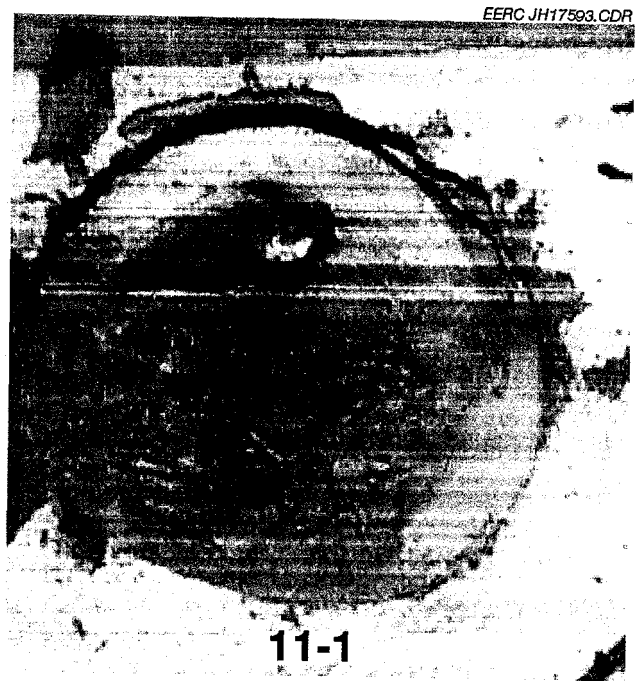


Figure 10. ORNL mullite composite ring removed from the sample holder after the March test run (ORNL #Jan 1 l-l).

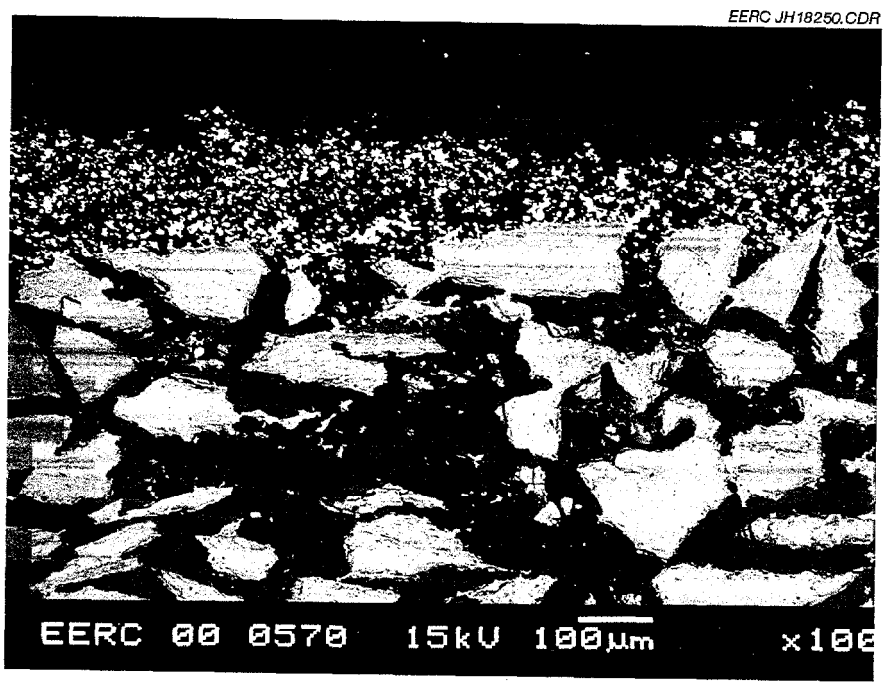


Figure 11. ORNL mullite composite and deposited ash at 100× magnification (ORNL #Jan 1 l-l).

*NMARL Sample 00-0668 Submitted by Virginie Vaubert, ORNL #B*

**Sample description:** Gray mullite cylinder 24 mm high by 62 mm diameter, with a wall thickness of 8 mm.

**Postexposure appearance:** Figure 12 shows the sample removed from the sample holder after the March test run. Ash deposit obscures much of the sample surface. No degradation was observed. Cross-sectioned sample set in epoxy remains gray.

SEM Morphology

The sample was described as being composed of mullite. Figure 13 shows a representative example of the material and deposited ash at 100× magnification. It reveals a porous field of ceramic masses largely separated from a band of ash across the top of the figure. SEM analysis of the bulk material indicated a composition of 48 wt% Al, 38 wt% 0, and 14 wt% Si. The composition of inclusions in the mullite grains-visible as light streaks-was 41 wt% Si, 38 wt% 0, 10 wt% Al, 7.5 wt% K, and 3 wt% Na. Some smaller grains in the substrate cross section contained more evenly balanced levels of Al and Si (25-26 wt% each with 38 wt% 0, 6 wt% K, 4 wt% Na, and 0.7 wt% Ca) or enriched Al (60 wt% with 25 wt% Si, 12 wt% 0, and 1 wt% K) with respect to the bulk material.

No subsurface corrosion was observed in the sample cross section. The material-ash interface appears limited to the surface of the ring. Ash filled the voids between the material at


Figure 12. ORNL #B mullite composite removed from the sample holder after the March test run.

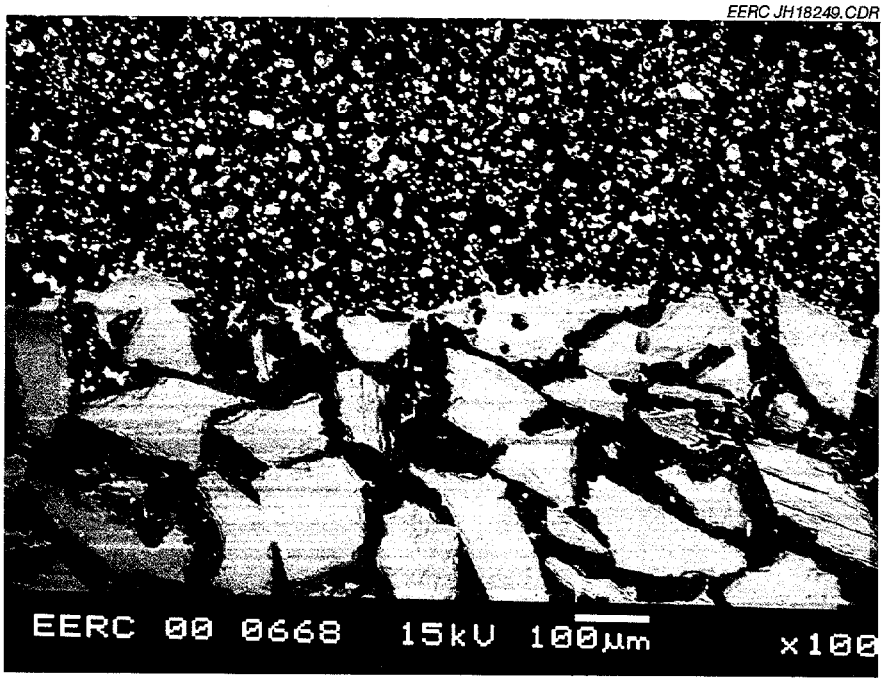


Figure 13. ORNL mullite composite and deposited ash at 100× magnification (ORNL #B).

the surface to a depth of <200 µm as observed in the figure. It did not penetrate or otherwise degrade the sample. Evidence of surface corrosion may be indicated by a thin discontinuous layer (<5 µm thick) of apparent corrosion product at the sample-ash interface. This layer is rich in calcium, aluminum, and silicon. Since flue gas was not forced through the sample, these results may vary from the performance of the material used as a filter.

The composition of the deposited ash layer was consistent with that of the convective pass ash deposit described in Table 1. The depth of the ash deposit on the sample ranged from less than 1 mm to greater than 70 mm.

### *NMARL Sample 00-0566 Submitted by Vinod Sikka, ORNL #1 7638*

**Sample description:** 3 1.5 $mm^2$ x 13-mm alloy cuboid with 13-mm-diameter hole in the center of larger surface; stainless steel-colored.

**Postexposure appearance:** Sample is coated with a flaky green layer. Similar green material is present on the floor of the pass under the sample rack as well. There is no ash bonded to the surface. Note that the reported duplicate sample came out of the test gray.

SEM Morphology

The metal is reported to contain 69.43 wt% Ni, 8.00 wt% Cr, 18.00 wt% Mo, 4.50 wt% Al, 0.05 wt% C, and 0.02 wt% B. Figure 14 shows a representative example of the material (at the

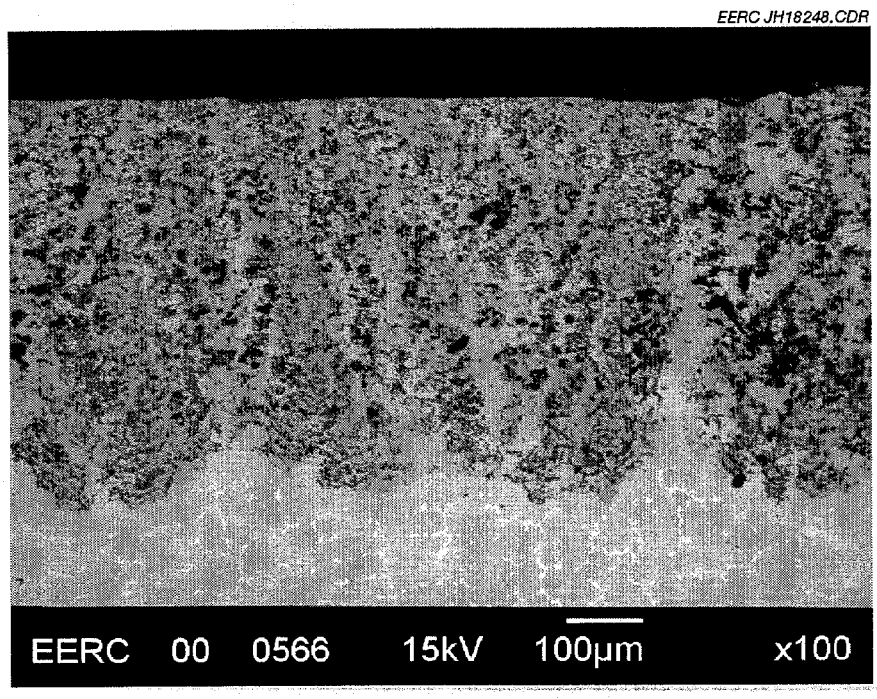


Figure 14. Surface corrosion at 100× magnification (ORNL #17638).

bottom of the photo) and surface corrosion at 100× magnification. It reveals in the alloy a pattern of bright streaks in a continuous field. SEM analysis of the bulk material indicated 68-79 wt% Ni, 8-18 wt% MO, 2-7 wt% Al, 4-l 1 wt% Cr, and l-2 wt% 0. The bright streaks contained less than 2 wt% Al, a lower concentration of Ni (3 l-35 wt%), and higher concentrations of MO (54-57 wt%) and Cr (8 wt%). The SEM analysis matches the reported content of alloy ORNL #17638.

Based on the cross section examined, the sample's surface underwent extensive smooth recession and oxidation. There was no attached ash deposit on the surface, but corrosion product covers the entire surface of the sample. At minimal thickness around the center opening where the sample rested on a 9.5-mm-diameter 3 16 steel rod, it varied in depth from 20 to 1000 µm. Figure 15 is a representative example of the corrosion product at 1500× magnification.

The corrosion product is heterogeneous, with pockets of metals and oxides. The corrosion product near the alloy interface (<120 µm from the alloy) included pockets similar to the alloy matrix described above and areas enriched in Ni. Examples of variations include regions with 37-47 wt% Ni, 20-48 wt% Cr, 4-24 wt% Al, trace Fe (<0.5 wt%), and 9 wt% 0; Ni-rich (77-81 wt%) regions containing 5-14 wt% Cr, 7 wt% Al, l-2 wt% Fe, and l-3 wt% 0; and nearly pure Ni-rich (90–97 wt%) regions associated with l-5 wt% 0, l-3 wt% Cr, and trace (<1 wt%) Al, Fe, and MO. Many of these combinations are found throughout the corrosion product. In contrast to the virgin alloy, MO concentrations in the corrosion product are at most 3 wt%.

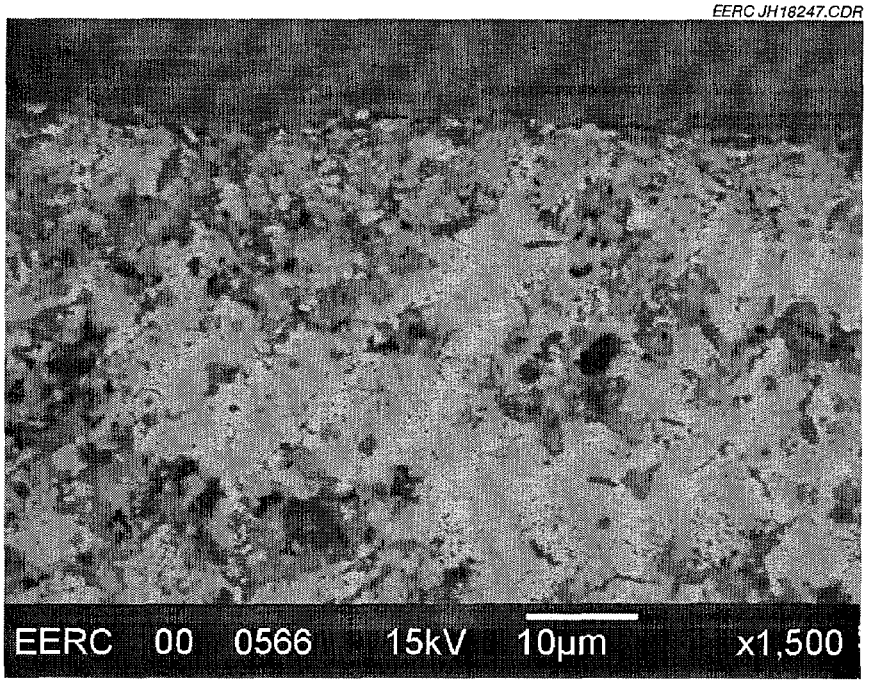


Figure 15. Surface corrosion at 1500× magnification (ORNL #17638).

Molybdenum shows up in the corrosion product close to the exterior surface (<40 µm deep), suggesting that the Mo has migrated toward the surface or escaped into the gas stream. From this region to the surface, Mo at 17 wt% was found associated with Ni (36 wt%), 0 (13 wt%), and Al (9 wt%). At the surface, pockets of alloy of similar content to the bright spots in the virgin alloy were observed. Some contained small amounts of 0 and S (67 wt% Mo, 26-31 wt% Ni, 2 wt% 0 and S, <2 wt% Cr, and <1 wt% Al), and others contained small amounts of Cl (48 wt% Ni, 43 wt% Mo, 3 wt% Cr, 2 wt% Al and Cl, and 1 wt% Fe). Oxidized nickel (86 wt% Ni, 12 wt% 0, <1 wt% Cu, Al and Fe) and matrix alloy (62 wt% Ni, 15 wt% Cr, 14 wt% Al, 5 wt% O, 2 wt% Fe, and <1 wt% S and Cl) were also present.

The main addition to metal alloy constituents in the corrosion sites was 0, indicating oxidation of the metal elements as the chief cause of corrosion. Low levels (2 wt% by weight) of sulfidation or halide attack were indicated. The absence of quantities of ash constituents present in the corrosion product indicates that the ash was not a factor in the alloy degradation.

### *NMARL Sample 00-0567 Submitted by Vinod Sikka, ORNL #17638*

**Sample description:** 3 1.5 $mm^2$ x 13-mm alloy cuboid with 13-mm-diameter hole in the center of larger surface; stainless steel-colored.

**Postexposure appearance:** Surface is no longer shiny. Aside from minor surface discoloration, the sample appears to have weathered the test well. There is little ash bonded to the surface. Note that the reported duplicate sample came out of the test green.

SEM Morphology

The metal is reported to contain 69.43 wt% Ni, 8.00 wt% Cr, 18.00 wt% Mo, 4.50 wt% Al, 0.05 wt% C, and 0.02 wt% B. Figure 16 shows a representative example of the cross-sectioned virgin material, corrosion product, and ash deposit at 100× magnification, It reveals a homogeneous field of alloy with dark spots caused by imperfect polishing of the sample cross-section surface. SEM analysis of the bulk material indicated 74 wt% Fe, 24 wt% Al, and 1.4 wt% Mo. Closer inspection of the sample at 1500× magnification (shown in Figure 17) reveals small white spots in the alloy, 2-4 μm in diameter, composed of 59-67 wt% Fe, 17-22 wt% Al, and 9-22 wt% Mo. Zirconium was also detected. The content of this sample is similar to that suggested for Sample #17682 supplied by ORNL, except for a high Mo content.

No subsurface corrosion was observed in the sample cross section, Very limited pitting was visible. The site near the middle of Figure 17 was typical. Maximum depth of penetration observed was 20 μm. The corrosion product in this pit was 64 wt% Al, 32 wt% 0, and 1.5 wt% Fe.

Limited smooth oxidation was also visible on the sample cross section. Depth of penetration was <10 μm. Content of the corrosion product varied from oxidation of Al and Fe (73 wt% Al, 24 wt% 0, and 2 wt% Fe) to Al and Fe with ash constituents (54 wt% Al; 7-8 wt% Fe; 1 l-23 wt% 0; O-13 wt% P; O-3 wt% Ca, Cl, Mg and Si; and 1 wt% Na).

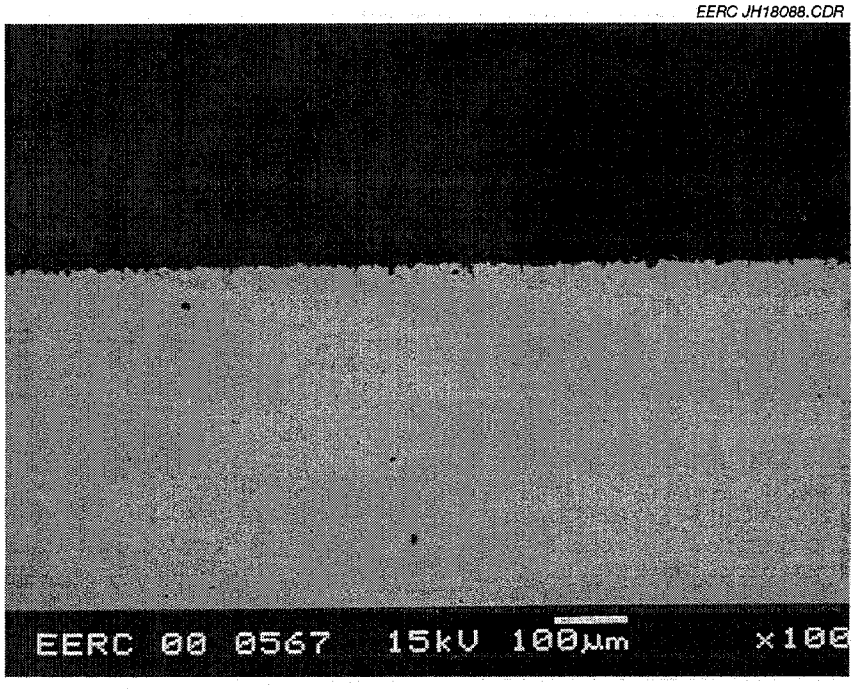


Figure 16. Cross-sectioned virgin material, corrosion product, and ash deposit at 100× magnification (ORNL #17638).

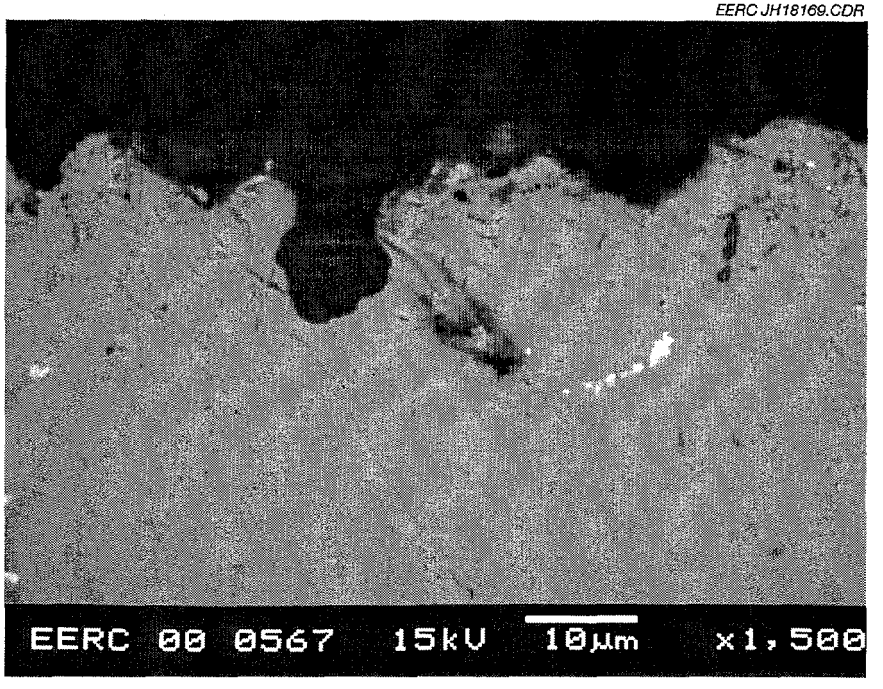


Figure 17. Pit in sample surface at 1500× magnification (ORNL #17638).

The ash adjacent to the corrosion product contained 18-24 wt% Ca, 10–22 wt% Fe, 10-23 wt% O, 13–15 wt% Al, 9-15 wt% Si, 3 wt% S, l-6 wt% Ti, l-3 wt% Na, and <3% Mg and P. This indicates an iron enrichment compared to the bulk ash deposits, which may indicate some migration of iron from the alloy into the deposit.

The main addition to metal alloy constituents in the corrosion sites was 0, indicating oxidation of the metal elements as the chief cause of corrosion. The absence of large quantities of ash constituents present at the corrosion sites indicates that the ash was not a factor in the alloy degradation.

### *NMARL Sample 00–0565 Submitted by Vinod Sikka, ORNL #17681*

**Sample description:** 3 1.5 $mm^2$ x 13-mm alloy cuboid with 13-mm-diameter hole in the center of larger surface; stainless steel-colored.

**Postexposure appearance:** The large mass of ash deposited on the sample separated easily from the sample. The surface is brown and dull through a thin layer of ash particle. The sample appears intact.

SEM Morphology

The metal is reported to contain 62.50 wt% Fe, 35.0 wt% Cr, and 2.5 wt% Si. Figure 18 shows a representative example of the cross-sectioned virgin material, corrosion product, and ash

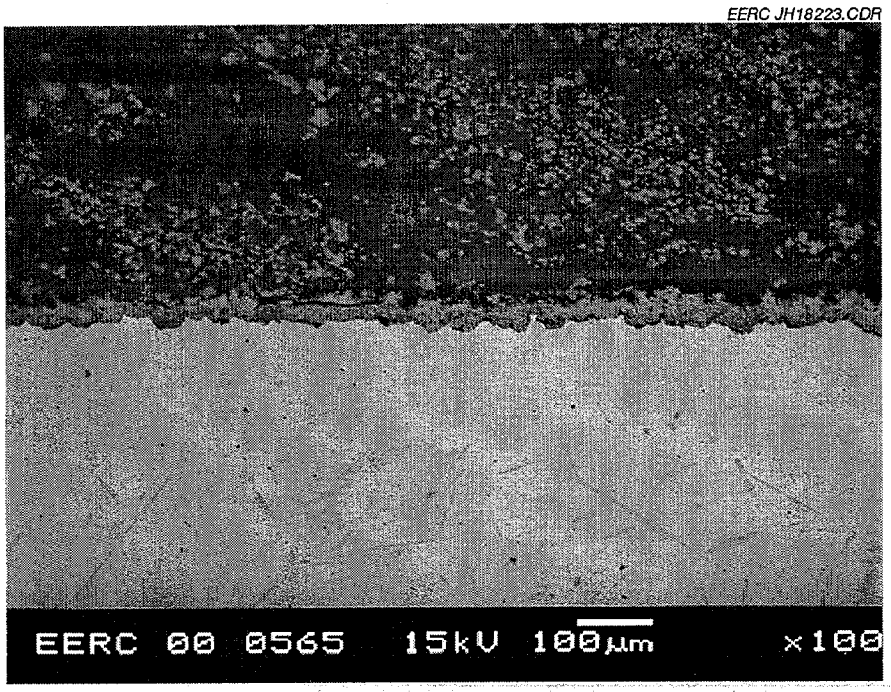


Figure 18. Cross-sectioned virgin material, corrosion product, and ash deposit at 100× magnification (ORNL #17681).

deposit at 100× magnification. It reveals a homogeneous field with occasional darker streaks. SEM analysis of the bulk material indicated 71.5-79 wt% Fe, 16-32 wt% Cr, and 1.5–4 wt% Si. The darker streaks contained higher proportions of Cr (92-94 wt%), less Fe (5 wt%) and 0 (2 wt%), and no Si.

The surface of the sample exhibited limited pitting and surface oxidation. Figure 19 shows one site of subsurface pitting at 1000× magnification. Depth and length of penetration were approximately 100 and 200 µm, respectively. The darker material filling the pit in Figure 19 comprises 36-73 wt% Cr, 6-41 wt% Al, and 17-20 wt% 0, with 0.4-3 wt% Si and l-2 wt% Fe. The lighter material at the surface of the pit is Cr (94 wt%) Fe (4 wt%) alloy which appears more resistant to the oxidation attack than the Fe-rich bulk material in the alloy.

Figure 20 shows surface pitting at 1500× magnification. The depth of the recession is approximately 50 µm. The alloy-corrosion product interface contains heterogeneous pockets of alloy elements and flue gas and ash components 0, Al, and S. Constituents include Fe-rich pockets (94 wt% Fe with l-2 wt% Al and Si); slightly oxidized Cr-rich alloy (80-92 wt% Cr, 2-5 wt% Fe, 4-16 wt% 0, and 0–2.3 wt% Si); oxidized alloy (45 wt% Cr, 29-34 wt% Fe, 12-16 wt% 0, and 6-9 wt% Si); Si-Cr-0 pockets (31-39 wt% Si, 30-36 wt% Cr, 20-29 wt% 0, and 3-4 wt% S); and Al-Cr combinations (44 wt% Al; 27 wt% Cr; 15 wt% O, 9 wt% Fe; 3 wt% Si; and <1 wt% S). The presence of Al and S at the interface suggests that ash and flue gas constituents assisted 0 in the corrosive degradation of the alloy materials.

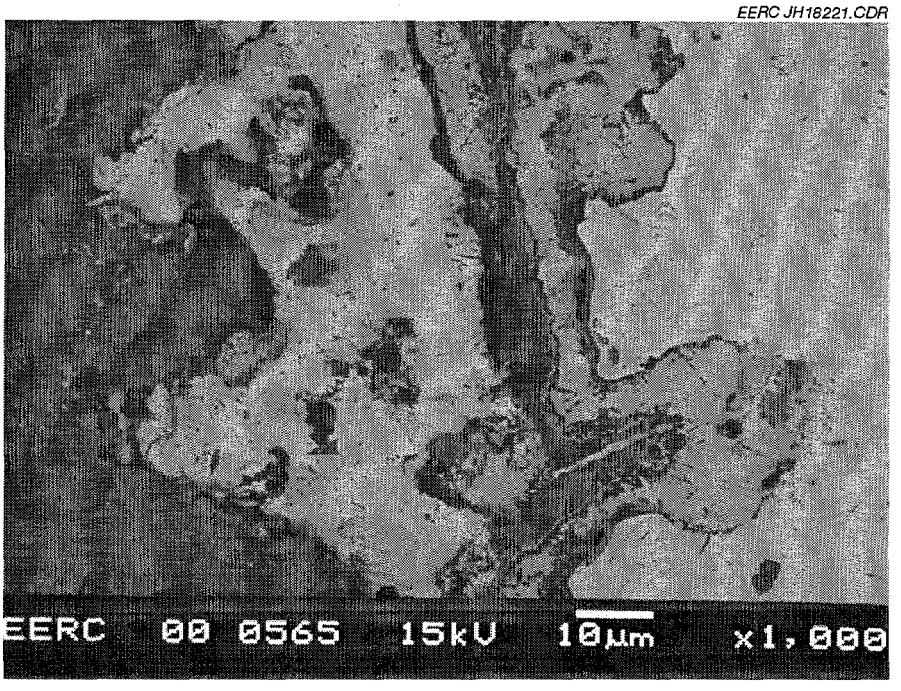


Figure 19. Subsurface pitting at 1000× magnification (ORNL #17681).

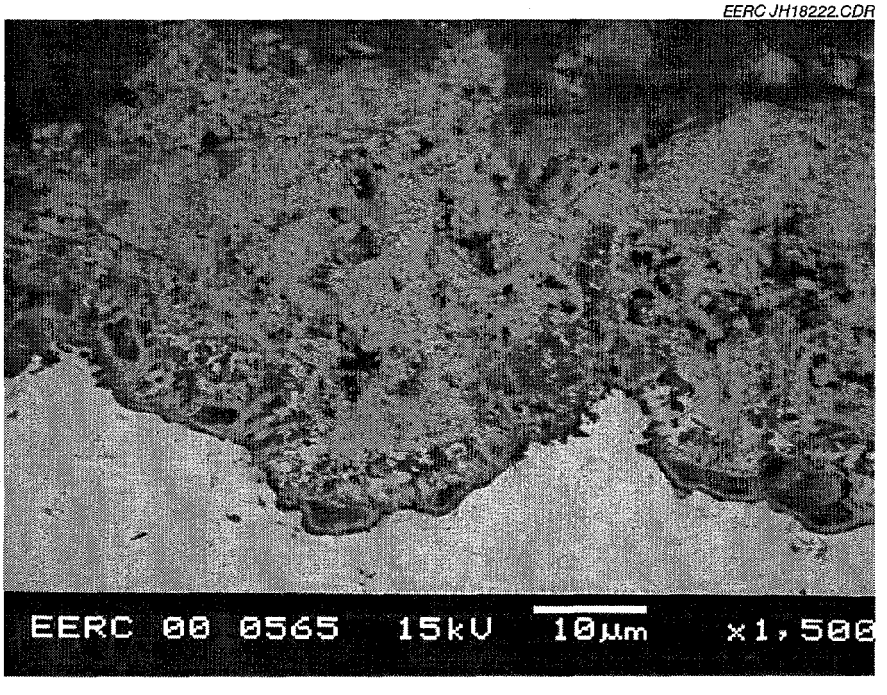


Figure 20. Virgin material and corrosion product at 1500× magnification (ORNL #17681).

The corrosion product itself, ranging in thickness from 20-50 μm, contained Cr-0, Si-Cr, Fe-Al-Cr, Si-Cr-0, Al-Fe-Cr-Ti, and Al-O-Fe pockets as listed in Table 2. Relative quantities of each type of corrosion product were not determined. As along the alloy interface, 0 and Al are conspicuous components of this region, indicating ash as well as oxidation attack on the sample.

TABLE 2

Surface Recession Corrosion Product Constituents

| Parameter, wt% | Cr-0 | Fe-Al-Cr | Si-Cr-0 | Al-Fe-Cr-Ti | Al-O-Fe |
|---|---|---|---|---|---|
| Cr | 72-84 | 19 | 36 | 26 | – |
| Fe | 2-4 | 53 | 3.5 | 13 | 15 |
| Si | l-9 | | 37 | 2 | <1 |
| **0** | 1 l-22 | – | 20 | – | 29 |
| Al | o-1.3 | 26 | | 29 | 54 |
| Ba | – | – | – | – | <1 |
| Ca | c l | – | – | – | – |
| *Cl* | – | – | – | 1.4 | – |
| S | – | – | 3 | 1 | – |
| Ti | – | – | – | 26 | – |

At the ash deposit interface, ash particles had the dominant presence. Silicon (17-52 wt%), 0 (28-44 wt%), Ca (O-23 wt%), and Al (O-6 wt%) were the main constituents. Present at trace amounts (<1 wt%) were Ba, Mg, Na, P, and S. Minor amounts of alloy materials (<9 wt% Cr, l-2 wt% Fe, and 2 wt% Ti) were observed in this region as well.

The main addition to metal alloy constituents in the corrosion sites were 0, Al, and S, indicating oxidation, Al attack, and sulfidation of the metal elements as the causes of corrosion. No halide attack was indicated. The presence of ash constituents present in the corrosion product indicates that the ash was a factor in the alloy degradation.

### *NMARL Sample 00-0569 Submitted by Vinod Sikka, ORNL #17682*

**Sample description:** 31.5 $mm^2$ x 13-mm alloy cuboid with 13-mm-diameter hole in the center of larger surface; stainless steel-colored.

**Postexposure appearance:** Surface is no longer shiny. Aside from minor surface discoloration, the sample appears to have weathered the test well. There is little ash bonded to the surface. Note that the reported duplicate sample came out of the test green.

SEM Morphology

The metal is reported to contain 74.85 wt% Fe, 25 wt% Al, 0.1 wt% Zr, 0.01 wt% B, and 0.05 wt% C. Figure 21 shows a representative example of the virgin material at 100× magnification. It reveals in the alloy a homogeneous field with occasional small bright spots. SEM analysis of the bulk material indicated 74 wt% Fe and 24 wt% Al, with trace amounts of MO, Zr, and Ti. The bright spots contained higher proportions of Zr (2-68 wt%) and MO (up to 6.5 wt%).

Subsurface corrosion was observed in the sample cross section at one location, shown in Figure 22 at 1500× magnification. The site was a pitted crack roughly parallel to the surface, 45 μm in length and 0.7-8 μm wide, with an average depth of 15 μm at center. The composition of material adjacent to the subsurface pitted crack was enriched in Al and reduced in Fe as compared to the surrounding alloy material. Specific concentrations were 47 wt% Al, 28 wt% 0, 19 wt% Zr, and 4 wt% Fe.

A second corrosion site in the form of a funnel-shaped pit stretching 25 μm deep into the sample and 20 μm wide at the sample surface was examined (Figure 23) at 1500× magnification. The material composition included 54 wt% Al, 23 wt% O, 17 wt% Fe, 2 wt% Zr, and cl wt% MO. As with the corrosion product at the other pit, the material contains more Al and less Fe than the virgin alloy, indicating probable oxidation of the metal alloy, Fe loss to the environment, and the formation of an aluminum oxide skin.

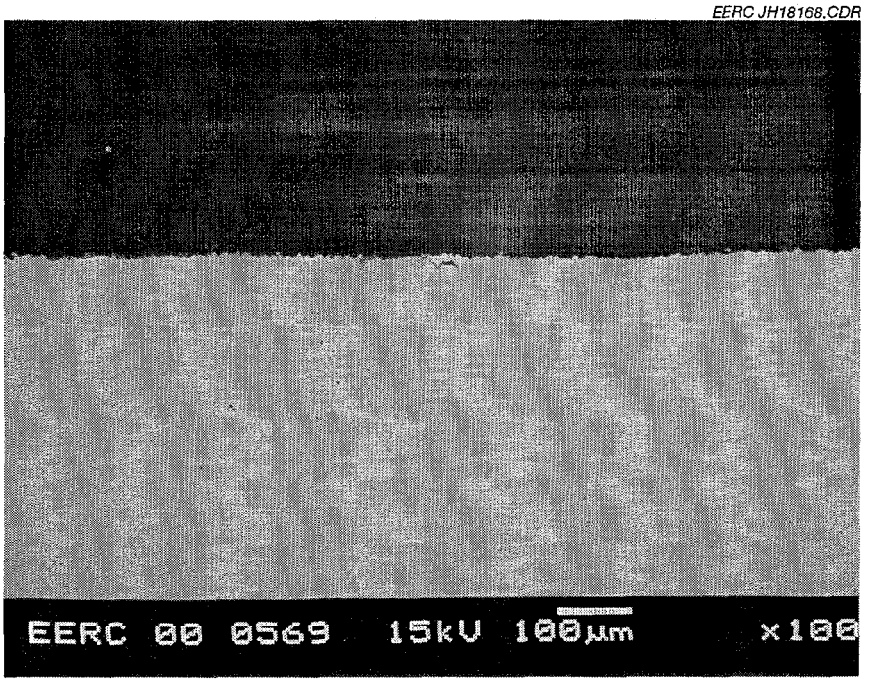


Figure 21. Cross-sectioned virgin material, corrosion product, and ash deposit at 100× magnification (ORNL #17682).

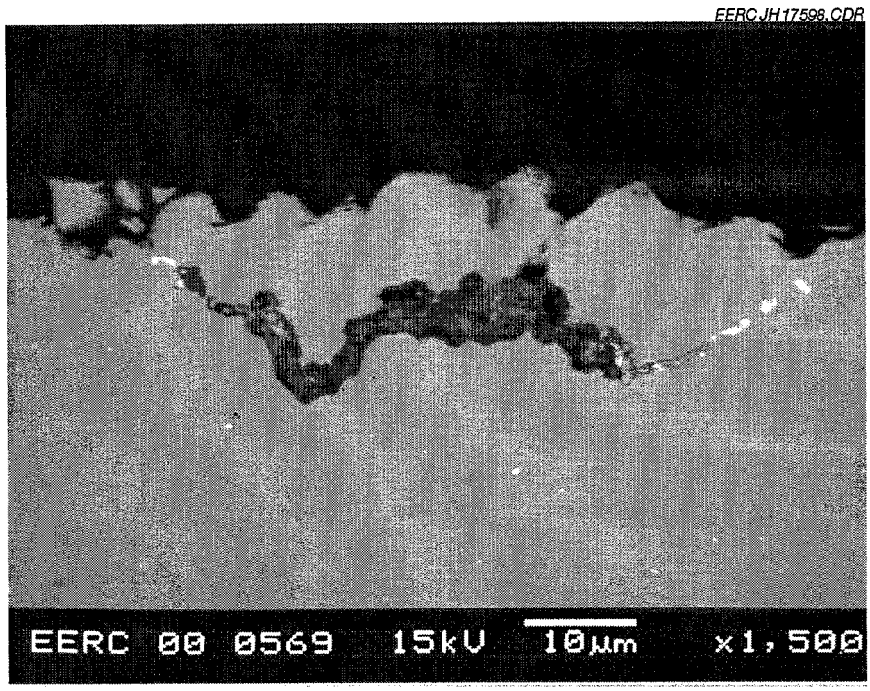


Figure 22. Subsurface corrosion at 1500× magnification (ORNL #17682).

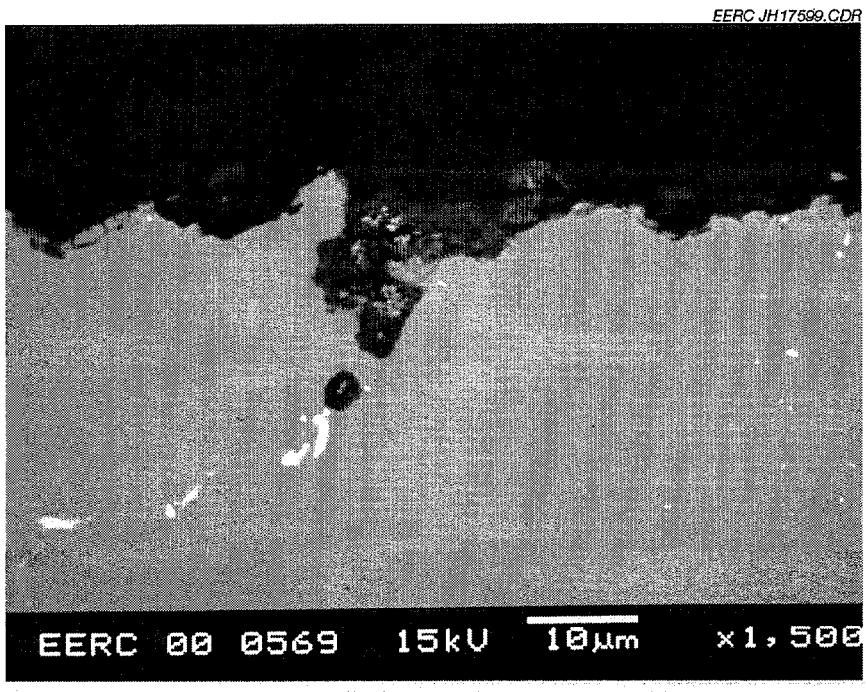


Figure 23. Surface corrosion at 1500× magnification (ORNL #17682).

Adjacent to both pits are pockets (l-2 × 2-5 μm) of increased Zr and MO concentrations in the metal on paths traceable to the corrosion conduit. This suggests that regions of high Zr/Mo concentration may invite corrosive action into the alloy.

The surface of the sample exhibited limited pitting and surface oxidation. The two sites of pitting described above, visible at the center of Figure 21 at 100× magnification, were within 100 μm of each other and the only sites in an 1140-μm length of sample surface cross section. Depth of penetration as described above was minimal.

Sulfur, Ca, and Cl at 2-4 wt% were identified near the exposed surface of the sample at three different points. The absence of large quantities of ash constituents present at either of the corrosion sites indicates that the ash was not a factor in alloy degradation. Along with occasional trace amounts of Cr, Ni, and P, the main addition to metal alloy constituents in the corrosion sites was 0. Oxidation and sulfidation of the metal elements were the chief causes of corrosion.

### *NMARL Sample 00–0568 Submitted by Vinod Sikka, ORNL #17682*

**Sample description:** 31.5 $mm^2$ x 13-mm alloy cuboid with 13-mm-diameter hole in the center of larger surface; stainless steel-colored.

**Postexposure appearance:** Sample is coated with a flaky green layer. Similar green material is present on the floor of the pass under the sample rack as well. There is no ash bonded to the surface. Note that the reported duplicate sample came out of the test gray.

SEM Morphology

The metal is reported to contain 74.85 wt% Fe, 25 wt% Al, 0.1 wt% Zr, 0.01 wt% B, and 0.05 wt% C. Figure 24 shows a representative example of the virgin material, a corrosion pit, and surface corrosion at 100× magnification. It reveals in the alloy a pattern of bright streaks in a continuous field. SEM analysis of the bulk material indicated 76-80 wt% Ni, 9-15 wt% MO, 2-7 wt% Al, 3-5 wt% Cr, and l-2 wt% 0. The bright streaks contained a trace amount of Al (<0.5 wt%), a lower concentration of Ni (38 wt%), and higher concentrations of MO (50 wt%) and Cr (7 wt%). Given the SEM analysis and the reported content of tested alloys, this sample is probably ORNL #17638.

Corrosion penetration into the alloy, shown in Figure 24, was visible at one location in the sample cross section examined. That area included a deep, narrow pit 200-300 μm wide extending 800 μm into the sample and a smaller adjacent site 200 by 300 pm that appeared to be the fringe of another pit. Both followed a corrosion conduit path parallel with the bright high-MO-content streaks noted above. Figure 25 shows the upper end of the exposed pit at 1500× magnification. The figure reveals dark boundaries of Al (58 wt%), 0 (39 wt%), and Ni (2 wt%) surrounding lighter patches of Cr (73 wt%), 0 (23 wt%), and Ni (3 wt%). The composition of the alloy interspersed among and adjacent to the corrosion products resembles the virgin metal except for the absence of Al, At this depth, oxidation of the alloy constituents appears to be the only corrosion source. The metal constituents have separated into two metal oxide complexes.

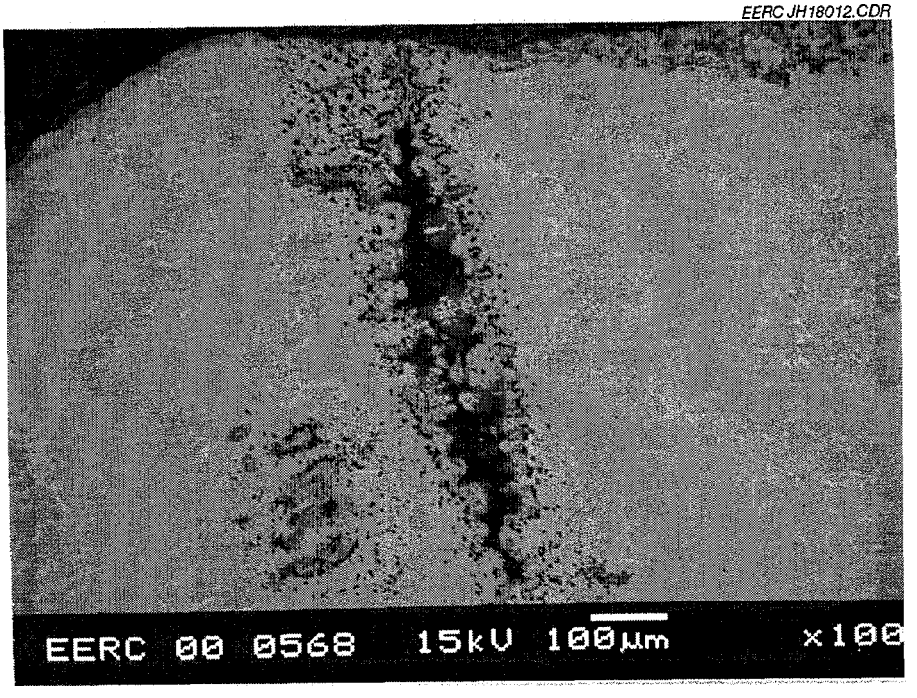


Figure 24. Virgin material, corrosion pit, and surface corrosion at 100× magnification (ORNL #17682).

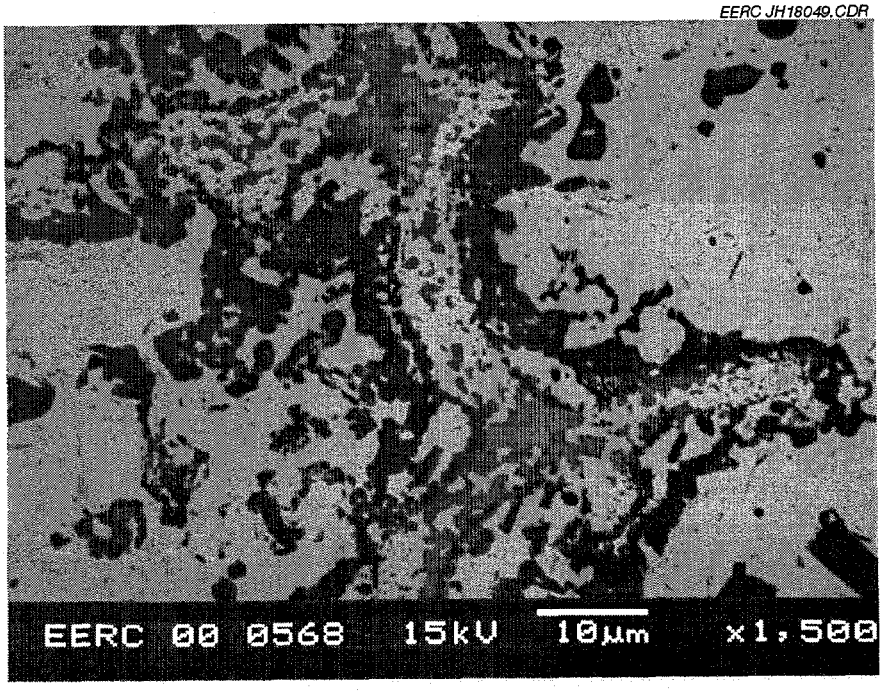


Figure 25. Outer end of exposed pit in Figure 24 at 1500× magnification (ORNL #17682).

The absence of Mo from the corrosion pit suggests that Mo may have been liberated from the alloy during the corrosion process.

In addition to the pit, the sample surface exhibited extensive smooth oxidation. The corrosion product covers the entire surface of the sample except around the center opening where the sample rested on a 9.5-mm-diameter 3 16 stainless steel rod. It varies in thickness from 20 to >750 μm. Figure 26 is a representative example of the corrosion product at its thickest point at 100× magnification. It is a broad, heterogeneous region containing areas of high Ni, Cr, and Mo content and oxidized areas of Al and Cr. Figure 27 illustrates the heterogeneity at 1500× magnification. The thickness of the corrosion product described below was 550 μm.

Corrosion products near the metal interface included Ni-rich, Cr-rich, and alloy-O-rich pockets. The Ni pockets containing 89-98 wt% Ni, <3 wt% Mo, <2 wt% Al, <5 wt% Cr, <3 wt% 0, and trace Ti are present from near the metal interface to within 70 μm of the surface in the region shown in Figure 26. Chromium-rich pockets containing 66 wt% Cr, 22 wt% 0, 5 wt% Al and Ni, and 2 wt% Mo occur simultaneously within about 120 μm of the metal interface. The oxidized pockets contained 34-44 wt% Cr, 26 wt% O, 13–27 wt% Al, 9-18 wt% Ni, and <2 wt% Mo and occurred within about 280 μm of the metal interface.

The constituents of the outermost layer of corrosion product include pockets of oxidized Ni, high Mo content, and a new proportion of metals and 0 in addition to the high Ni content described above. These combinations are found from about 150 μm from the surface outward. The oxidized Ni (80 wt% Ni, 14 wt% 0) pockets also contained 2 wt% Cr, <5 wt% Mo, and trace amounts (<0.3 wt%) of the ash constituents Si, S, Cl, P, K, and Ca.

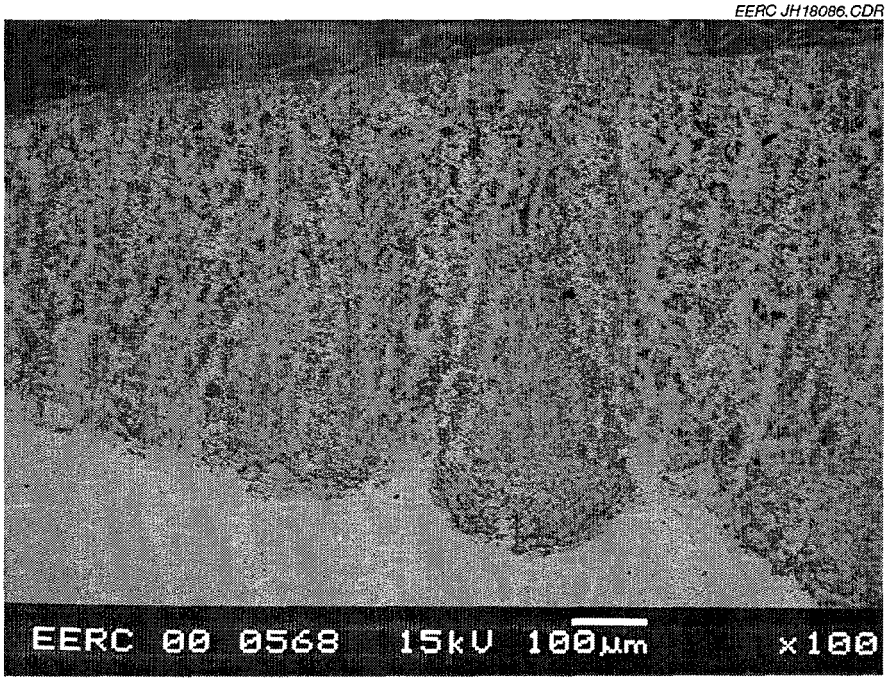


Figure 26. Corrosion product at thickest point at 100× magnification (ORNL #17682).

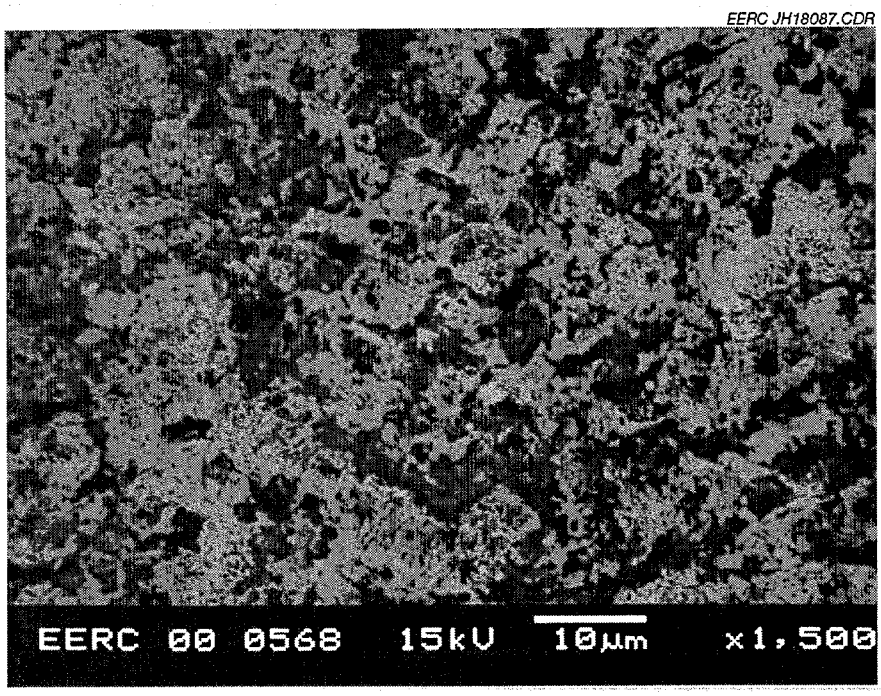


Figure 27. Corrosion product heterogeneity at 1500× magnification (ORNL #17682).

Mo-rich pockets contained 41-54 wt% MO, 25-37 wt% Ni, 17 wt% O, 0.8–7 wt% Cr, <2 wt% Al, and l-2 wt% S. The oxidized metal amalgams in this region contain more Ni (37 wt%) and less Cr (10–17 wt%), with similar amounts of Al (23 wt%), 0 (20-26 wt%), and MO (<3 wt%).

The main addition to metal alloy constituents in the corrosion sites was 0, indicating oxidation of the metal elements as the chief cause of corrosion. No sulfidation or halide attack was indicated. The absence of quantities of ash constituents present in the corrosion product indicates that the ash was not a factor in the alloy degradation.

### *NMARL Sample 00-0564 Submitted by Vinod Sikka, ORNL #1 7433*

**Sample description: 3** 1.5 $mm^2$ x 13-mm alloy cuboid with 13-mm-diameter hole in the center of larger surface; stainless steel-colored.

**Postexposure appearance:** The large mass of ash deposited on the sample separated easily from the sample. The surface is dull gray and covered with patches of ash particles. The sample initially appeared to have weathered the test well. However, as the ash was removed from the sample, a large mass on one side of the sample was uncovered.

SEM Morphology

The metal is reported to contain 44.25 wt% Fe; 3 1 wt% Ni; 20 wt% Cr; 2.0 wt% Mn; 1.5 wt% Mo; 0.40 wt% V; 0.25 wt% Ti, Nb, and Si; 0.09 wt% C; and 0.005 wt% B. Figure 28 shows a representative example of the cross-sectioned virgin material, corrosion product, and ash deposit at 100× magnification. It reveals a homogeneous field of alloy, the largest corrosive intrusion into the sample, and some smaller pits. SEM analysis of the bulk material indicated 82-85 wt% Fe, 1 l-15 wt% Al, and l-2 wt% Cr. This content more closely matches an aluminum-poor version of the reported content of ORNL #17682.

The sample underwent corrosion exhibited by both pitting and smooth recession of the surface. Figure 28, a portion of the sample cross section at 100× magnification, shows the largest deep pit in the sample, extending 2000 μm into the metal alloy, as well as the shallow pitting and smooth recession representative of the rest of the sample surface. Depth of shallow pitting and smooth recession were 50-350 and <20 μm, respectively. Figure 29 shows a typical pit at 1500× magnification. Chemistry at the alloy-corrosion product interface of pits and recession areas was constant. Constituents included 78-83 wt% Al, 3-l 1 wt% Fe, 4-9 wt% 0, 1–6 wt% S, <2 wt% Cr and Cl, and 1 wt% Si, suggesting the formation of an Al-O skin, oxidation and sulfidation attack, and loss of Fe from the sample.

The corrosion product contains areas with element proportions similar to those at the alloy interface as well as areas higher in Fe (20-25 wt% Fe, 63 wt% Al, 3-5 wt% Cr, 4 wt% 0, and 2-3 wt% Si). At 67-83 wt%, Al remains the dominant element at the sample's surface, likely

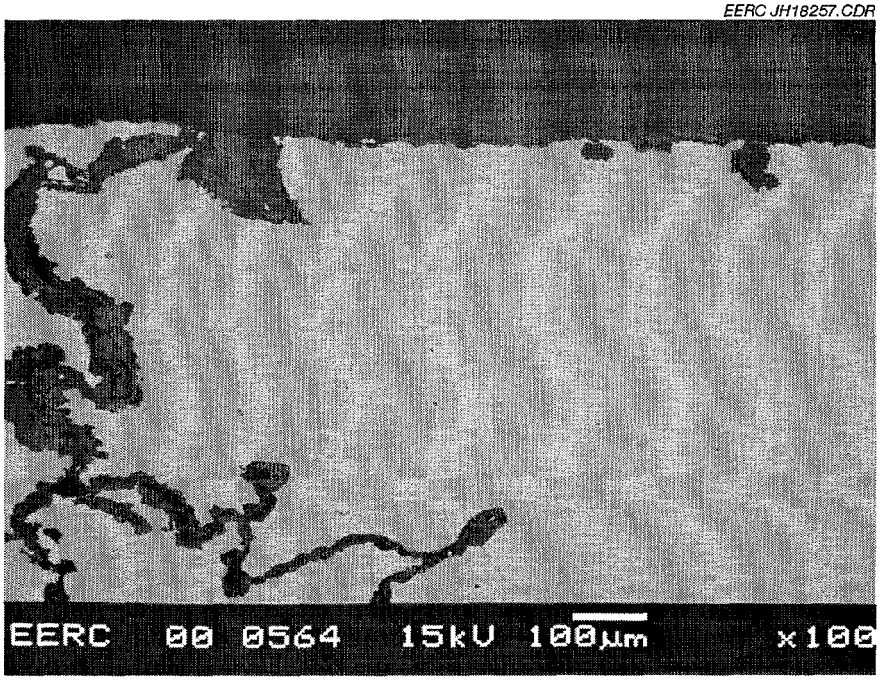


Figure 28. Cross-sectioned virgin material, corrosion product, and ash deposit at 100× magnification (ORNL #17433).

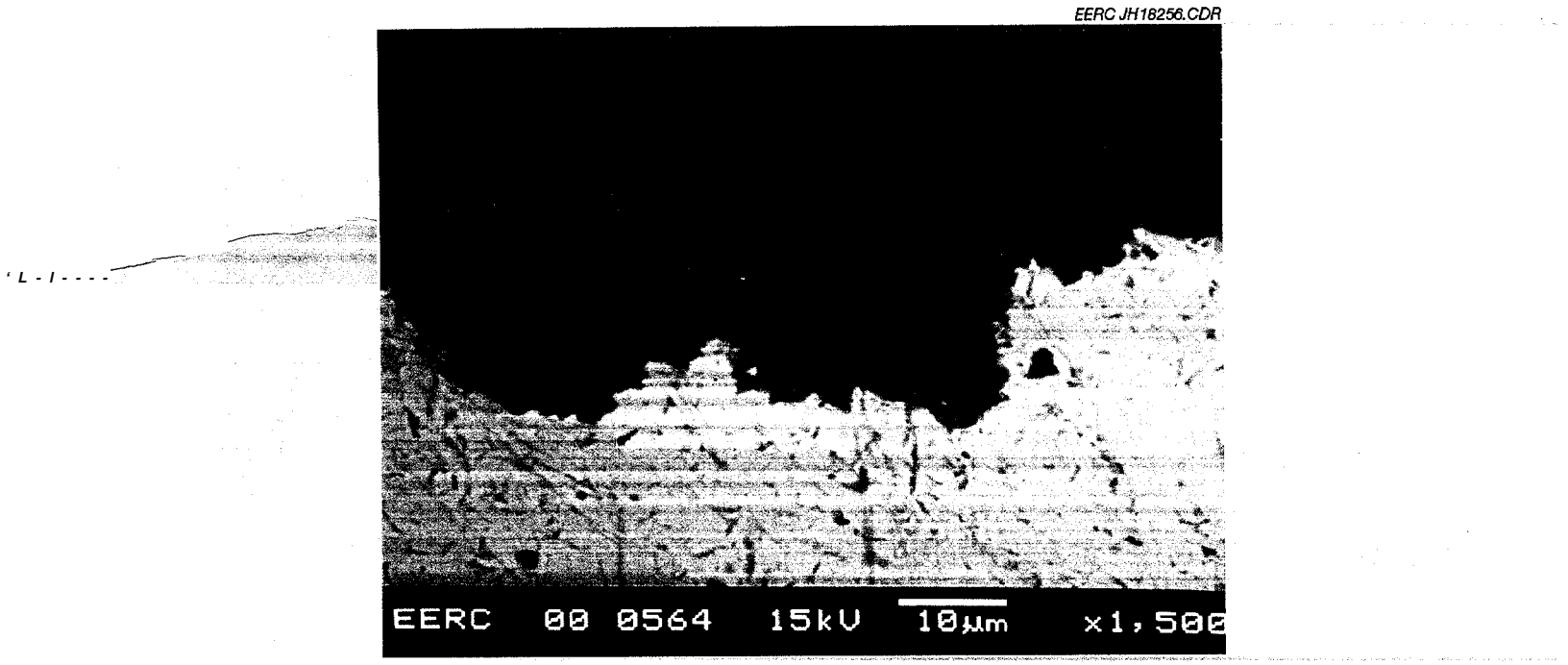


Figure 29. Typical pit at 1500× magnification (ORNL #17433).

having formed a partially oxidized layer with the 1 l-20 wt% 0 present. Minor constituents at the sample surface include 2-7 wt% Fe, l-2 wt% Cl, and 2 wt% S and Si.

As noted in the physical description above, a large mass formed on the sample during the 200-hour exposure to flue gas. The mass, as shown in Figure 30, is a mirror image cross section of what was analyzed. It formed over one edge of the sample (13.5 mm wide) and along one side of the sample (16 mm long) toward the center hole. Depth of the mass ranged from 6.5 mm at the edge to 8.2 mm around the corner to 4.9 mm along the side, tapering to the thickness of the smooth recession (20 µm). Figure 3 1 shows the alloy-corrosion product interface at 100× magnification. Constituents in this region included pockets of Fe (99 wt%, white streaks on the figure); pockets of 52-60 wt% Fe, 22-29 wt% Al, 13 wt% 0 with 2 wt% Mn, and l-4 wt% Cr; and pockets of 90 wt% Fe and 8 wt% 0. Much of the corrosion product in this mass resembled Figure 32, a porous region of 49-94 wt% Fe, O-33 wt% Al, and 4-12 wt% 0 3400 µm thick. The very dark spots and cracks in this figure are open areas of the sample filled with mounting epoxy. The layered structure in Figure 33 occurred 1500 µm from the surface. The light bands contained 76-86 wt% Fe; 4-9 wt% Al; 6-l 1 wt% 0; and <1 wt% Ca, Cl, and Cr. Darker areas contained 46-54 wt% Al, 2-25 wt% O, 17–26 wt% Fe, 2-3 wt% Cr, and l-2 wt% Cl. Figure 34 overlaps Figure 33 and depicts the structure at the surface of the corrosion mass. No change in concentration ratios of constituents was observed in this. region.

The main addition to metal alloy constituents in the corrosion sites was 0, indicating oxidation of the metal elements as the chief cause of corrosion. Minor sulfidation and halide attack likely occurred near the alloy-corrosion product interface given the small amounts of S

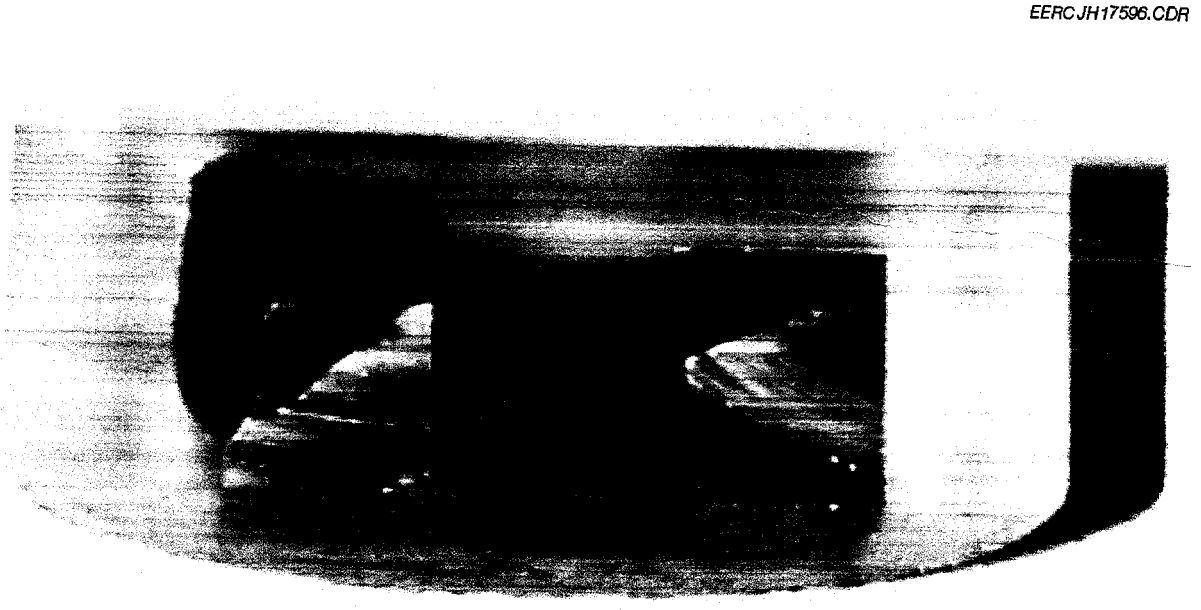


Figure 30. Corrosion product mass on cross-sectioned sample (ORNL #17433).

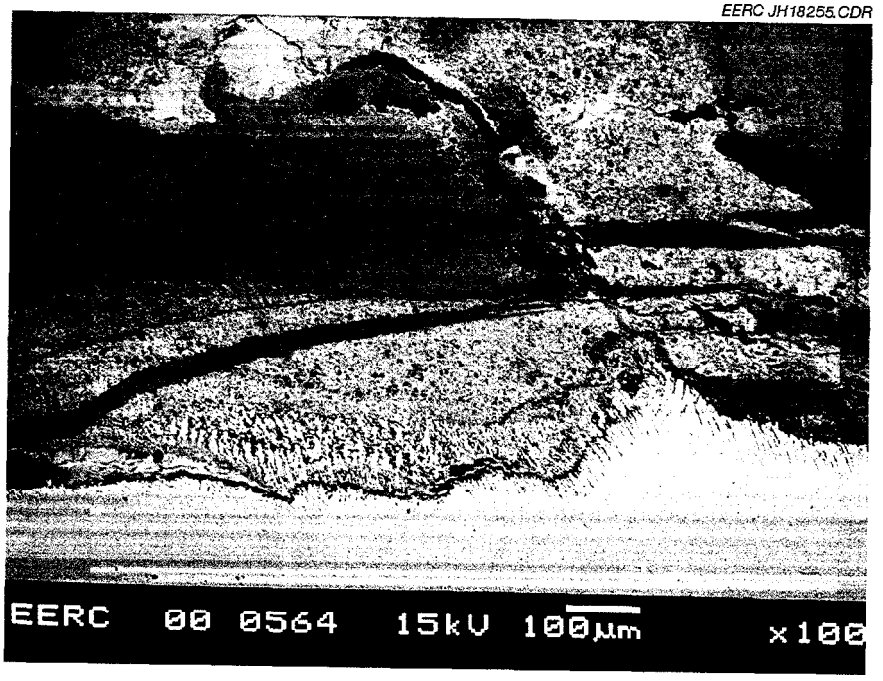


Figure 3 1. Alloy--corrosion product interface at 100× magnification (ORNL #17433).

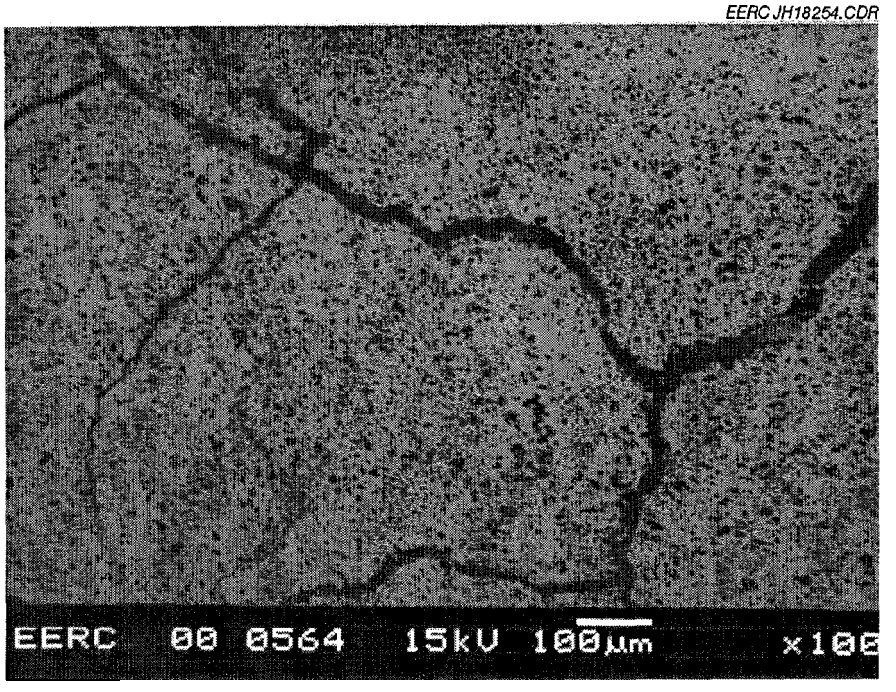


Figure 32. Porous region of corrosion product mass (ORNL #17433).

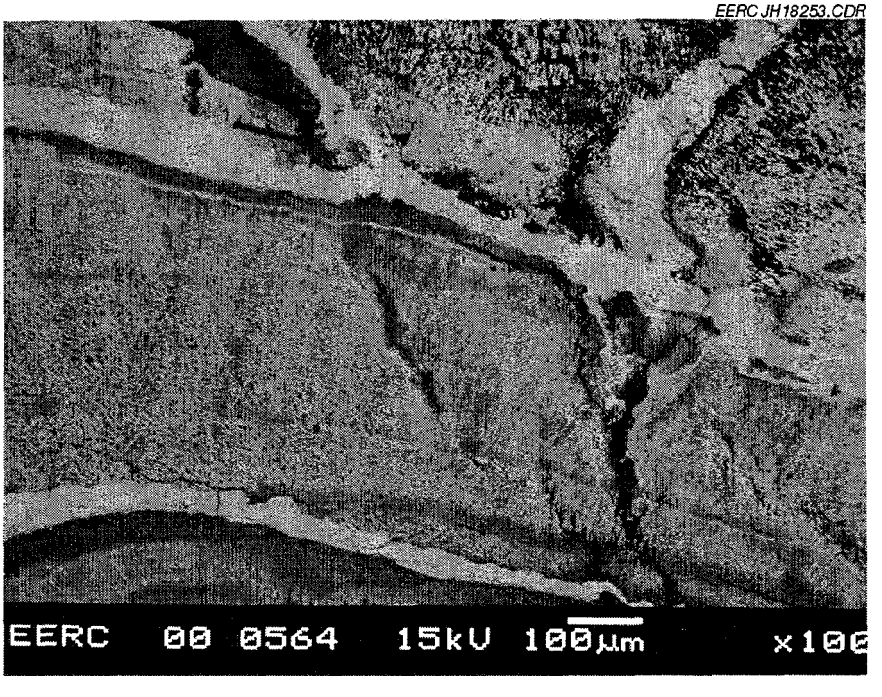


Figure 33. Stratified region of corrosion product mass (ORNL #17433).

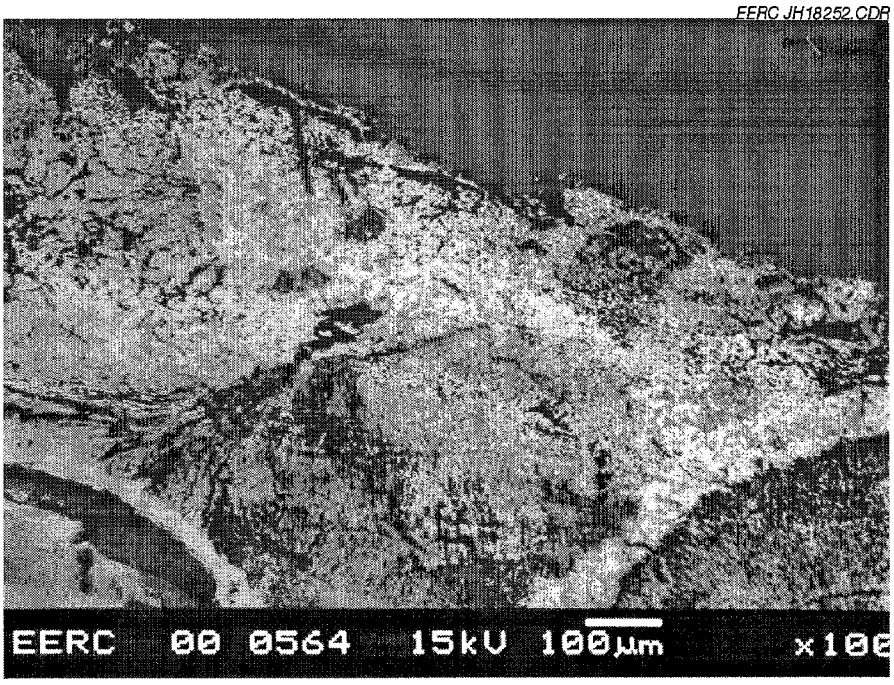


Figure 34. Corrosion product mass at the surface-ash interface (ORNL #17433).

(2-6 wt%) and Cl (<3 wt%) present in these areas. The absence of ash constituents present in the corrosion product indicates that the ash was not a significant factor in alloy degradation.

The sample surface has no attached ash since the ash deposited on the sample was removed prior to analysis.

## RESULTS AND DISCUSSION OF THE JUNE 2000 TEST

### Samples Exposed in the June Test

Additional samples to be installed in the SFS and TRDU were received prior to the June test run. ORNL personnel sent 19 metal alloy samples and 12 ceramic rings. Fourteen duplicate samples of metal alloys were approximately 32 mm square and 1 to 3.4 mm thick. An exposure temperature below 700°C in the SFS was requested for these samples. Five additional alloy coupons contained Cr, Ta, and MO. These included a 9-mm-diameter rod 152 mm long, and four identical cylinders 24 mm in diameter and approximately 12.5 to 12.8 mm high. The 12 ceramic rings were approximately 59 to 63.5 mm in diameter and 15 to 3 1 mm long, with a wall thickness ranging from 8 to 13.5 mm. All samples were described as mullite, gelcast. Four were thinner-walled white rings, and eight were thick-walled gray rings.

Personnel from SMC sent six alloy samples for inclusion in the June test. They included duplicate sample disks 48 mm in diameter and 5.5 to 9 mm thick and two duplicate samples

approximately 46 to 50.5 mm square. The metal content of these samples has not been disclosed. One of each pair of SMC samples was installed in the TRDU. All alloy samples, except for the rod, included a 12-mm-diameter hole for mounting.

The 19 metal alloys from ORNL, three alloys from SMC, and 12 ceramic samples were installed in the SFS for the June test, along with several samples exposed during the SFS operation in March. Fourteen duplicate ORNL samples were installed in an elbow between process air heaters and the first set of shell-and-tube heat exchangers. Figure 35 shows the sample rack as it was lowered into position in the SFS. The Cr/Ta alloy rod was partially embedded in the refractory just downstream of the slag screen to be exposed to slag, ash, flue gases, and temperatures in excess of 1510°C. Figure 36 shows the installed Cr/Ta rod. The other four Cr/Ta alloy coupons, all 12 ceramic rings, and the ceramic rings and two alloys previously exposed in the SFS but not analyzed were installed on the three-tiered Iconite rack in the convective pass of the SFS 330 mm beyond the CAH. Figure 37 indicates the upstream appearance of the samples in position prior to the system being sealed for the June test.

### June Test Conditions

Once the gradual heating of the system on natural gas was accomplished, the samples were exposed during an initial 14 hours of combustion conditions while firing an eastern Kentucky bituminous coal. The high ash fusion temperature of this coal forced the EERC to add limestone to the coal feed to reduce the viscosity of the ash depositing in the slag screen. However, this measure was not sufficient to prevent an operation shutdown after the initial 14 hours of operation because of plugging of the slag screen. The remains of the Cr/Ta alloy rod were

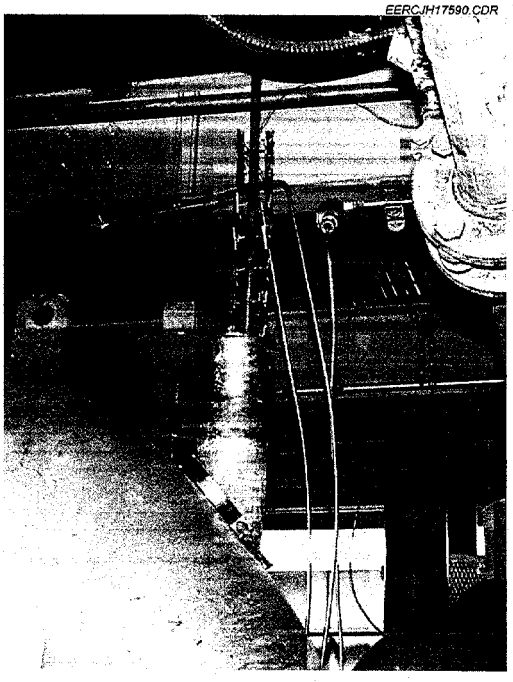


Figure 35. Sample rack being lowered into the SFS.

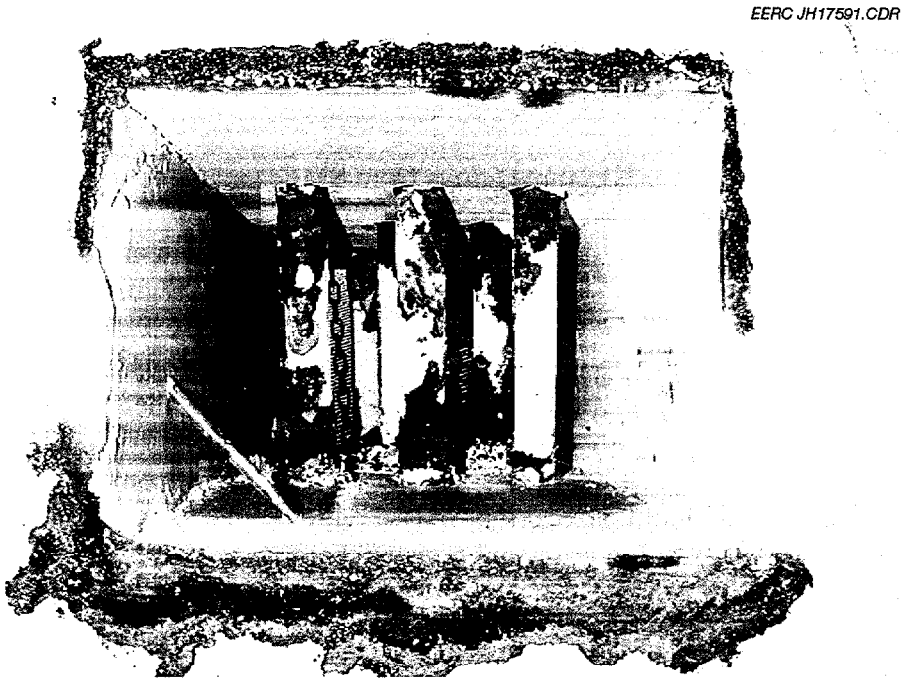


Figure 36. The installed ORNL Cr/Ta rod.

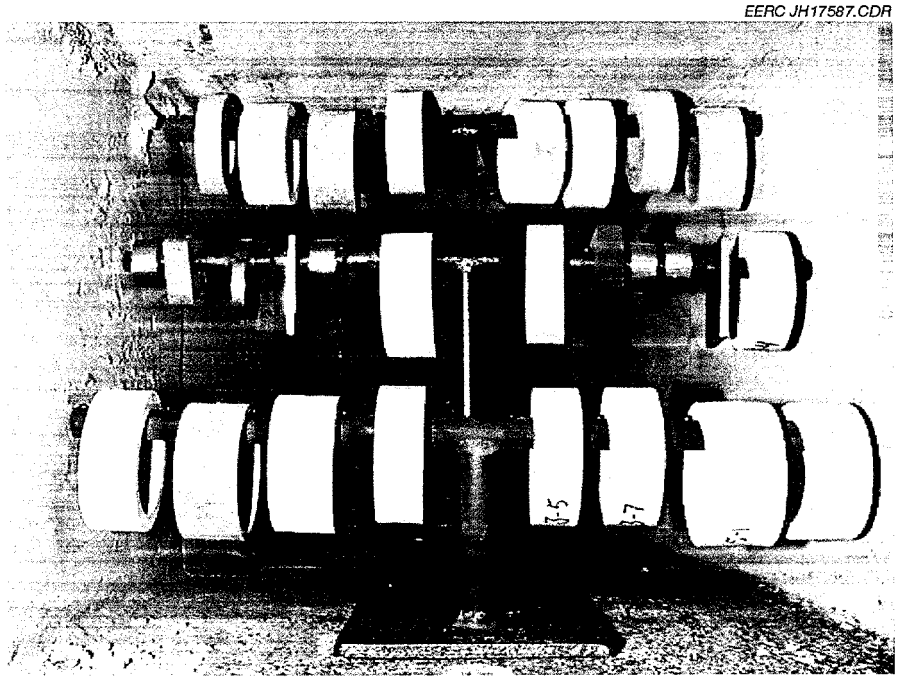


Figure 37. Upstream appearance of samples before the June test.

removed during maintenance of the slag screen area after the initial 14 hours of operation. The rod had succumbed to the intense temperature and corrosive effects of the slag and flue gas to which it was exposed. One of the three pieces of sample recovered during maintenance of the slag screen was embedded in epoxy and analyzed by SEM. The results of this analysis follow this section. The remaining ceramic and alloy samples were exposed to an additional 150 hours of combustion conditions while firing another eastern Kentucky bituminous coal from the Prater Creek Mine that had a lower ash fusion temperature.

The Prater Creek coal contained 1.7 wt% moisture, 5.1 wt% ash, and 0.94 wt% sulfur. The heating value was 31,459 kJ/kg on an as-fired basis. These data are similar to the eastern Kentucky bituminous coals previously fired. Coal ash was analyzed for ash fusion properties under oxidizing conditions. Results indicate a softening temperature of 1372 °C and a fluid temperature of 1411 °C. The fluid temperature of the Prater Creek coal ash was slightly lower than values observed for previously fired eastern Kentucky bituminous coals successfully fired and comparable to the high end of the temperature range observed for the Illinois No. 6 fuel previously fired.

The average flue gas flow rate through the slag screen and convective pass/elbow during the first 14 hours of coal firing was 685 and 948 scfm, respectively. The composition of the gas (on a dry basis) near the slag screen was 143 ppm SO,, 458 ppm NO,, 59 ppm CO, 3.1% 0,, and 14% CO,, with $N_2$ as the remainder. The composition at the baghouse exit was 374 ppm SO,, 575 ppm NO,, 59 ppm CO, 4.5% 0,, and 12.9% CO,, with $N_2$ as the remainder. The flue gas to which the coupons were exposed had a composition between these two points of analysis at 950°C. A profile of the flue gas temperature at three thermocouples (TCs) located near the sample positions is shown in Figure 38. The vertical lines at 33 and 47 hours indicate the initiation and termination of coal feed during the initial 14 hours of coal firing. TC SS Out was located near the position of the Cr/Ta rod. The temperature range in this region was 1420°–1540°C; average temperature was 15 10°C. Measurements during subsequent runs indicate that temperature variation across the duct is no more than 2°C. TC 409 was located just downstream of the CAH pass sample rack during the run. The temperature ranged from about 910” to about 960°C; average temperature was 950°C. TC 502 was located near the samples at the elbow between process air heaters and the first set of shell-and-tube heat exchangers. The temperature ranged from about 660” to about 710°C; average temperature was 690°C. The figure indicates a large temperature drop at TC SS Out resulting from the transition from gas to coal feed. Refractory temperatures reach equilibrium approximately 40 hours into the run, with the result that flue gas temperatures level out as well.

Once the system was repaired after the initial 14 hours of coal firing, the test run resumed for 150 hours of coal firing using the Prater Creek eastern Kentucky bituminous coal. The average flue gas flow rate through the convective pass and elbow during this portion of the test was 948 scfm. The composition of the gas (on a dry basis) at the baghouse exit was 336 ppm SO,, 504 ppm NO,, 19 ppm CO, 5.4% $O_2$, and 12.6% CO,, with $N_2$ as the remainder. A profile of the flue gas temperature at the two TCs located near the sample positions is shown in Figure 39. The vertical lines at 30 and 180 hours indicate the initiation and termination of coal feed. The temperature at TC 409 ranged from about 870” to about 995°C; average temperature was 930°C.

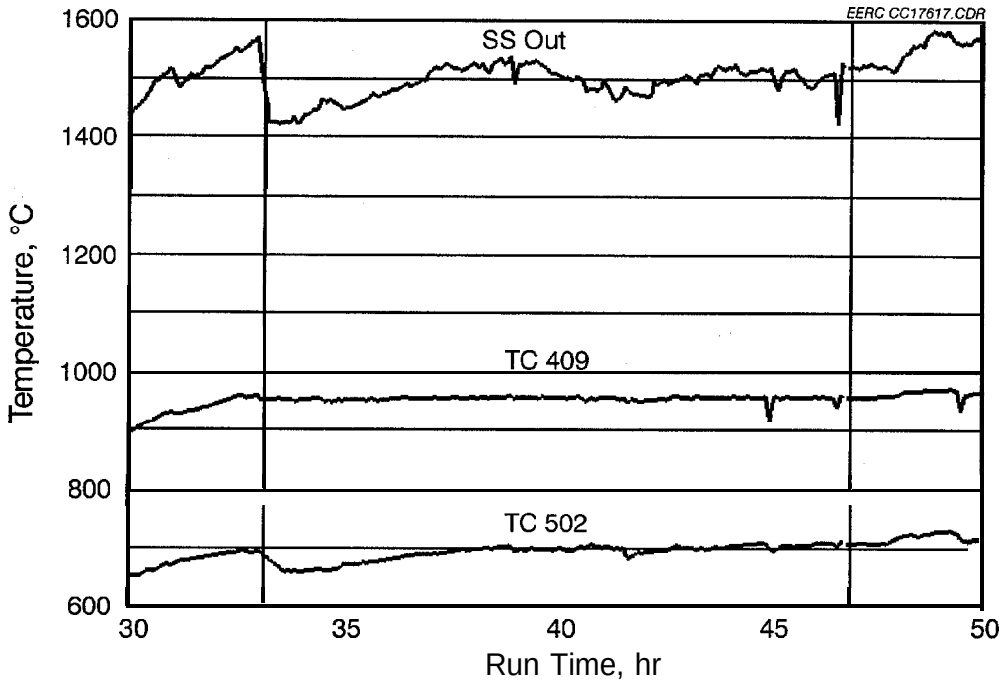


Figure 38. Flue gas temperatures near three sample positions.

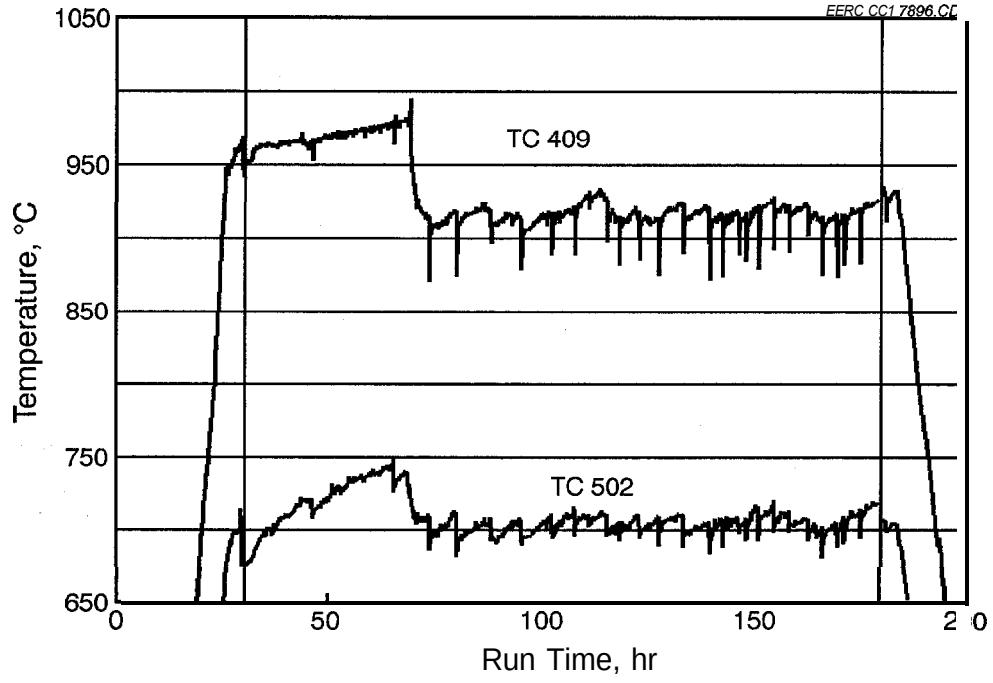


Figure 39. Profile of temperatures near two sample positions.

TC 502 was located near the samples at the elbow between process air heaters and the first set of shell-and-tube heat exchangers. The temperature ranged from about 676” to about 750°C; average temperature was 708 °C. The gradual temperature increase exhibited between commencement of coal feed and Hour 69 was caused by a decrease in quench flow rate caused by the gradual degradation of the TC upstream of the CAH tubes. That TC is used to control the amount of cold flue gas entering the quench zone. Operators replaced that degraded TC 69 hours into the run. They also switched the introduction rate of downstream gas entering the quench zone from temperature control to flow control. As a result, temperature levels cycled periodically with the cleaning of the quench zone.

The CAH pass samples were examined and photographed in place after the test run was completed. Figure 40 shows the extent of the sintered ash deposit on the upstream surfaces of samples at the end of the test. In addition, ash filled the open areas in the center of each ceramic ring. Downstream deposition on the samples is shown in Figure 41. Ash deposit weights were lower than those deposited during the March test with the Powder River Basin coal.

The composition of the ash deposits formed on the coupons is given in Table 3 along with the analyses of the coal ashes that were used for the initial and final portions of the tests.

As Table 3 indicates, both of the Kentucky coals contained much higher levels of Si and Al and much less Ca than the Cordero Rojo coal fired in March. Also, the first Kentucky coal fired contained the highest levels of Si and Al and very low levels of Fe or basic elements, explaining the very high viscosity of the slag. In contrast, the second Kentucky coal that was fired for most of the time contains much more Fe, which decreases the viscosity of the slag. A comparison of

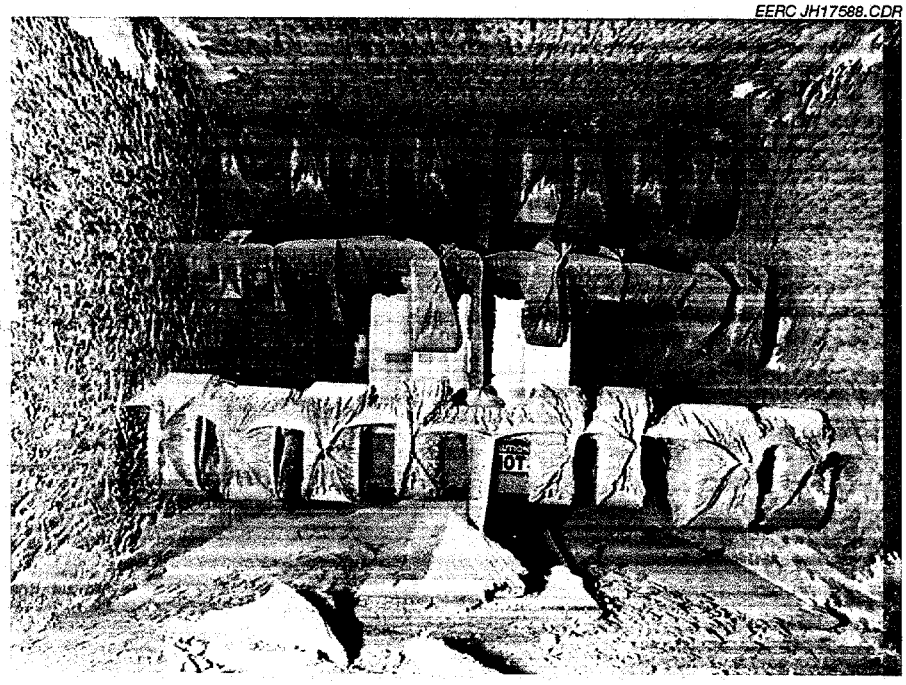


Figure 40. Upstream surfaces after the June test.

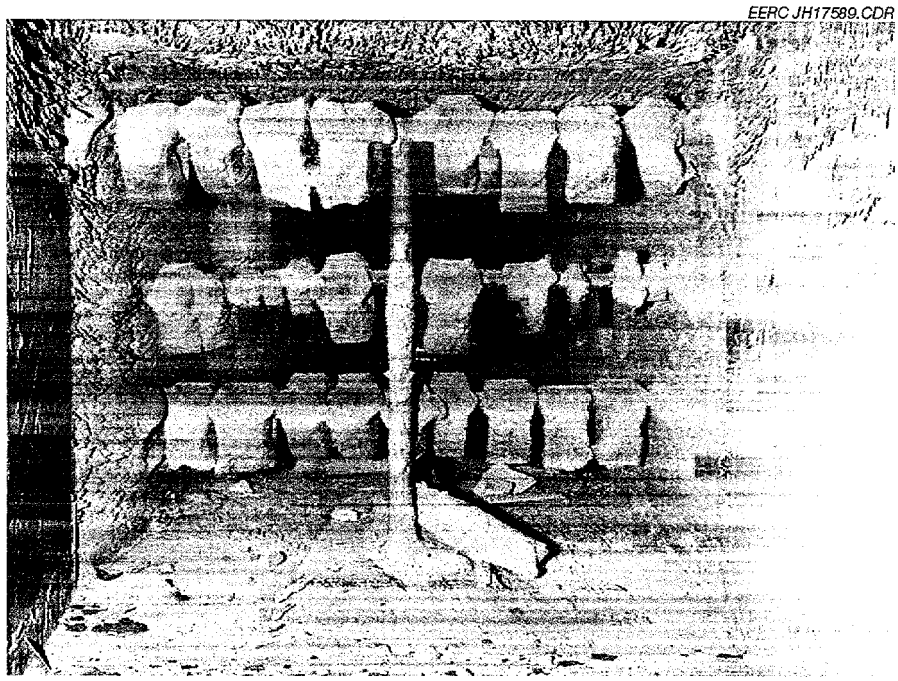


Figure 41. Downstream deposition.

the coal ashes and the inner and outer layers of the ash-fouling deposits that formed on the coupons shows that the inner layer, next to the materials, had a composition very similar to that of the first coal ash, except for much higher levels of calcium due to the limestone addition that was used to help the slag flow. SEM analyses of the inner ash deposit showed that the calcium had reacted with the aluminosilicate ash particles to form particles with an anorthitelike composition. If so, then the calcium should be locked in a relatively unreactive form and should not significantly attack the oxide coatings on alumina-forming alloys or alumina-rich ceramics at these temperatures.

The outer layer of the deposits, which was away from the materials, had an ash composition much closer to that of the second coal fired. SEM analyses showed that only 3% of the outer ash deposit was composed of iron oxide particles. The great bulk of the material was composed of Fe-rich aluminosilicate particles which again are relatively unreactive to alumina coatings.

After the combustion test, the sample rack was carefully removed from the SFS. The coupons in the CAH pass were separated from each other and the rack, maintaining as much ash on the samples as possible. Each sample was examined and photographed, with care being taken not to dissociate the ash from the coupon. Visual inspection of the rings revealed no changes because of the exposure. Some rings underwent SEM analysis to determine corrosion and erosion effects not visible to the eye. The remainder of the samples will be returned to the submitter or cleaned and reinstalled in the SFS for further high-temperature exposure during a future test.

TABLE 3

Composition of the Initial and Final Kentucky Coal Ashes and the Convective Pass Deposits (normalized sulfur-free oxide basis)

| Oxides, wt % | Initial Kentucky Coal | Final Kentucky Coal | Inner Ash Deposit | Outer Ash Deposit |
|---|---|---|---|---|
| $SiO_2$ | 56.5 | 40.2 | 49.7 | 36.4 |
| $Al_2O_3$ | 32.6 | 25.9 | 26.7 | 23.9 |
| $Fe_2O_3$ | 4.4 | 23.9 | 5.2 | 24.0 |
| $TiO_2$ | 1.9 | 1.0 | 2.1 | 1.7 |
| $P_2O_5$ | 0.1 | 0.2 | 0.2 | 0.3 |
| CaO | 0.8 | 3.9 | 11.6 | 9.0 |
| MgO | 1.3 | 2.1 | 1.3 | 1.2 |
| $Na_2O$ | 0.3 | 0.4 | 0.6 | 0.6 |
| $K_2O$ | 2.0 | 2.3 | 2.6 | 2.8 |
| $SO_3$[1] | 0.2 | 4.8 | 0.5 | 0.4 |

[1] Normalized with other oxides.

In contrast to the ceramic rings, all metal coupons installed in the CAH pass exhibited effects of surface corrosion. Visual inspection showed discoloration of all metal sample surfaces. SEM analyses of these samples is described in the following section of this report.

The alloy coupons installed in the elbow between process air heaters and the first set of shell-and-tube heat exchangers were coated with a very light layer of ash on both the upstream and downstream sides. Figure 42 shows the samples after they were removed from the SFS. Visual inspection indicates that all samples probably underwent surface corrosion. Half of the samples were analyzed by SEM.

### SEM Analyses of Coupons Exposed During the June 2000 Test

SEM analysis of the coupons prior to exposure was not performed.

#### *NMARL Sample 00-0669 Submitted by Mike Brady, ORNL CrTa Rod*

**Sample description:** Shiny, gray alloy rod 156 mm long, 9 mm diameter, weighing 92.745 g. Figure 36 shows the sample embedded in the refractory materialdownstream of the slag screen in the SFS.

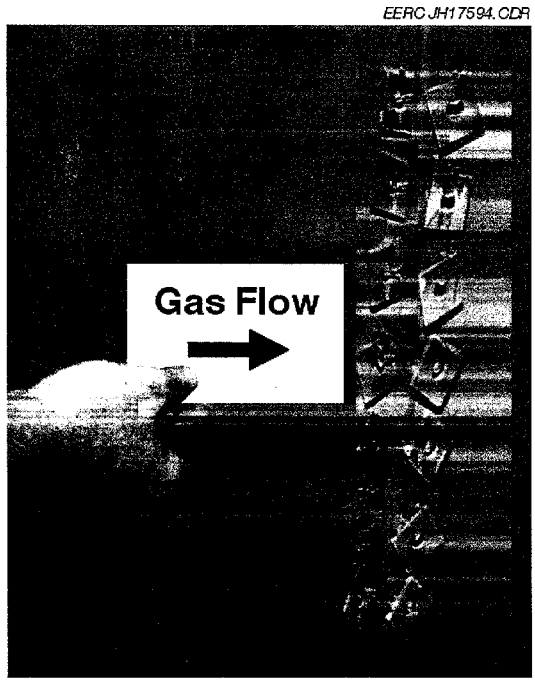


Figure 42. Samples after removal from the SFS.

**Postexposure appearance:** Approximately 70% of the sample was retrieved from the SFS in three sections. They were blackened and brittle. Figure 43 shows the sample removed from the quench zone after 14 hours of flue gas exposure at the start of the June 2000 test run. The mean lengths of the three pieces were approximately 21 mm, 32 mm, and 60 mm. The ensemble weighed 33.35 g.

SEM Morphology

The sample was reported to contain 83 wt% Cr, 16 wt% Ta, 5 wt% MO, 0.8 wt% Si, 0.2 wt% La, and 0.05 wt% Ti. Figure 44 shows a representative example of the sample remains after exposure at 100× magnification. It reveals a heterogeneous mass-a field of medium gray with light and dark portions in sample cross-section surface. SEM analysis of the sample revealed no evidence of virgin alloy material remaining after exposure. Analysis of the medium gray material indicated a high level of Cr with some 0 and Al and small amounts of Ta, Fe, and Si. This was common to all areas examined regardless of proximity to the sample surface. The lightest regions were high in Ta (54-57 wt%), with Si, Cr, and 0 and trace amounts (<2 wt %) of Ti, Fe, and P. Dark regions contained either high levels of ash constituents with small amounts of Cr and Ta or nearly pure $SiO_2$. Black areas in the figure indicate voids filled with epoxy during sample preparation. The shading in SEM photographs is limited by the sensitivity of the backscatter detector. Therefore, regions of the same shade may contain different constituents or different concentrations of the same constituents. Table 4 summarizes the concentration ranges of multiple analyses by region shade.

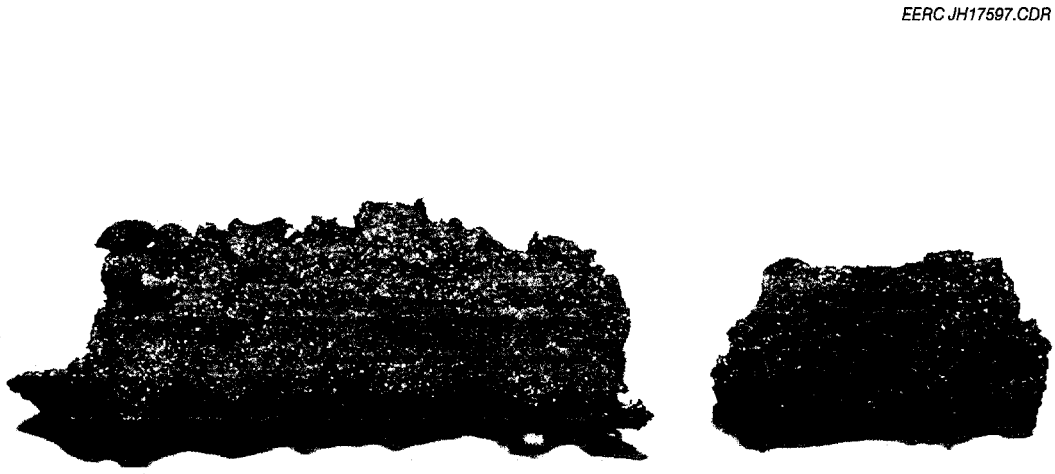


Figure 43. ORNL Ca-Ta alloy rod removed from the quench zone after 14 hours of flue gas exposure.

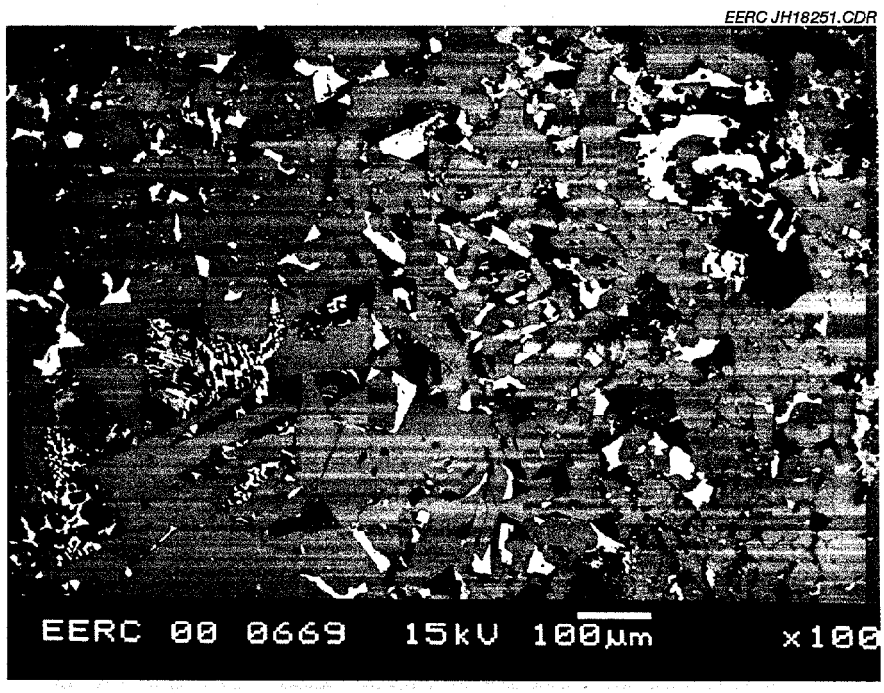


Figure 44. Representative example of sample remains after exposure at 100× magnification (ORNL Ca-Ta alloy rod).

TABLE 4

Elemental Content of Regions in Figure 44 by Shade

| Element, wt% | White | Light Gray | | Medium Gray | | Dark Gray | |
|---|---|---|---|---|---|---|---|
| Mg | – | – | – | – | – | <1 | – |
| Al | – | – | 0.6 | 1-3 | 14.5 | 11-14 | – |
| Si | 19-20 | – | – | c l | – | 34-36 | 58-62 |
| P | 0.4-0.6 | – | – | – | – | – | – |
| Ca | – | – | – | – | – | 11 | – |
| Fe | <1 | 82.6 | 14.2 | <1 | – | – | – |
| Ti | o-2 | – | – | – | – | – | – |
| 0 | 8-9 | – | 18 | 20 | 22 | 19-35 | 36-38 |
| Cr | 14-16 | 10.6 | 7.7 | 72-78 | 61 | 1-9 | <2 |
| MO | – | 3.8 | 57.4 | – | – | – | – |
| Ta | 54-57 | 2.2 | – | o.-5 | – | 2–4 | – |

The presence of heterogeneous combinations of metal alloy constituents and high levels of ash constituents (up to 61% Si, 8-38% 0, <15% Al, ~13% Ca) suggest corrosion by the coal slag.

### *NMARL Sample 01-0029 Submitted by Mike Brady, ORNL Sample A*

**Sample description:** Shiny, gray alloy ring 12.8 mm high by 24 mm diameter, with a wall thickness of 5.5-6.5 mm.

**Postexposure appearance:** Figure 45 shows the sample removed from the sample holder downstream of the CAH after the June test run. Flue gas flow across the sample was from left to right. The ash deposit broke off from the sample, leaving a fine coating of ash. What can be seen of the sample surface appears dull dark gray and brown, with indications of corrosion.

SEM Morphology

The sample was reported to contain 83 wt% Cr, 16 wt% Ta, 5 wt% MO, 0.8 wt% Si, 0.2 wt% La, and 0.05 wt% Ti. Figure 46 shows a representative example of the sample and ash deposit at 100× magnification. It reveals a heterogeneous sample mass of irregular shapes in shades ranging from light to dark gray covered with a thin discontinuous oxide layer and a light coating of ash particles. SEM analysis of the bulk alloy material sample indicated an overall composition of 52 wt% Cr, 28 wt% Ta, 11 wt% Si, 6 wt% MO, and 4 wt% 0. Figure 47 shows the alloy in greater contrast and detail at 500× magnification. Analysis of the larger white portions of the alloy indicate high Ta content (48 wt%), with some Cr (30 wt%), Si (16 wt%), MO (4 wt%), and 0 (1 wt%). The medium gray material contained high Cr (72 wt%), with MO (14 wt%), Ta (5 wt%), 0 (4 wt%), and Si (2 wt%). The shading in SEM photographs is limited


A

Figure 45. Sample removed from the sample holder after the June test run (ORNL Sample A).

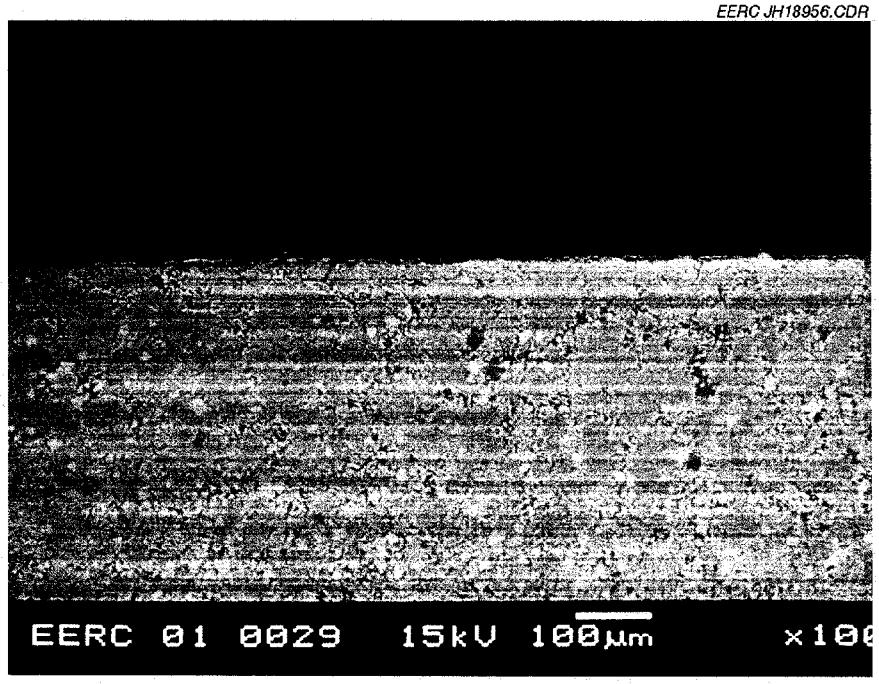


Figure 46. Example of material and deposited ash at 100× magnification (ORNL Sample A).

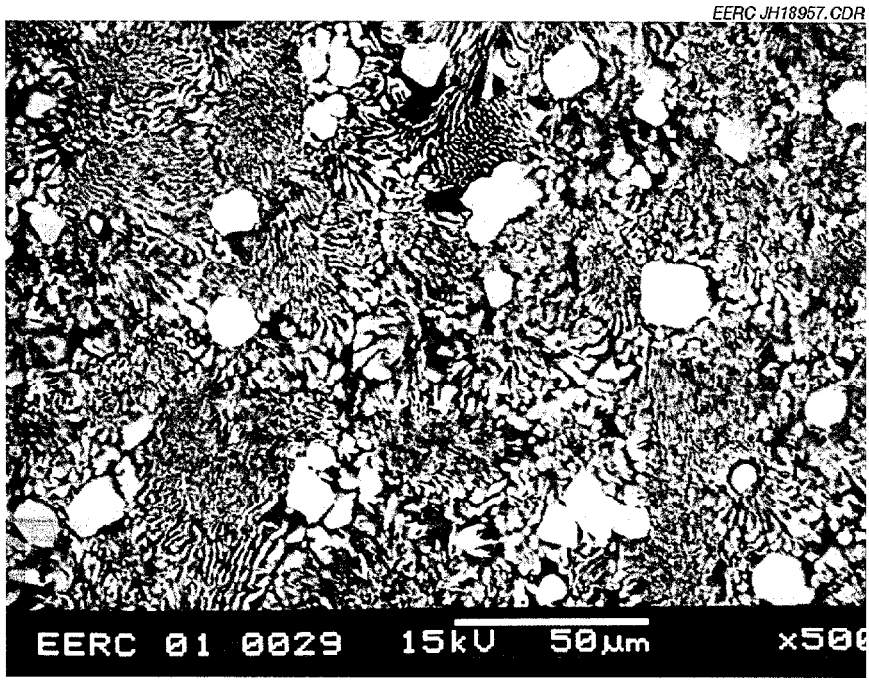


Figure 47. Example of material and deposited ash at 500× magnification (ORNL Sample A).

by the sensitivity of the backscatter detector. Therefore, regions of the same shade may contain different constituents or different concentrations of the same constituents.

No subsurface corrosion was observed in the sample cross section. No obvious pitting occurred at the sample surface. There is, however, a very distinctive discontinuous oxide layer across the sample surface that can be seen in the upper left corner of Figure 48. The oxide layer is composed of two sections: the inner layer which is nearly white and the outer layer which is dark gray and barely visible in the figure. The bright inner layer contains more Ta than Cr, with some Si, 0, and traces of Fe. The outer layer is Cr (64 wt%) and 0 (22 wt%), with some Si (8 wt%) and traces of flue gas constituents, Fe, Ca, Al, Cl, P, and Mg. At the corrosion layer-ash interface, Si (13-2 1 wt%) replaced some of the Cr (38-42 wt%) in the Cr-0 layer. There is also high Ca (12-20 wt%) and trace Al, **Fe,** and Mg. The oxide layer is about 14 µm at its thickest. No obvious erosion was observed.

The composition of the fine deposit of ash on the sample surface coincides with the ash deposit composition of other samples analyzed.

### *NMARL Sample 01-0023 Submitted by Mark Janney, ORNL #3-1*

**Sample description:** Pale gray mullite ring 19.5 mm high by 61 mm diameter, with a wall thickness of 13.5 mm.

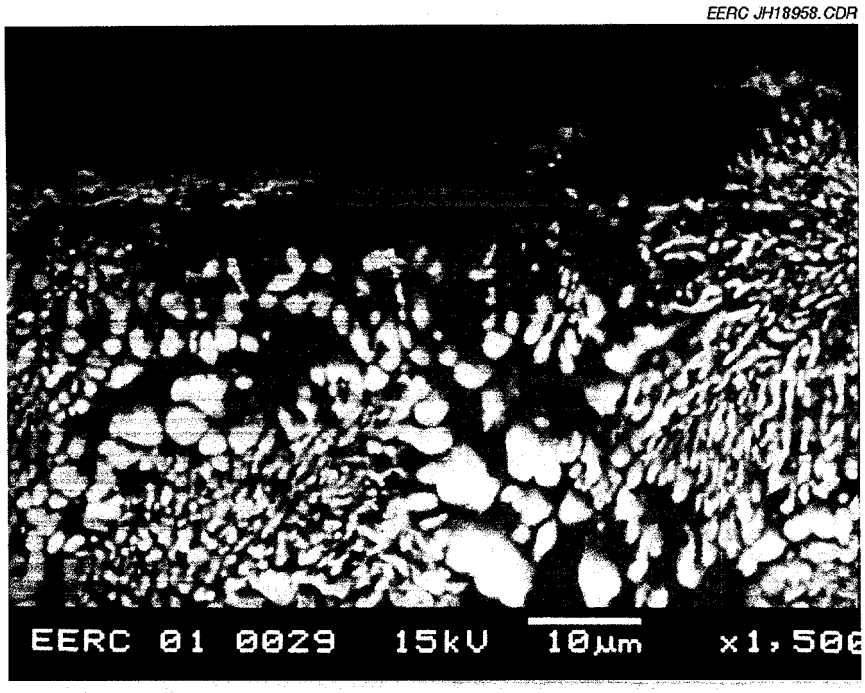


Figure 48. Sample at 1500x magnification (ORNL Sample A).

**Postexposure appearance:** Figure 49 shows the sample removed from the sample holder after the June test run. Flue gas flow across the sample was from left to right. The ash deposit obscures much of the sample surface. No degradation was observed visually. The bare leeward ring surface is brown, presumably from a light coating of ash particles. The cross-sectioned sample set in epoxy looks light gray. The upstream face of the cross-sectioned sample is well covered by an ash deposit up to 22 mm thick.

SEM Morphology

The sample was described as being composed of mullite. Figure 50 shows a representative example of the material and deposited ash at 100× magnification. SEM analysis of the bulk material indicated a composition of 48 wt% Al, 36 wt% 0, and 15 wt% Si. Inclusions in the bulk material seen as light gray streaks in the figure were present throughout the sample. Their average composition was 9.7 wt% Al, 37 wt% 0, and 43 wt% Si, with 7 wt% K, 2 wt% Ca, and trace amounts of P and Na. Because of their morphology and location, these inclusions are most likely an artifact of manufacturing rather than evidence of corrosive exposure from flue gas.

Ash penetration into the ring structure was minimal, but there was no gas flow through the material. No subsurface corrosion was observed in the sample cross section. Ash filled the voids between the mullite grains at the surface to a depth of less than 200 µm as observed in the figure. Some mullite-ash interaction was apparent at the surface of the ring. Figure 51 illustrates the typical appearance of surface corrosion, a discontinuous layer of material ranging from less than 1 µm to 7 µm thick at 1500× magnification. Constituents in the corrosion product include 0

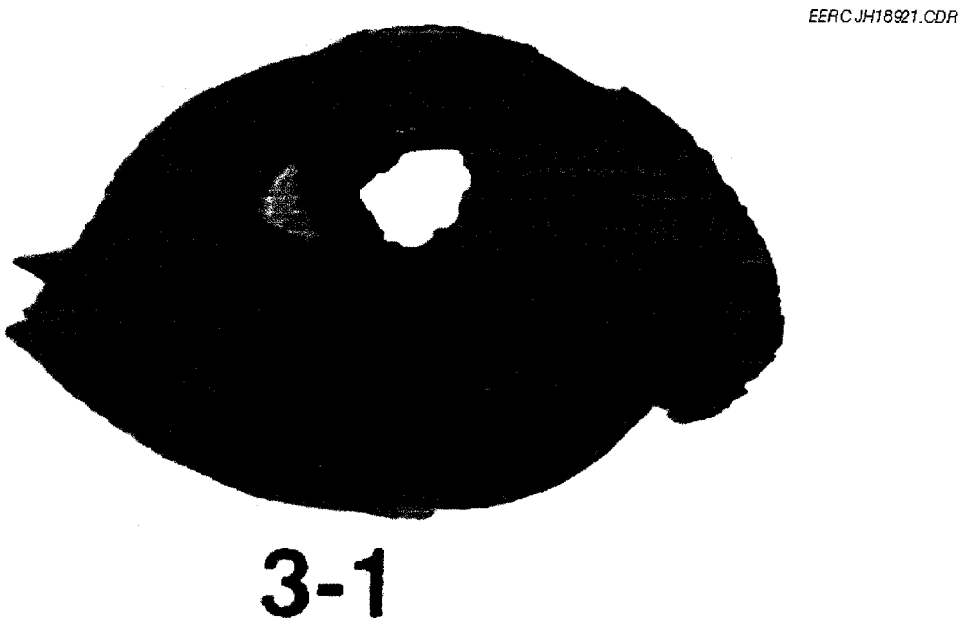


Figure 49. Sample removed from sample holder after the June test run (ORNL #3-1).

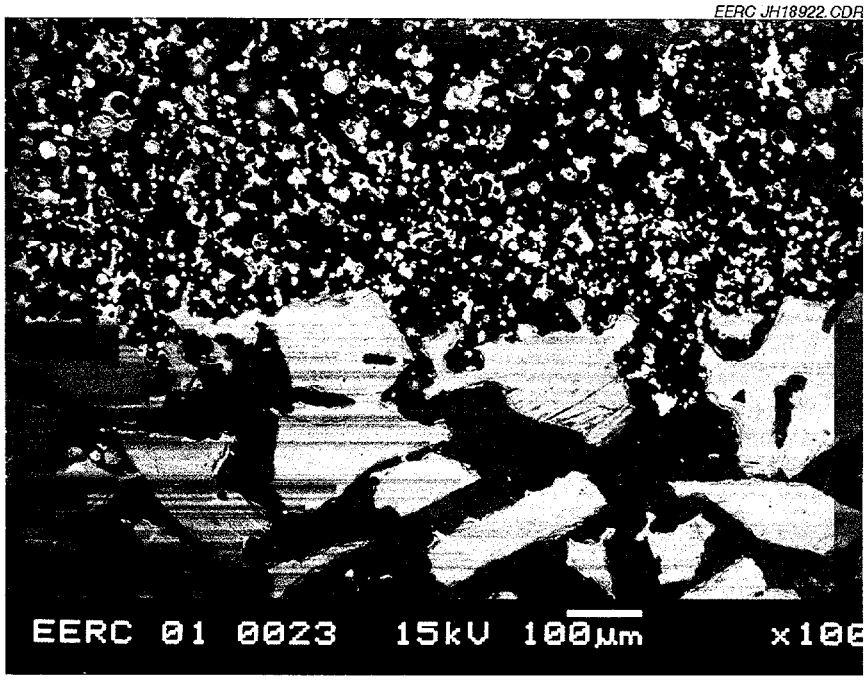


Figure 50. Example of material and deposited ash at 100× magnification (ORNL #3-1).

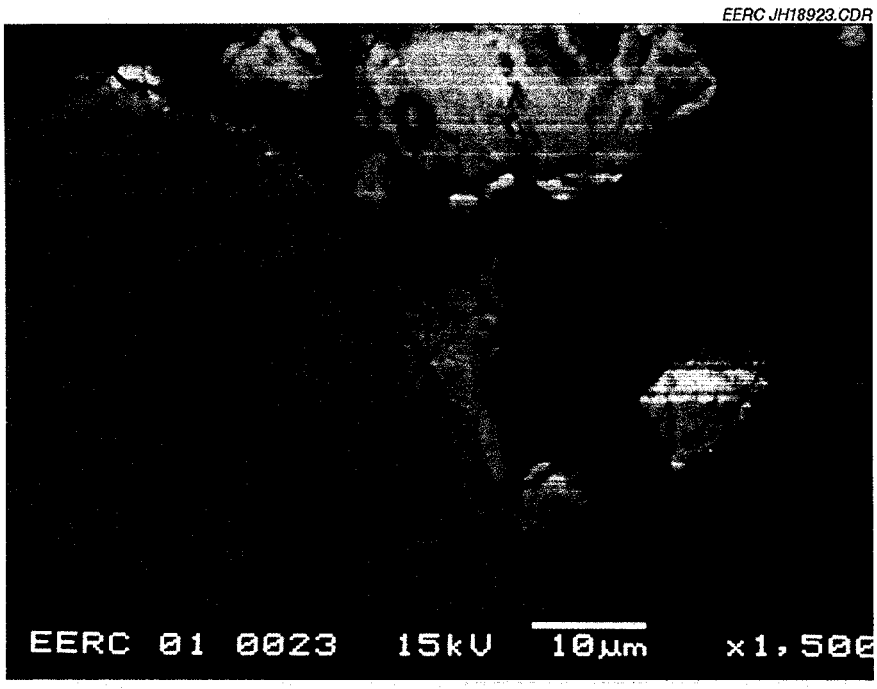


Figure 5 1. Typical appearance of surface corrosion at 1500× magnification (ORNL #3-1).

(28-35 wt%), Al (18-26 wt%), Si (1 l-25 wt%), Ca (12-21 wt%), Fe (3-l 1 wt%), P (2-8 wt%), Ti, Mg, and S (less than 3 wt% each). Occasional lumps of Ca-rich aluminosilicate ash particles fused with corrosion product are visible in both figures. These measure up to 30 µm in diameter. The SEM analysis indicates that Ca did not diffuse into the mullite. However, it is not clear whether the mullite diffused into the ash deposit because Al, Si, and 0 are constituents common to both.

Composition of the deposited ash layer was consistent between samples installed in the convective pass. The buff-colored ash next to the mullite surface is 17 wt% Al, 29 wt% Si, 37 wt% O, 4 wt% Ca, 3 wt% Fe, 2 wt% Ti, and 3 wt% S and K, with traces of Cr and Mg. This reflects the composition of the ash from the coal fired during the first 14 hours of the test. The outer and much thicker layer of dark rust-brown ash is 14 wt% Al, 23 wt% Si, 31 wt% O, 7 wt% Ca, 17 wt% Fe, 1 wt% Ti, 1 wt% Mg, and 2 wt% S and K. It reflects the composition of the ash from the coal during the last 186 hours of the test.

### *NMARL Sample 01-0024 Submitted by Mark Janney, ORNL #3-2*

**Sample description:** Pale gray mullite ring 17-17.5 mm high by 59.5 mm diameter, with a wall thickness of 13-13.5 mm.

**Postexposure appearance:** Figure 52 shows the sample removed from the sample holder after the June test run. Flue gas flow across the sample was from left to right. The ash deposit obscures much of the sample surface. No degradation was observed. The bare leeward ring

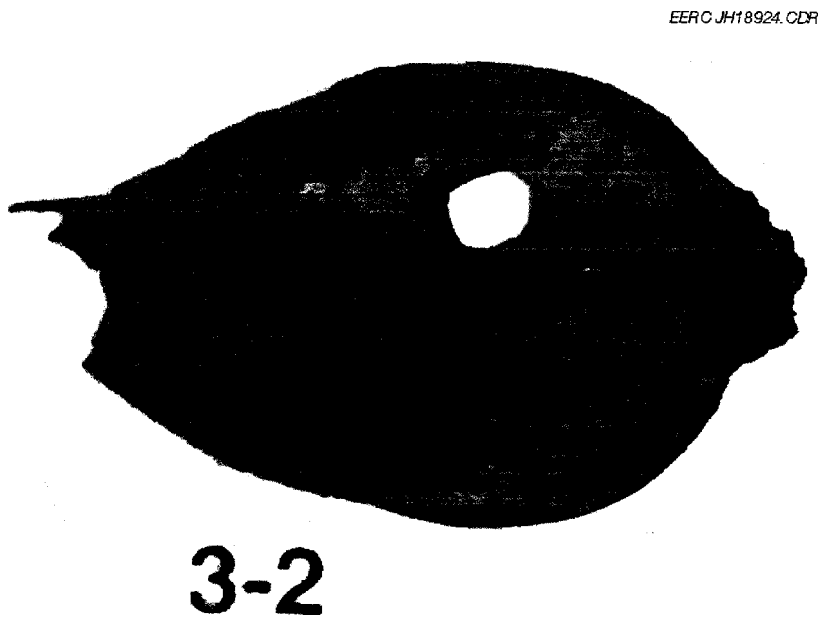


Figure 52. Sample removed from the sample holder after the June test run (ORNL #3-2).

surface is brown, presumably from contamination by ash particles. The cross-sectioned sample set in epoxy looks light gray. The upstream face of the cross-sectioned sample is well covered by an ash deposit ranging from 2 to 14 mm thick.

*SEM* Morphology

The sample was described as being composed of mullite. Figure 53 shows a representative example of the material and deposited ash at 100× magnification. It reveals a porous field of ceramic grains largely separated from a band of ash across the top of the figure. SEM analysis of the bulk material indicated a composition of 48 wt% Al, 38 wt% 0, and 14 wt% Si. The composition of inclusions in the grains-visible as light streaks-included 4-18 wt% P in place of some of the Al and 0 in the bulk material.

No subsurface corrosion was observed in the sample cross section. Ash filled the voids between the material at the surface to a depth of <215 μm. It did not penetrate or otherwise degrade the sample interior. The material-ash interaction appears limited to the surface, although there was no gas flow through the ring. Evidence of very minor surface corrosion was present as occasional patches at the sample-ash interface. Figure 54 shows at 1500× magnification an example area of corrosion 14 μm deep by 36 μm wide formed on a piece of ceramic aggregate to the right of the more porous aggregate piece at the far left of Figure 53. SEM analysis of the very light gray and white regions embedded in the perimeter of the light gray ceramic base material indicates a reduction in Al (15-28 wt%), an increase in Si (28-32 wt%), and inclusion of ash components Ca (6-10 wt%) and Fe, Na, Mg, P, Ti, and Ba at trace levels (<1 wt% each).

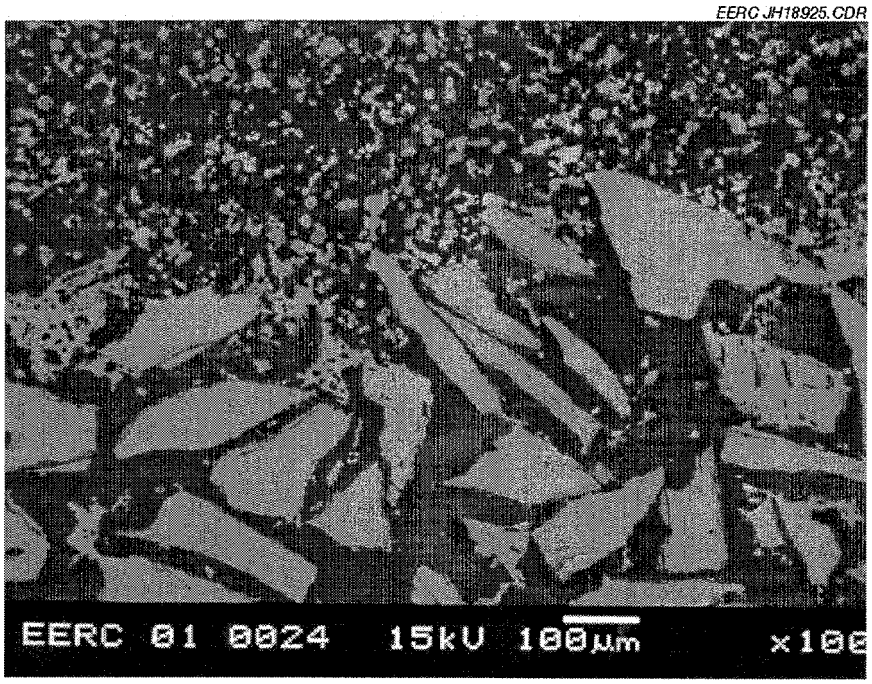


Figure 53. Example of material and deposited ash at 100× magnification (ORNL #3-2).

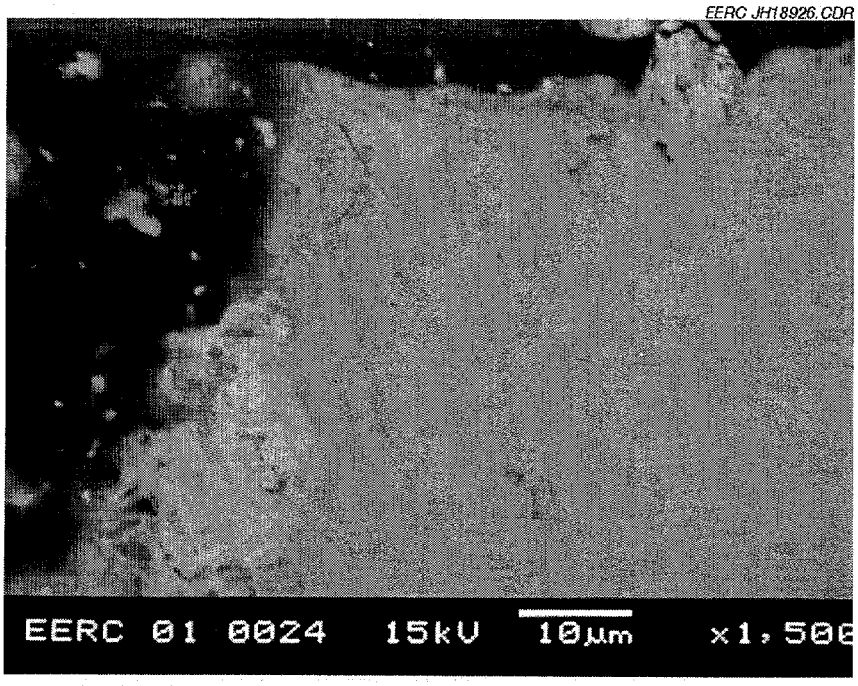


Figure 54. Typical appearance of surface corrosion at 1500× magnification (ORNL #3-2).

The ceramic material at the corners appeared to have more corrosion product present than the rest of the upstream surface of the sample. Figure 55 shows one corner at 100× magnification. The flue gas flow is from the top of the photo to the bottom. The figure shows corrosion on several grains, with thicknesses ranging from <5 μm to 22 μm. The corrosion product in these corner areas includes more Fe (up to 29 wt%) than the rest of the upstream surface, consistent with the Fe content of the ash deposited at the corners.

The change in fuel coal was evident in the deposition layers on this sample. The composition of the ash layer deposited across the width of the upstream face was consistent between samples installed in the convective pass. The dark reddish brown ash deposit was in direct contact with the ceramic material at the corners where the upstream face (cylinder wall) met the side face (top and bottom, doughnut-shaped surface of the cylinder).

### *NMARL Sample 01-0025 Submitted by Mark Janney, ORNL #3-3*

**Sample description:** Pale gray mullite ring 19-20 mm high by 60 mm diameter, with a wall thickness of 13-14 mm.

**Postexposure appearance:** Figure 56 shows the sample removed from the holder after the June test run. Flue gas flow across the sample was from left to right. Ash deposit obscures much of the sample surface. No sample degradation was visually observed. The bare leeward ring surface is brown, presumably from ash particles. The cross-sectioned sample set in epoxy looks light gray. The thickness of the ash deposit on the sample ranged from 2 to 18 mm.

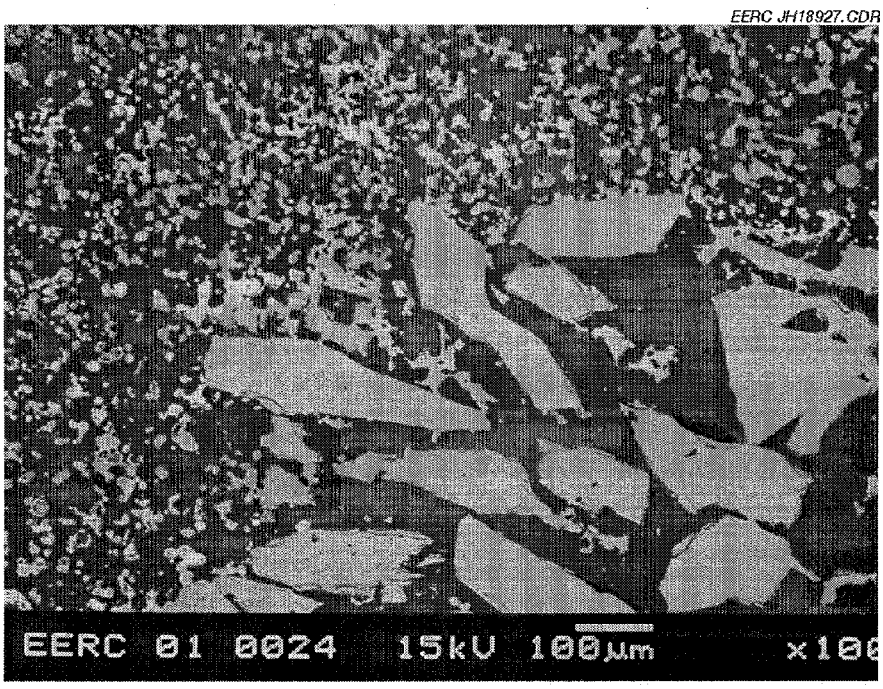


Figure 55. Typical appearance of surface corrosion at 100× magnification (ORNL #3-2).

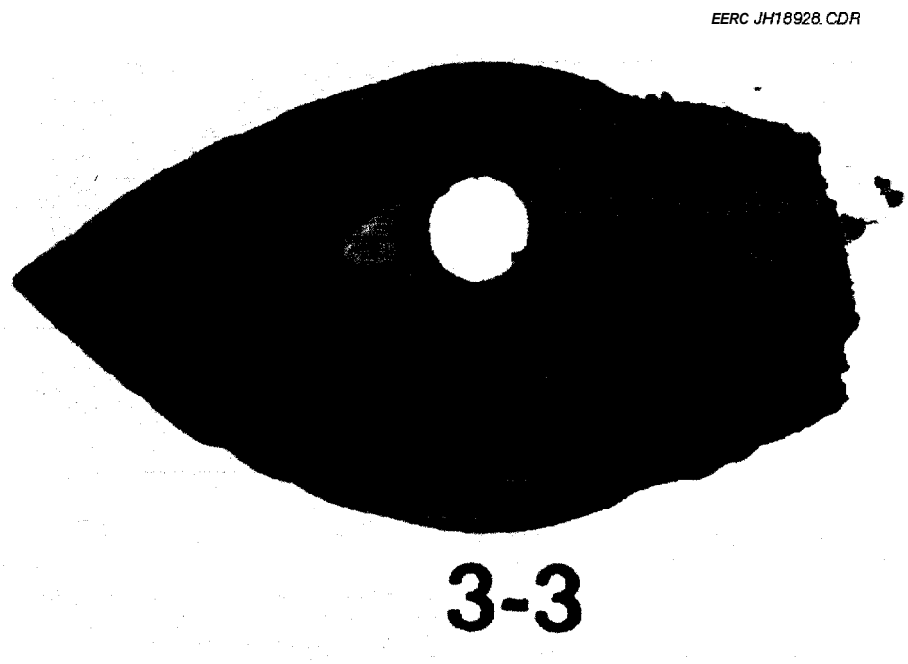


Figure 56. Sample removed from the sample holder after the June test run (ORNL #3-3).

*SEM* Morphology

The sample was described as being composed of mullite. The sample surface directly facing oncoming flue gas (upstream surface) was examined. Figure 57 shows a representative example of the material and deposited ash at 100× magnification. It reveals a porous field of ceramic grains largely separated from a band of ash across the top of the figure. SEM analysis of the bulk material indicated a composition of 47 wt% Al, 38 wt% 0, and 14 wt% Si. Inclusions in the grains seen as light gray streaks in the figure were present throughout the sample. Their composition was similar to the inclusions observed in Sample 01-0023 (ORNL#3-1). Because of their morphology and location, these inclusions are most likely artifacts of manufacturing rather than evidence of corrosion by the flue gas or ash.

No subsurface corrosion was observed in the sample cross section. Ash filled the voids between the material at the surface. Rare ash particles were observed at a depth of 260 μm; most filled pores to a depth of only 50-60 μm. The ash did not penetrate or otherwise degrade the sample interior, although there was no gas flow through the sample. The material-ash interface appears limited to the surface. Evidence of very minor corrosion was present as thin coatings or blobs of corrosion product at the sample-ash interface. Figure 58 shows at 1500× magnification a typical area of corrosion on the ceramic chunk to the right of center in Figure 57. SEM analysis of the center mass of corrosion product showed that darker gray areas were ceramic material with 2 wt% Ca incorporated, whereas light gray and white regions contained greater percentages of ash constituents Ca (16-35 wt%), Fe (2-8 wt%), Ti (3-5 wt%), and Na, Mg, P, S, and K at trace levels (<2 wt% each). This example, with dimensions of 43 μm by 28 μm, was the largest cross

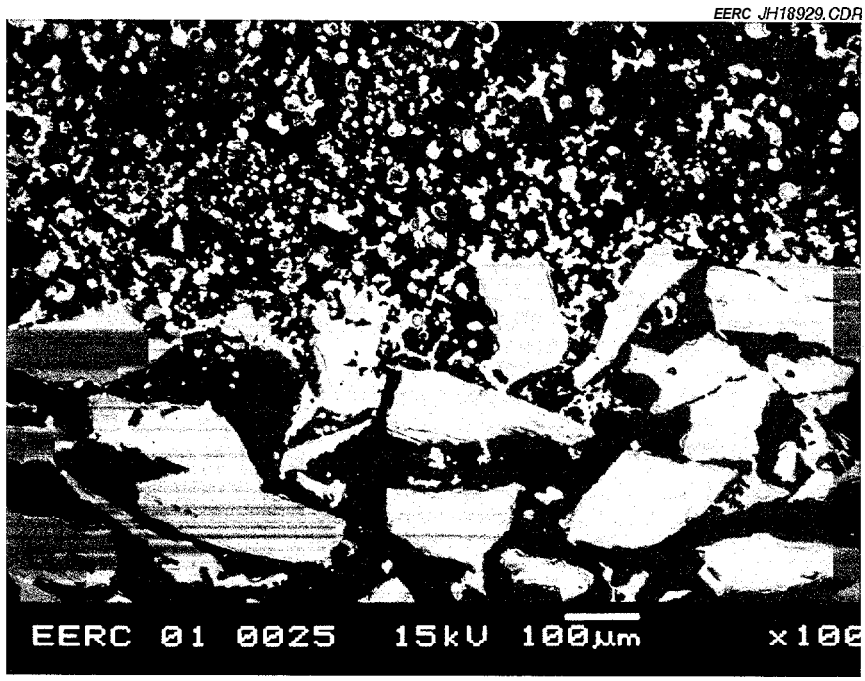


Figure 57. Example of material and deposited ash at 100× magnification (ORNL #3-3).

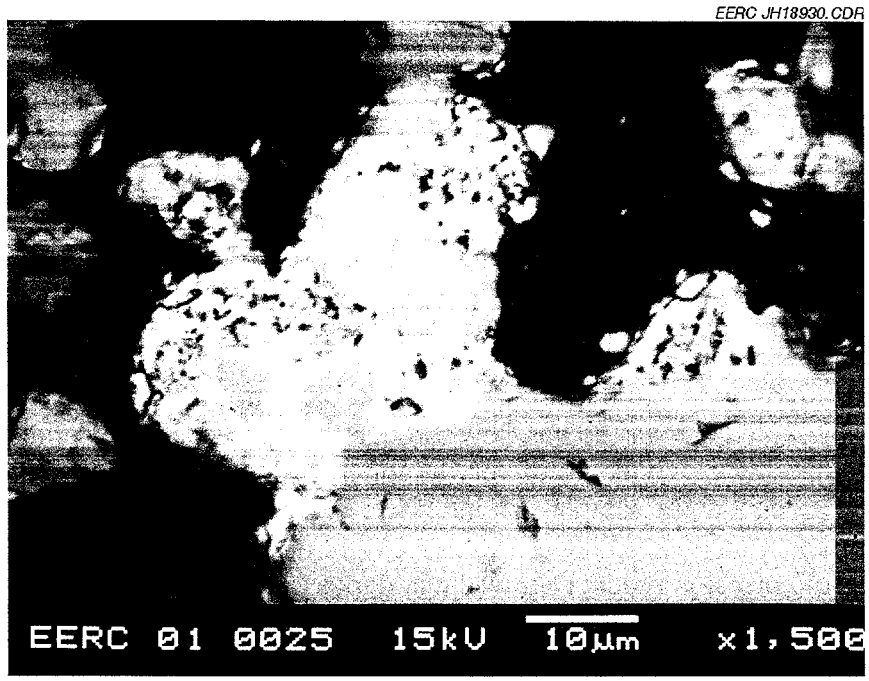


Figure 58. Typical appearance of surface corrosion at 1500× magnification (ORNL #3-3).

section of corrosion product observed for this sample. The texture of the corrosion product, whether in thin coatings or blobs attached to the surface, appears porous. The corrosion product at the corners of this sample was similar in content and frequency to the rest of the sample surface. The SEM analysis indicates that ash constituents did not diffuse into the mullite. However, it is not clear whether the mullite diffused into the ash deposit at the corrosion product interface because of the similarity in composition between the mullite and some constituents of the ash deposit and the irregularity of the ceramic-ash boundary.

As was true for all of the samples, the change in fuel coal was evident in the deposition layers on this sample. The composition of the inner ash layer deposited over all but the very corner of the upstream face was consistent with that of the ash deposits on other samples installed in the convective pass. The thickness of the ash deposit on the sample ranged from less than 1 mm to greater than 70 mm.

### *NMARL Sample 01-0026 Submitted by Mark Janney, ORNL #3-4*

**Sample description:** Pale gray mullite ring 19.5-20 mm high by 60.5 mm diameter, with a wall thickness of 13.5 mm.

**Postexposure appearance:** Figure 59 shows the sample removed from the sample holder after the June test run. Flue gas flow across the sample was from left to right. Ash deposit obscures much of the sample surface. No sample degradation was visually observed. The bare leeward ring surface is brown, presumably from contamination with ash particles. The

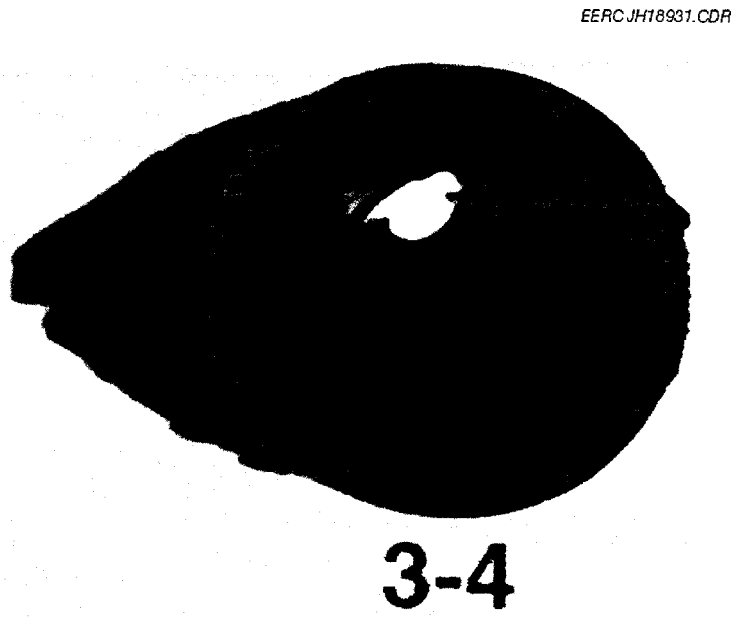


Figure 59. Sample removed from the sample holder after the June test run (ORNL #3-4).

cross-sectioned sample set in epoxy looks light gray. The depth of the ash deposit on the sample ranged from less than 1 to 23 mm.

*SEM* Morphology

The sample was described as being composed of mullite. The sample surface directly facing oncoming flue gas (upstream surface) was examined. Figure 60 shows a representative example of the material and deposited ash at 100× magnification, a porous field of ceramic grains largely separated from a band of ash across the top of the figure. SEM analysis of the bulk material indicated a composition of 48 wt% Al, 36 wt% 0, and 16 wt% Si. Inclusions in the grains seen as light gray streaks in the figure were present throughout the sample. Their average composition was 11 wt% Al, 36 wt% 0, and 40 wt% Si, with 9 wt% IS, 2 wt% Ca, and trace amounts of P and Na. As was true for the other mullite rings, because of their morphology, composition, and location, these inclusions are most likely artifacts of manufacturing rather than evidence of corrosive exposure from flue gas or ash.

No subsurface corrosion was observed in the sample cross section. Ash filled the voids between the grains at the surface. Ash particles were observed to a depth of 305 μm. The ash did not penetrate or otherwise degrade the sample interior, although there was no gas flow through the sample. The material-ash interface appears limited to the surface. Evidence of surface corrosion was present as thin coatings and blobs of corrosion product at the sample-ash interface. Figure 61 shows at 1500× magnification a typical area of corrosion on the right side of the ceramic grain to the right of center in Figure 60. SEM analysis at the ceramic material-corrosion product interface revealed an influx of Ca ranging from 3 to 25 wt%. A mean 4 wt% Fe and trace

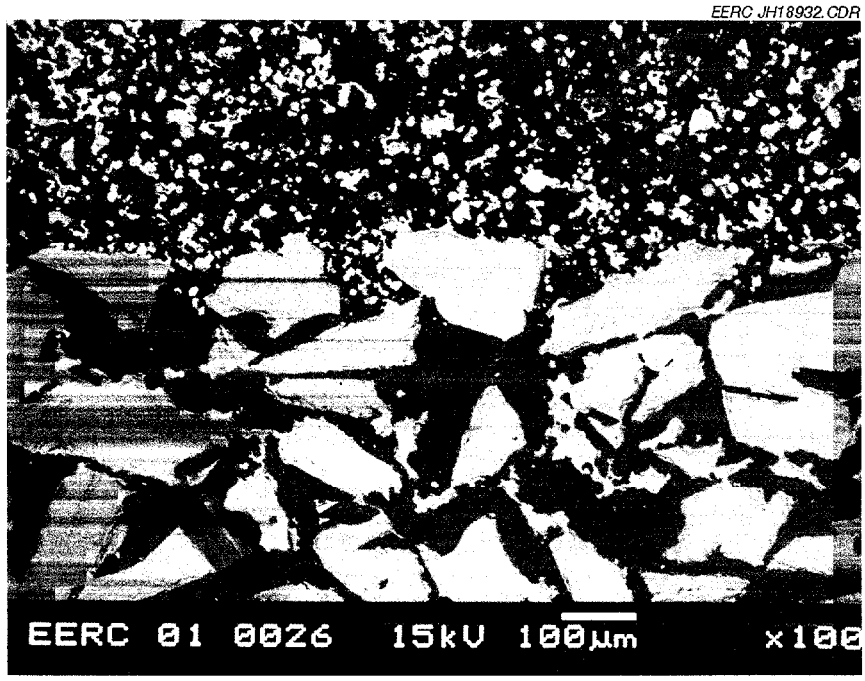


Figure 60. Example of material and deposited ash at 100× magnification (ORNL #3-4).

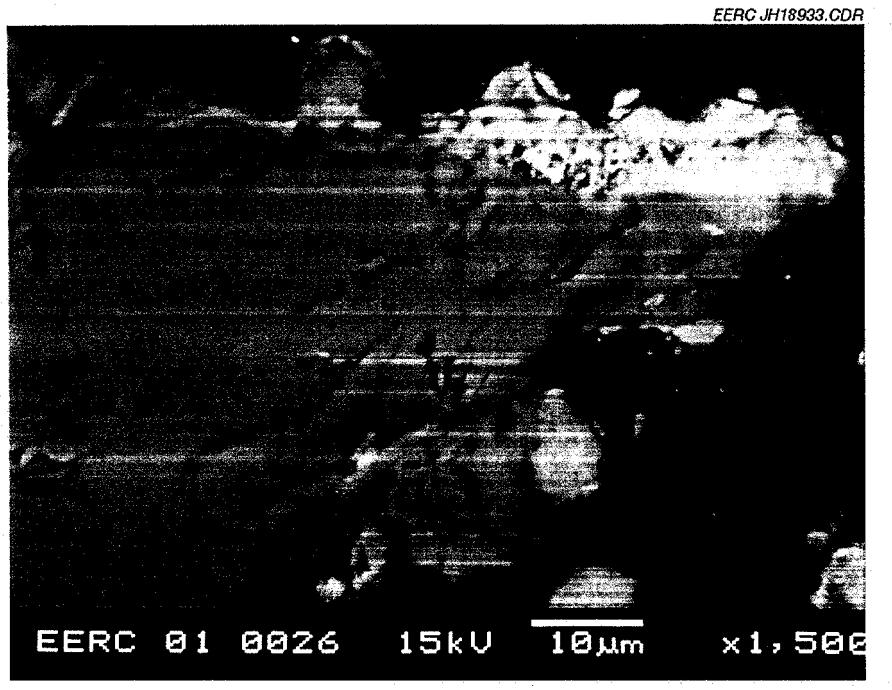


Figure 6 1. Typical appearance of surface corrosion at 1500× magnification (ORNL #3-4).

levels of other flue gas constituents were also present. The blobs of corrosion product were generally <10 µm thick. The corrosion product at the corners of this sample was similar in content and frequency to the rest of the sample surface. The SEM analysis indicates that ash constituents did not diffuse into the mullite. However, it is not clear whether the mullite diffused into the ash deposit at the corrosion product interface because of the similarity of the composition of the mullite and the constituents of the ash and the irregularity of the ceramic-ash boundary.

As was true with the other samples, the change in fuel coal was evident in the deposition layers on this sample. The composition of the ash layer deposited over the center 18 mm of the upstream face was consistent between samples installed in the convective pass.

### *NMARL Sample 01-0027 Submitted by Mark Janney, ORNL #5-1*

**Sample description:** White mullite cylinder 3 1 mm high by 63 mm diameter, with a wall thickness of 8 mm.

**Postexposure appearance:** Figure 62 shows the sample removed from the sample holder after the June test run. Flue gas flow across the sample was from left to right. Ash deposit obscures much of the sample surface. No degradation was observed. The bare leeward ring surface ranges in color from brown to rusty brown to dirty white, presumably from contamination with ash particles. The cross-sectioned sample set in epoxy looks white. The thickness of the ash deposit on the sample ranged from less than 1 mm at the corners to 13 mm.

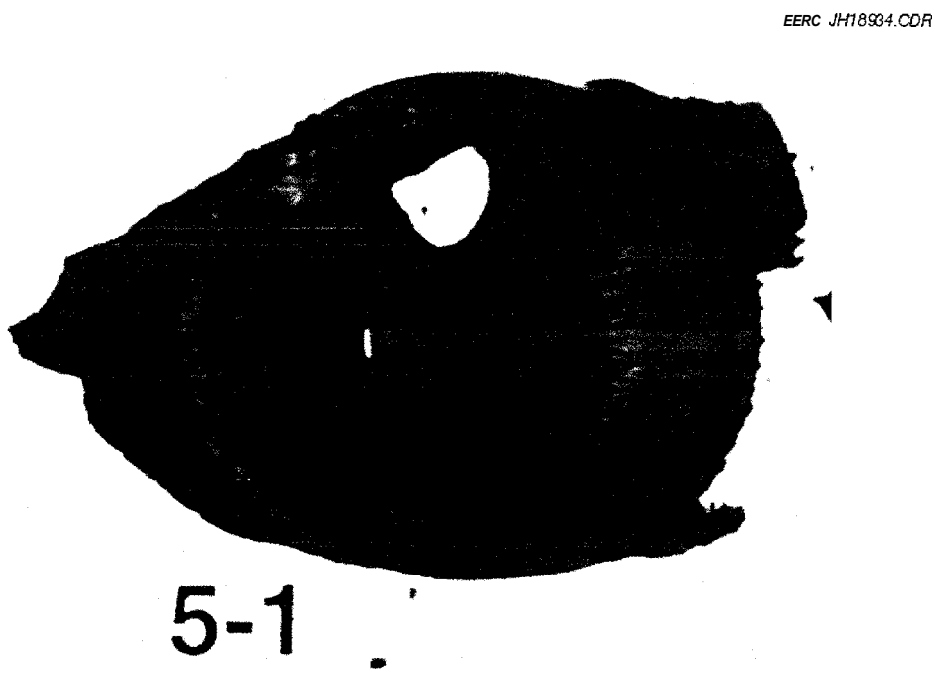


Figure 62. Sample removed from the sample holder after the June test run (ORNL #5-1).

*SEM* Morphology

The sample was described as being composed of mullite. The sample surface directly facing oncoming flue gas (upstream surface) was examined. Figure 63 shows a representative example of the material and deposited ash at 100× magnification, a porous field of ceramic grains largely separated from a band of ash across the top of the figure. SEM analysis of the bulk material indicated a composition of 47 wt% Al, 37 wt% 0, and 15 wt% Si. Inclusions in the bulk material seen as light gray streaks in the figure were present throughout the sample. Their average composition was 12 wt% Al, 37 wt% 0, and 39 wt% Si, with 7 wt% K, 2 wt% Ca, and trace amounts of Na and Fe. Because of their composition, morphology, and location, these inclusions are most likely artifacts of manufacturing rather than evidence of corrosive exposure from flue gas or ash. The surface of this sample exhibited large irregular depressions as large as 370–530 μm deep and 1220 μm wide. Although filled with ash, there appeared to be no corrosive or erosive effects causing the depressions.

No subsurface corrosion was observed in the sample cross section. Ash filled the voids between the material at the surface. Ash particles were observed to a depth of 255 μm. The ash did not penetrate or otherwise degrade the sample interior, although there was no flow of gas through the sample. The material-ash interface appears limited to the surface grains. Evidence of surface corrosion was present as thin coatings and blobs of corrosion product at the sample-ash interface. Figure 64 shows at 1500× magnification a typical area of corrosion on the left side of the ceramic grain on the left side of Figure 63. SEM analysis at the ceramic material-corrosion interface revealed that the two light areas under the blob of corrosion product were high in Si

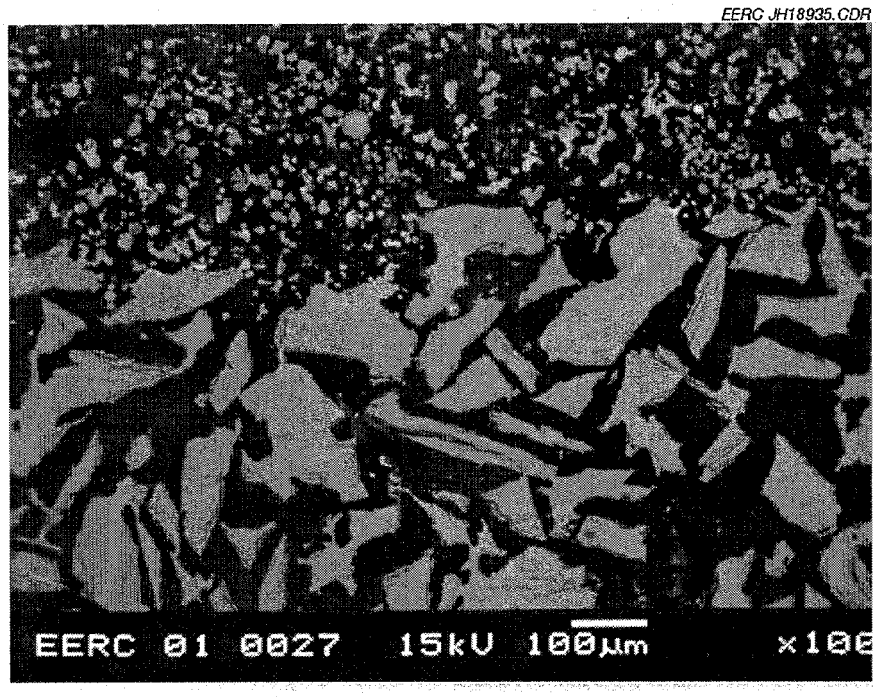


Figure 63. Example of material and deposited ash at 100× magnification (ORNL #5-1).

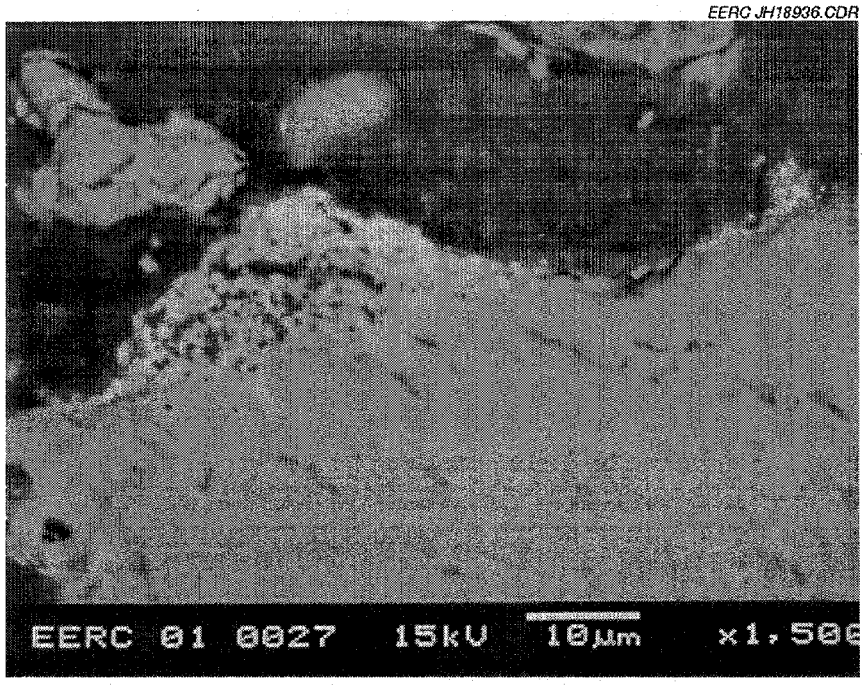


Figure 64. Typical appearance of surface corrosion at 1500× magnification (ORNL #5-1).

(28 wt%) and Ca (21 wt%), with 34 wt% O, 15 wt% Al, and traces of Fe, K, Na. and Ba. These sites extending 4 μm from the surface, were the only penetrating the sample material. Constituents in the blobs of corrosion product varied in concentration and included in order of decreasing content Ca, Si, Al, and Fe, with traces levels of Mg, Ti, P, and Na. The coverage of the surface corrosion was sporadic, ranging from <1 μm to 12 μm thick. The corrosion product coverage at the corners of this sample was more consistent and 3-6 μm thick, with a few blobs extending 23 μm from the sample surface. Constituents in the corrosion product at the corners of the upstream face were the same as regions nearer the center of the sample cross section, but had higher Fe levels, resulting from direct exposure to the higher Fe concentration of the coal ash generated during the second phase of the test run. SEM analysis indicates that ash constituents did not diffuse into the mullite. However, it is not clear whether the mullite diffused into the ash deposit at the corrosion product interface because of the similarity in composition of the mullite to many constituents of the ash and the irregularity of the ceramic material boundary.

The change in fuel coal was evident in the deposition layers on this sample. The composition of the ash layer deposited over the center of the upstream face was consistent between samples installed in the convective pass.

### *NMARL Sample 01-0028 Submitted by Mark Janney, ORNL #5-2*

**Sample description:** White mullite cylinder 23 mm high by 63.5 mm diameter, with a wall thickness of 8 mm.

**Postexposure appearance:** Figure 65 shows the sample removed from the sample holder after the June test run. Flue gas flow across the sample was from left to right. Ash deposit obscures much of the sample surface. No degradation was observed. The cross-sectioned sample set in epoxy looks white. The sample is bare of ash deposits at the corners, but has deposit as thick as 16 mm on the upstream surface.

SEM Morphology

The sample was described as being composed of mullite. The sample surface directly facing oncoming flue gas (upstream surface) was examined. Figure 66 shows a representative example of the material and deposited ash at 100× magnification, a porous field of ceramic grains largely separated from a band of ash across the top of the figure. SEM analysis of the bulk material indicated a composition of 58 wt% Al, 22 wt% 0, and 18 wt% Si. Inclusions in the grains seen as light gray streaks in the figure were present throughout the sample. Their average composition was 13 wt% Al, 26 wt% 0, and 48 wt% Si, with 8 wt% K, 2 wt% Ca, and 1 wt% Na. Because of their morphology, composition, and location, these inclusions are most likely artifacts of manufacturing rather than evidence of corrosive exposure from flue gas or ash.

No subsurface corrosion was observed in the sample cross section. Ash filled the voids between the material at the surface. Ash particles were observed to a depth of 220 μm. Most were deposited <80 μm deep in the surface irregularities. The ash did not penetrate or otherwise degrade the sample interior, although there was no gas flow through the sample. The

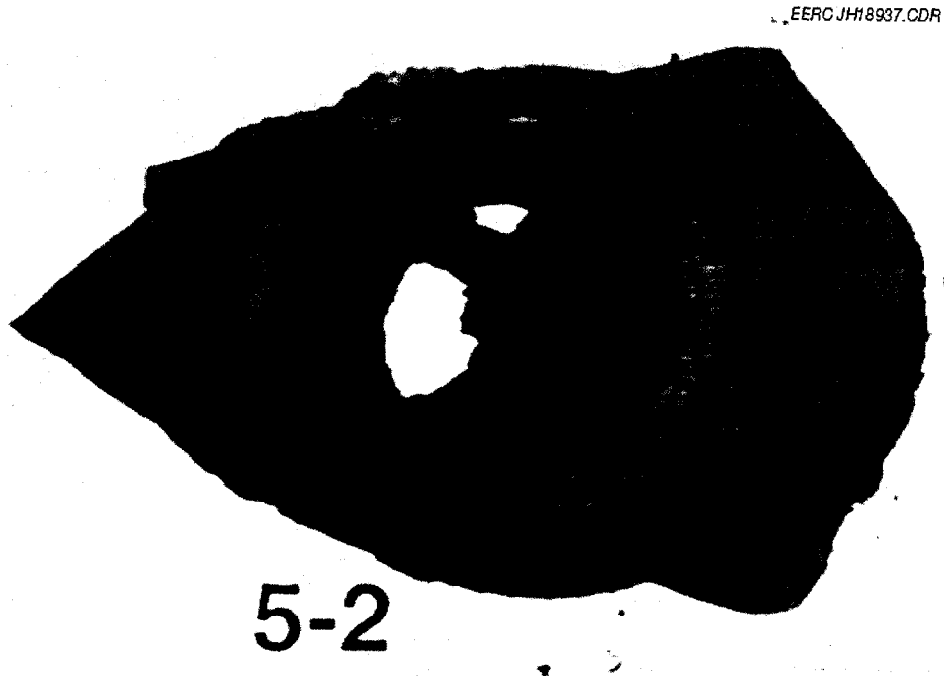


Figure 65. Sample removed from the sample holder after the June test run (ORNL #5-2).

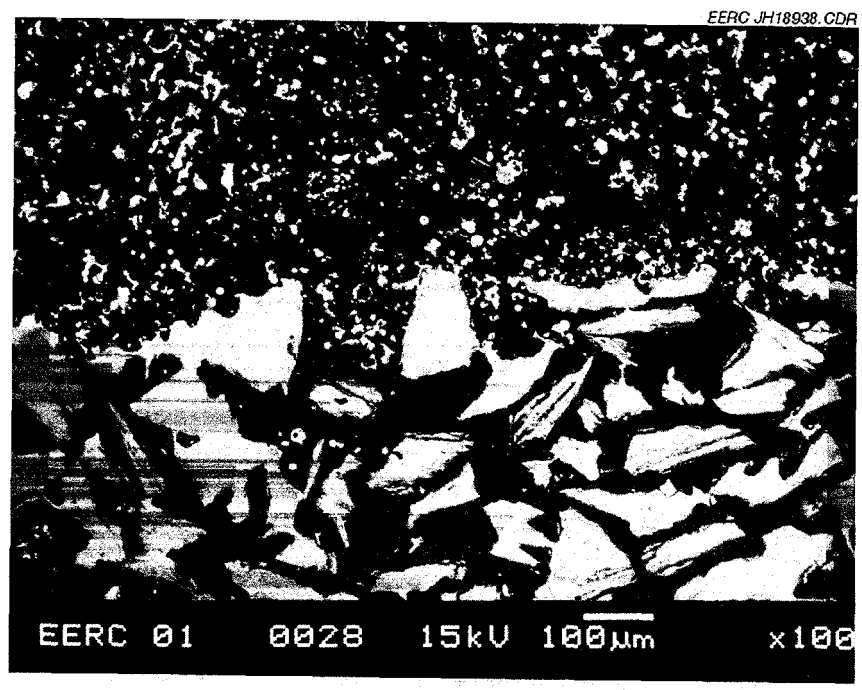


Figure 66. Example of material and deposited ash at 100× magnification (ORNL #5-2).

material-ash interface appears limited to the surface grains. Evidence of minor surface corrosion was present as thin coatings and blobs of corrosion product at the sample-ash interface. Figure 67 shows at 1500× magnification a typical area of corrosion on the ceramic chunk on the far left side of Figure 66. SEM analysis at the ceramic material-corrosion product interface revealed high Si (23-31 wt%), Ca (13-24 wt%), and Fe and Mg (0–4 wt%) enrichment, and reduced Al (32 wt%) and 0 (6-23 wt%) content. Constituents in the blobs of corrosion product varied in concentration and included in order of decreasing content Si, 0, Ca, Al, Fe, and Ti, with trace levels of Mg, P, Na, and Ba. The coverage of the surface corrosion was sporadic, ranging from <1 μm to 30 μm thick. The corrosion product layer at the corners of this sample was more consistent and 3-6 μm thick, with a few blobs extending 23 μm from the sample surface. Constituents in the corrosion product at the corners of the upstream face were the same as regions nearer the center of the sample cross section, but had higher Fe levels, as a result to direct exposure to the higher Fe concentration of the coal ash generated during the second phase of the test run.

Figure 68, the edge on one mullite grain at the corner, shows the area of greatest heterogeneity in the sample. Most of this material is corrosion product, as all but the darkest regions are enriched with ash constituents. The greatest deviation from other regions of the cross section examined appear in the medium gray area at the right side of the figure. Although this appears to have been ceramic material originally, it contains 32 wt% Si; 22 wt% Al; 5 wt% each Ca, Fe, and K; and 2 wt% each Na, Mg, and Ba. This indicates either fortuitous slicing of this sample at the ceramic-corrosion product interface or diffusion of flue gas components into the ceramic material at the comer. It is hypothesized that this area exhibits the highest reaction to corrosive forces because of its location. Ash deposition at the center of the sample's upstream

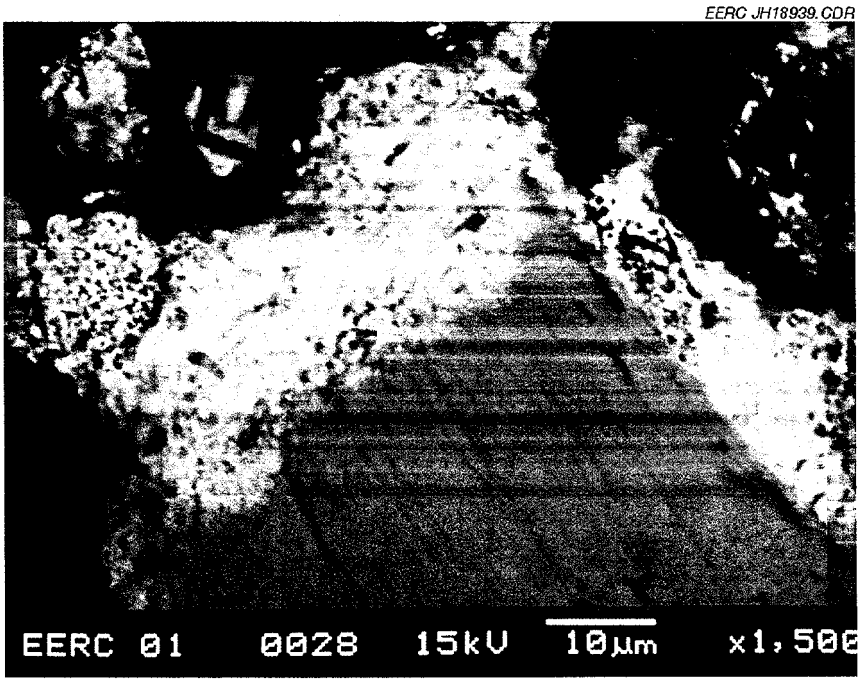


Figure 67. Typical appearance of surface corrosion at 1500× magnification (ORNL #5-2).

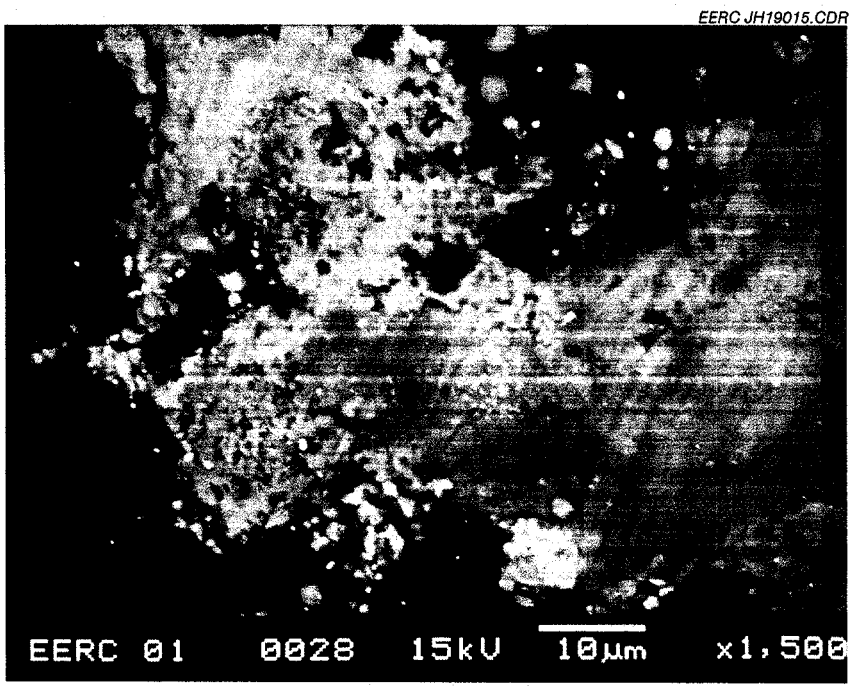


Figure 68. Surface corrosion site at 1500× magnification (ORNL #5-2).

face caused constant movement of flue gas past this exposed corner. Although it is difficult to state confidently, there appears to be no significant erosion of the sample.

With the exception of the area in Figure 68, **SEM** analysis indicates that ash constituents did not diffuse into the mullite. However, it is not clear whether the mullite diffused into the ash deposit at the corrosion product interface because of the similarity of the composition of the mullite to some constituents of the ash and the irregularity of the ceramic material boundary.

As was true for all of the samples, the change in fuel coal was evident in the deposition layers on this sample. The composition of the ash layer deposited over the upstream face was consistent between samples installed in the convective pass.

### *NMARL Sample 01-0030 Submitted by Honeywell, HACI #0257-01-001-1-6*

**Sample description:** Charcoal gray SiC/SiC ring 25 mm high by 60 mm diameter, with a wall thickness of 3 mm, previously exposed during the Cordero Rojo test in March 2001.

**Postexposure appearance:** Figure 69 shows the sample removed from the sample holder after the June test run. Flue gas flow across the sample was from left to right. Ash deposit obscures much of the sample surface. No material degradation was observed. Cross-sectioned sample set in epoxy remains very dark gray.


Figure 69. Sample removed from the sample holder after the June test run (HACI #0257-01-001-1-6).

*SEM* Morphology

The sample was described by Honeywell as SiC fibers in a SiC matrix. The sample was prepared for SEM analysis according to Honeywell instructions. Figure 70 is a backscattered electron image of the sample material and ash deposit at 100× magnification. It shows a cross section of weave of lengthwise and crosswise fibers, amorphous bundles and voids, amorphous binder at the surface, and a light layer of ash. The darkest areas are mounting epoxy. SEM analysis of the sample matrix indicated a composition of 49 wt% C, 46 wt% Si, and 5 wt% 0 in the fiber bundles and 32 wt% C, 66 wt% Si, and 2 wt% 0 in the matrix. It must be noted that the C in the mounting epoxy may interfere with accurate analysis of C in samples.

No subsurface corrosion was observed in the sample cross section. The material-ash interface appears limited to the surface of the sample. The depth of the ash deposit on the sample ranged from less than 1 mm to greater than 30 mm. Figure 71 is a backscattered electron image of the sample material-ash deposit at 1500× magnification. The sample matrix, medium gray mass at the bottom of the figure, appears unimpaired by the light gray ash layer at its surface. Composition of the deposited ash layer was consistent with that of the ash deposits on other samples installed in the convective pass. No signs of corrosion or erosion were indicated throughout the sample cross section, although a thin surface layer less than 30 microns thick was rich in calcium and silicon, which indicates some interaction with the ash constituents.

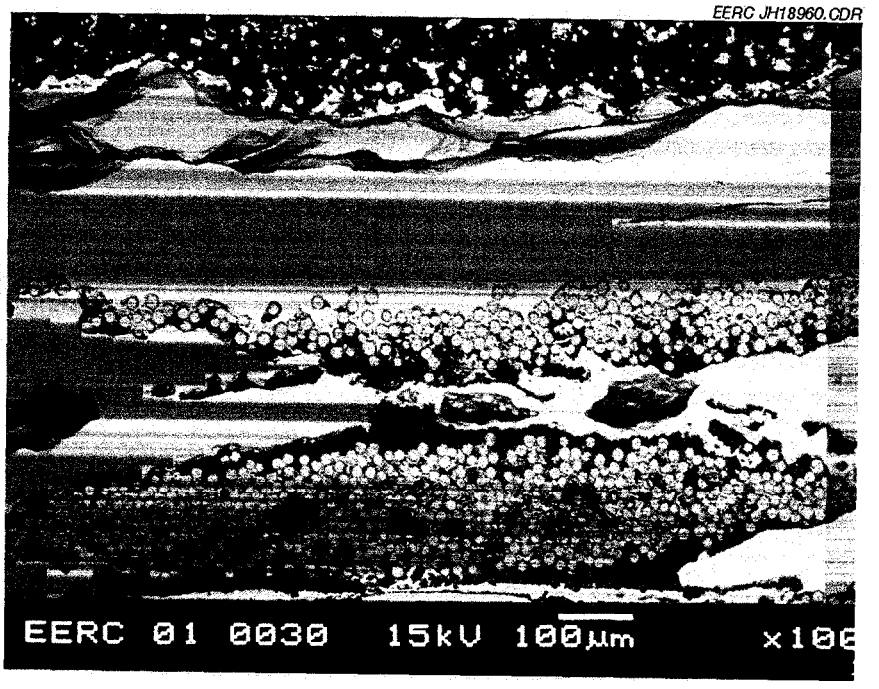


Figure 70. Sample material and ash deposit at 100× magnification (HACI #0257-01-001-1-6).

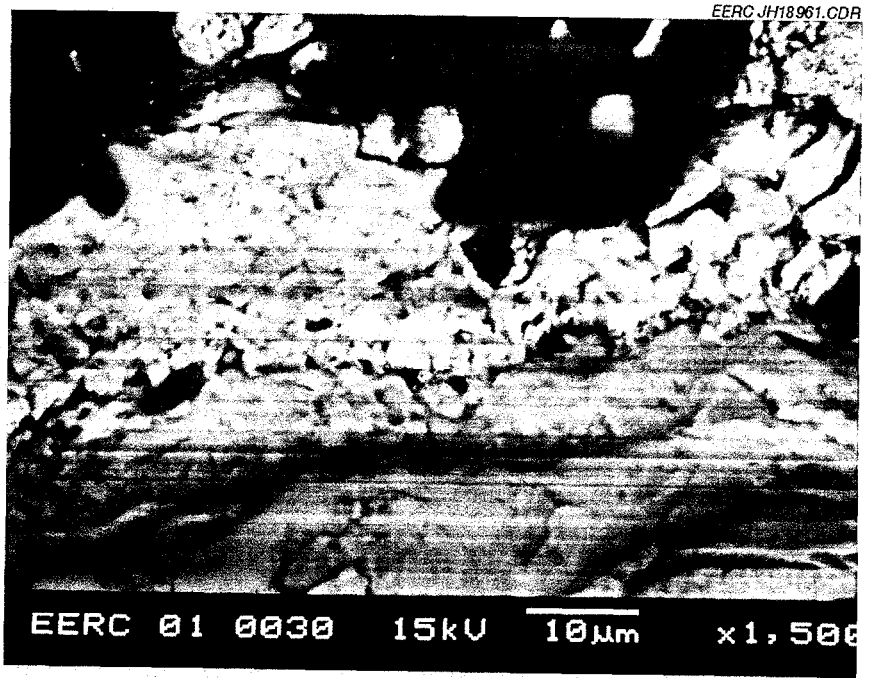


Figure 7 1. Sample material and ash deposit at 1500× magnification (HACI #0257-01-001-1-6).

*NMARL Sample 01-0033 Submitted by Mark Harper, #Thermie-020-l*

**Sample description:** 5.5-mm-thick disk of Thermie Alloy cut from a 48-mm-diameter rod, flattened on one edge; shiny, chrome-colored.

**Postexposure appearance:** Figure 72 shows the sample removed from the sample holder after the June test run. Flue gas flow across the sample was from left to right. The large mass of ash deposited on the sample separated easily from the sample. The surface is gray-brown and dull. The sample appears intact, with indications of surface corrosion.

SEA4 Morphology

Thermie Alloy 020 is reported to contain 52 wt% Ni, 25 wt% Cr, 20 wt% Co, 1.7 wt% Ti, and <1 wt% Si and Al. Figure 73 shows a representative example of the cross-sectioned alloy material, products of corrosive activity, and ash deposit at 100× magnification. The alloy material appears as a homogeneous field. SEM analysis of the bulk material indicated 47 wt% Ni; 25 wt% Cr; 20 wt% Co; 2 wt% Nb, 0, Ti, and Fe; and trace (<1 wt%) Si and Al. Alloy in the corrosion zone is of similar composition.

Subsurface corrosion in the sample cross section includes a region extending 35 μm deep into the sample. Figure 74 shows this region at 1500× magnification. Oxidation appears to be the major mode of corrosion in these areas, especially the formation of aluminum oxide. Dark gray intrusions in the subsurface include increased concentrations of Al and 0 and low levels of Ni, Cr, and Co. Light gray intrusions include increased concentrations of Ti, Al, and 0 and lower

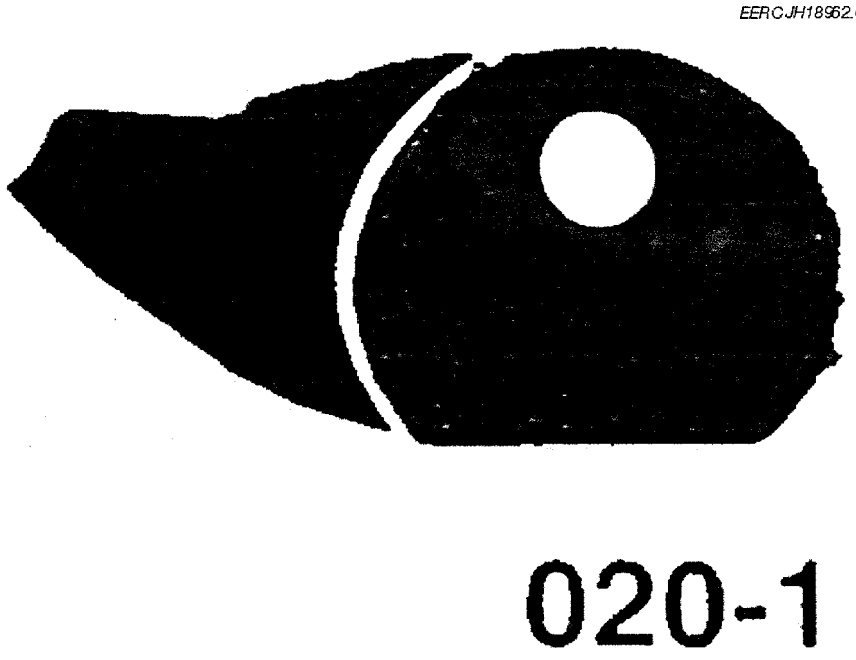


Figure 72. Sample removed from the sample holder after the June test run (#Thermie-020-1).

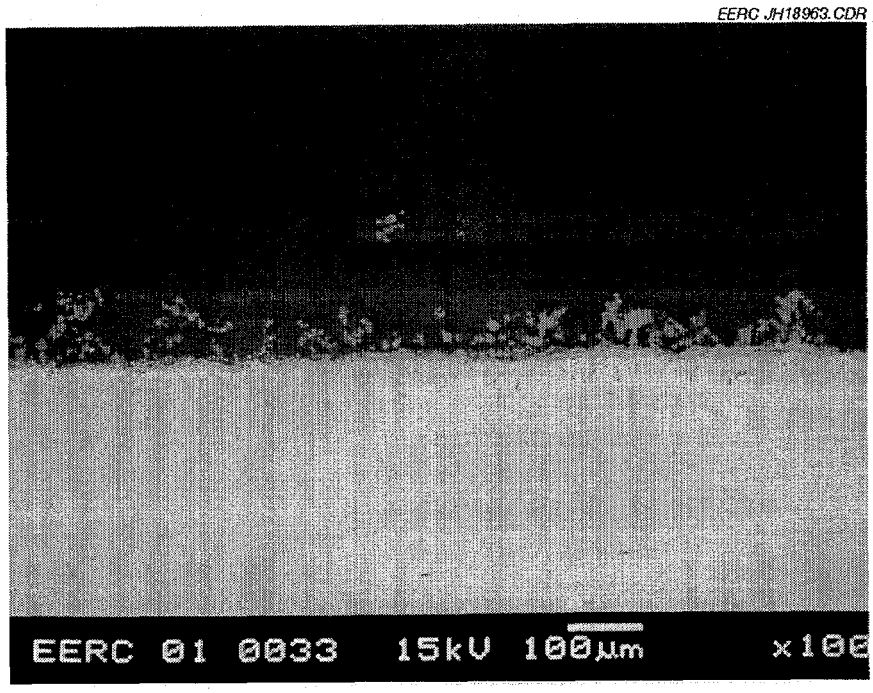


Figure 73. Cross-sectioned alloy material, products of corrosive activity, and ash deposit at 100× magnification (#Thermie-020-1).

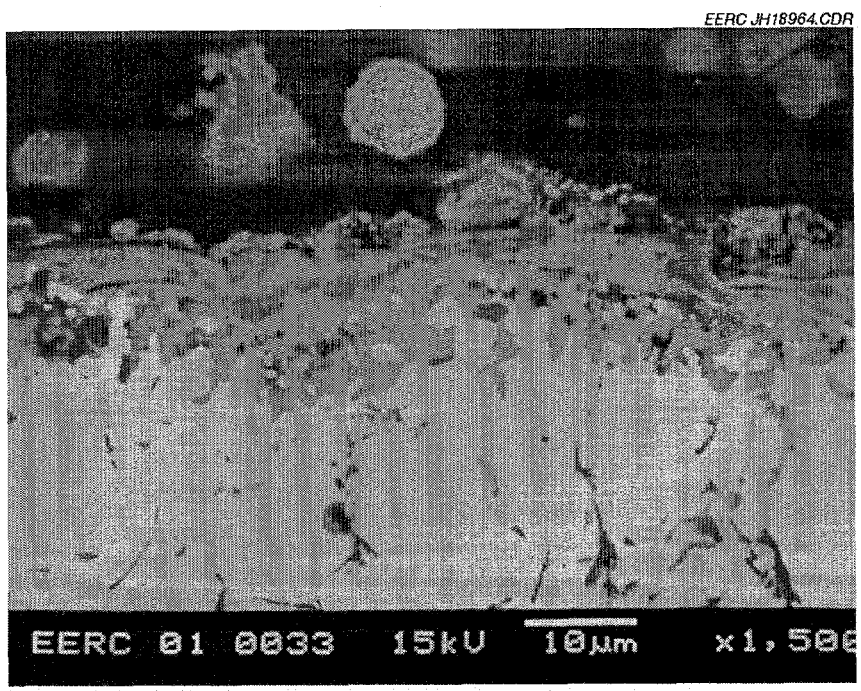


Figure 74. Example of cross-sectioned alloy material, products of corrosive activity, and ash deposit at 1500× magnification (#Thermie-020-1).

levels of Ni, Co, and Cr. This subsurface corrosion appears across the near-surface of the sample throughout the cross section examined.

The surface of the sample is covered with a continuous layer of corrosion product as shown in Figure 74. This surface layer contains small amounts of ash constituent Ca (<4 wt%) incorporated into the corrosion layer. Light gray fingers of corrosion material reaching into the alloy show enrichment of Ti, 0, and Al and depletion of Ni and Co. The Cr concentration remained relatively constant between the different gray levels. Dark gray areas include 0, Si, and Al in place of Ni and Co. The light gray surface layer comprises mostly Cr and 0; other constituents are present in trace levels if at all, suggesting oxidation as the main flue gas attack on the sample and chromium oxide layer formation. No sulfidation or halide attack was indicated. No signs of erosion were indicated. Assuming the Si and Al in the corrosion product represent concentration of alloy constituents, the absence of significant amounts of ash constituents in the corrosion product indicates that the ash was not a factor in alloy degradation.

The ash deposit on the upstream face of the sample was originally up to 35 mm thick. Too little ash remained on the sample after removal from the rack to perform an adequate SEM area scan analysis of the deposit.

### *NMARL Sample 01-0034 Submitted by Mark Harper, #956-1*

**Sample description:** 50-mm x 49-mm alloy sheet quadrilateral 4 mm thick, with a 12.5-mm-diameter hole in the larger surface; shiny chrome-colored.

**Postexposure appearance:** Figure 75 shows the sample removed from the sample holder after the June test run. Flue gas flow across the sample was from left to right. The large mass of ash deposited on the sample separated easily from the sample. The surface is gray-brown and dull through a fine layer of ash. The sample appears intact, with indications of surface corrosion.

*SEM* Morphology

Metal Alloy 956 is reported to contain 73-75 wt% Fe, 19-21 wt% Cr, 4.5 wt% Al, 0.1-0.5 wt% Ti, and 0.5 wt% $Y_2O_3$. Figure 76 shows a representative example of the cross-sectioned alloy material, corrosion layer, and ash deposit at 100× magnification. The alloy material appears as a homogeneous field. SEM analysis of the bulk material indicated 74 wt% Fe, 20 wt% Cr, and 4 wt% Al.

The sample cross section exhibited no signs of subsurface corrosion or penetration of ash constituents beyond the surface corrosion layer.

The surface of the sample contains a continuous layer of corrosion product as shown in Figure 77 at 1500× magnification. The dark gray corrosion material adjacent to the alloy comprises 57 wt% Al, 34 wt% O, 3 wt% Fe, and 2 wt% Ti and Cr. Light gray spots in this area contain more Ti (up to 9 wt%). Near the corrosion product-ash interface, Ca, Si, and traces of Mg, P, S, K, Ba, and V appear. The overall effect is formation of a protective aluminum oxide

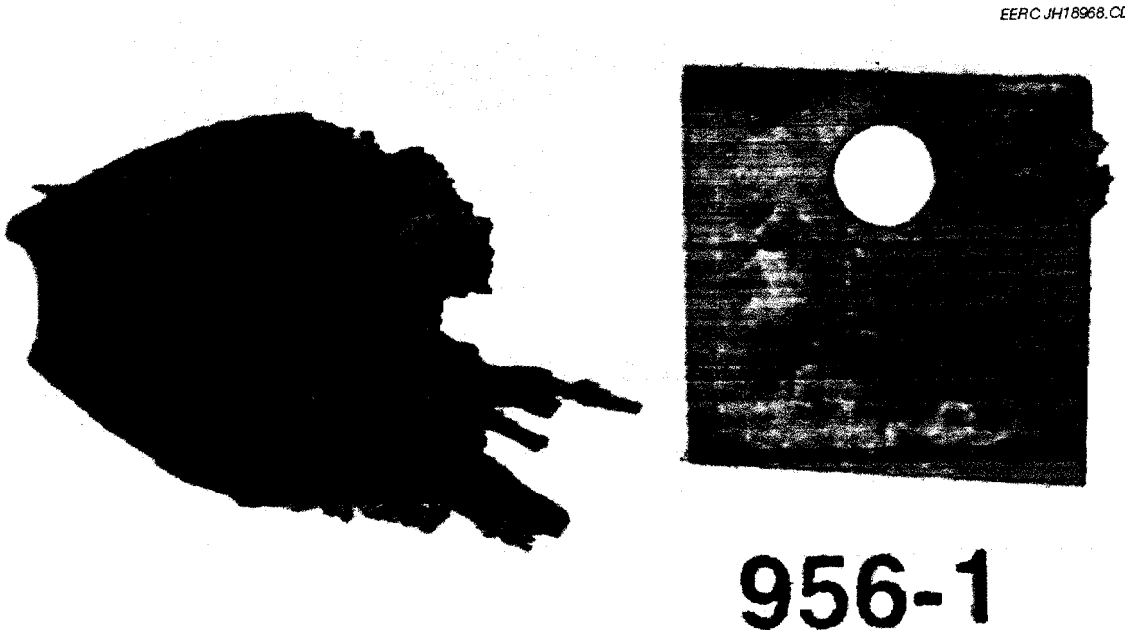


Figure 75. Sample removed from the sample holder after the June test run (#956-1).

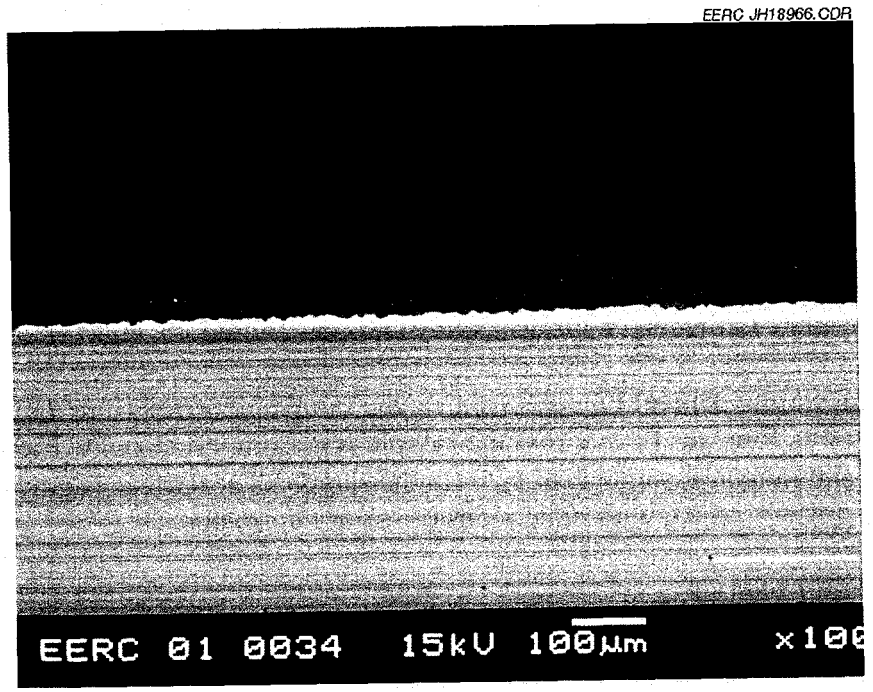


Figure 76. Example of cross-sectioned alloy material, corrosion layer, and ash deposit at 100× magnification (#956-l).

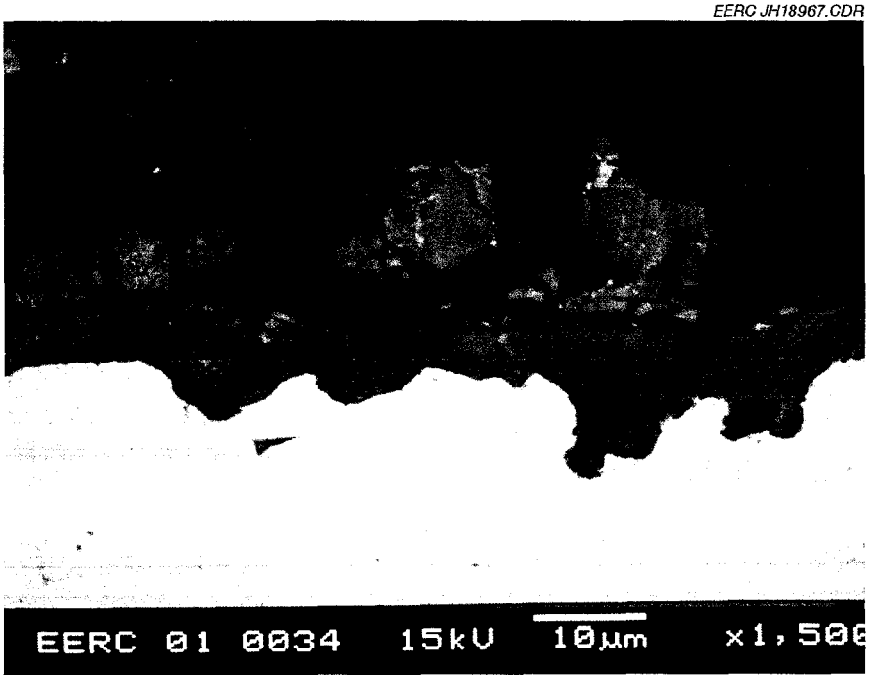


Figure 77. Example of cross-sectioned alloy material, corrosion layer, and ash deposit at 1500× magnification (#956-l).

layer 4 to 15 µm thick, limiting penetration of ash constituents beyond the outer corrosion layer and into the alloy. No sulfidation or halide attack was indicated. No signs of erosive attack were indicated.

The ash deposit on the upstream face of the sample was originally up to 35 mm thick, but too little remained for adequate SEM analysis.

### *NMARL Sample 01-0035 Submitted by Mark Harper, #803-1*

**Sample description:** 51-mm x 48-mm alloy sheet quadrilateral 3 mm thick, with a 12.5-mm-diameter hole in the larger surface; shiny chrome-colored.

**Postexposure appearance:** Figure 78 shows the sample removed from the sample holder after the June test run. Flue gas flow across the sample was from left to right. The large mass of ash deposited on the sample separated easily from the sample. The surface is gray-brown and dull. The sample appears intact, with indications of surface corrosion.

*SEM* Morphology

Metal Alloy 803 is reported to contain 35-36 wt% Ni, 35 wt% Fe, 25 wt% Cr, <1.5 wt% Mn, <1 wt% Si and C, <0.75 wt% Cu, 0.15-0.60 wt% Al and Ti, and <0.015 wt% S. Figure 79 shows a representative example of the cross-sectioned alloy material, corrosion layer, and ash

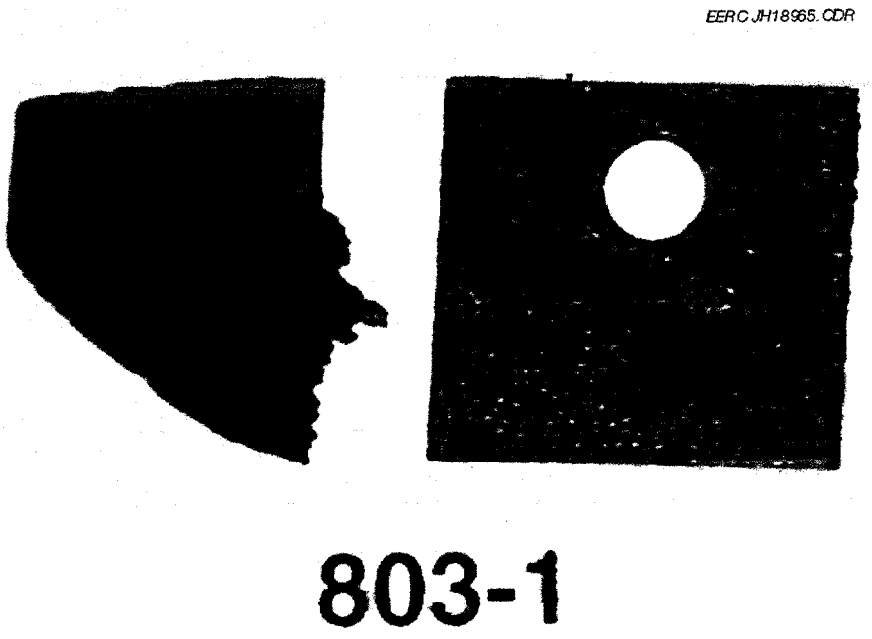


Figure 78. Sample removed from the sample holder after the June test run (#803-l).

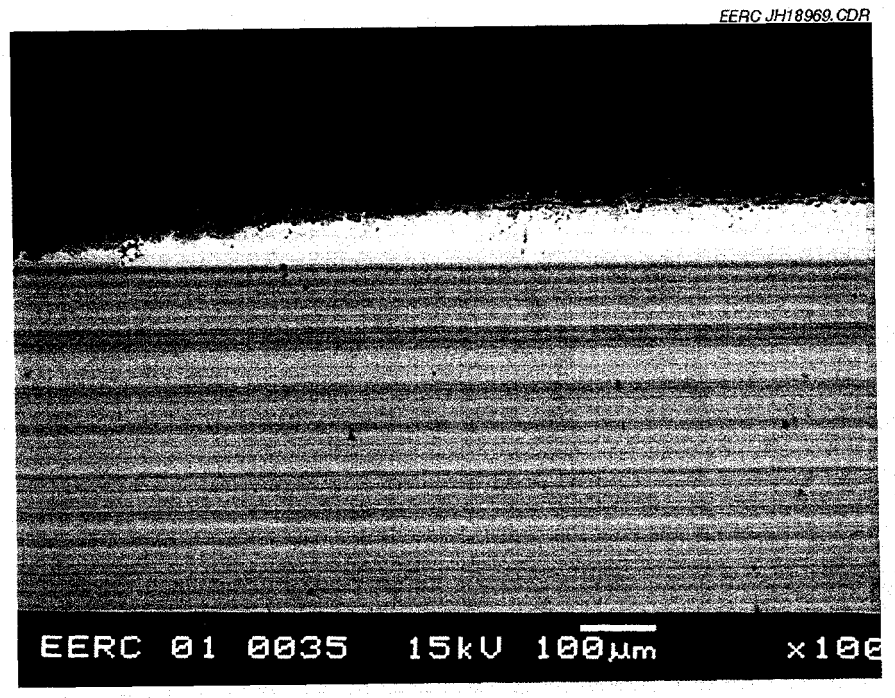


Figure 79. Sample surface at 100× magnification (#803-l).

deposit at 100× magnification. The alloy material appears as a homogeneous white field. SEM analysis of the bulk material indicated 38 wt% Ni, 36 wt% Fe, 23 wt% Cr, and 1 wt% 0. Occasional light gray spots appearing in the alloy are depressions in the sample cross section representing holes in the alloy material.

Subsurface corrosion occurs sporadically in the upper 70 μm of the sample. Figure 80 shows the sample surface just right of center in Figure 79 at 600× magnification. Most of the intrusions in Figure 80 are hollow pores in the alloy. The medium gray patches associated with these intrusions are composed of 50 wt% Cr, 20 wt% Ti, 20 wt% O, 4 wt% Al, and 2 wt% Ni and Fe, indicating oxidative penetration into the subsurface.

The surface of the sample contains a continuous, irregular layer of corrosion product. Figure 81 shows the area left of center in Figure 80 at 1500× magnification. The dark gray corrosion material adjacent to the alloy comprising 52 wt% Ti, 26 wt% Cr, 10 wt% Fe, 8 wt% Ni, and 2 wt% 0 indicates a shift in alloy concentration. Closer to the gas interface, oxidation has led to the formation of a chromium titanium oxide layer. The corrosion layer in this area also includes a large separation. The lighter gray layer above the crack is chromium (72 wt%) oxide (21 wt%), with pockets of TiO and TiOMn. In addition, ash particles sticking to the corrosion layer surface appear as entrained spheres. These spheres incorporate Cr, with ash constituents Al, Si, 0, and Mn. The corrosion layer was approximately 40 μm thick. No sulfidation or halide attack was indicated. No signs of erosive attack were indicated.

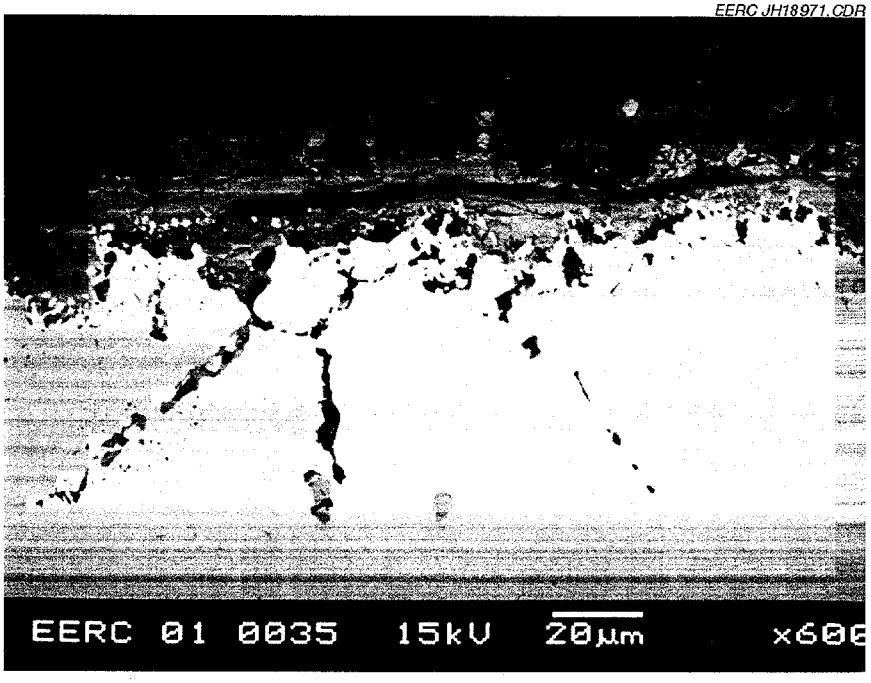


Figure 80. Sample at 600× magnification (#803-1).

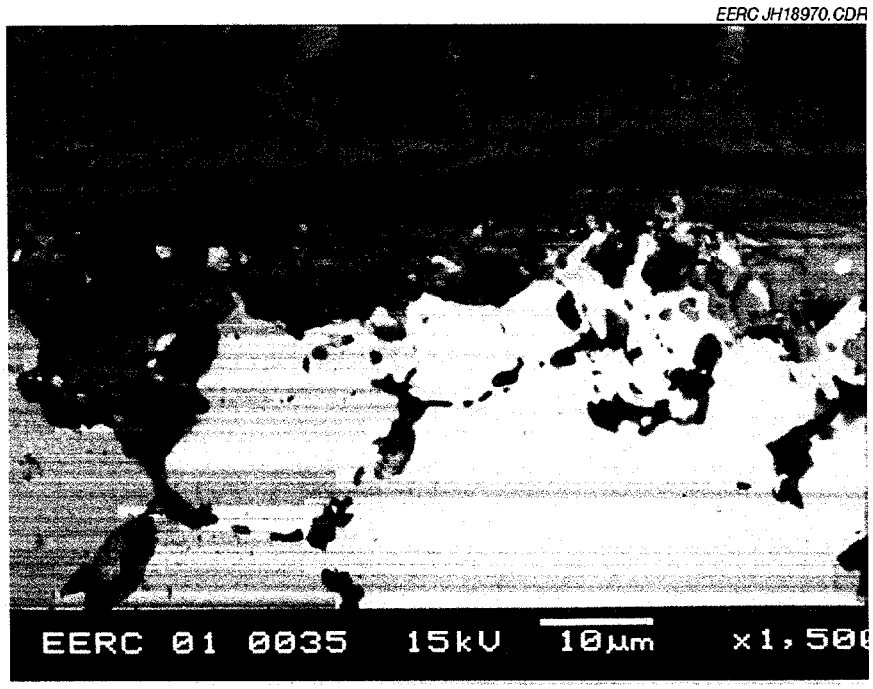


Figure 81. Sample surface at 1500× magnification (#803-l).

The ash deposit on the upstream face of the sample was originally up to 40 mm thick. Too little ash remained on the sample after removal from the rack to perform adequate SEM analysis of the material.

### *NMARL Sample 01-0031 Submitted by Vinod Sikka, ORNL #17681 (4)*

**Sample description:** 31.5 $mm^2$ x 13-mm alloy cuboid with 13-mm-diameter hole in the center of larger surface; stainless steel-colored. Previously exposed on the Cordero Rojo test.

**Postexposure appearance:** Figure 82 shows the sample removed from the sample holder after the June test run. The large mass of ash deposited on the sample separated easily from the sample. The surface is brown and dull through a thin layer of ash particle. The sample appears intact, with indications of surface corrosion.

*SEM* Morphology

Metal Alloy 17681 is reported to contain 62.50 wt% Fe, 35.0 wt% Cr, and 2.5 wt% Si. Figure 83 shows a representative example of the cross-sectioned alloy material, corrosion product, and ash deposit at 100× magnification. It reveals a homogeneous field of alloy material. SEM analysis of the bulk material indicated 61 wt% Fe, 36 wt% Cr, 1.75 wt% Si, and 1 wt% 0. Although not present in the photo, the alloy material also contained occasional darker streaks with higher proportions of Cr (93 wt%), less Fe (4 wt%), some 0 (2 wt%), and no Si.

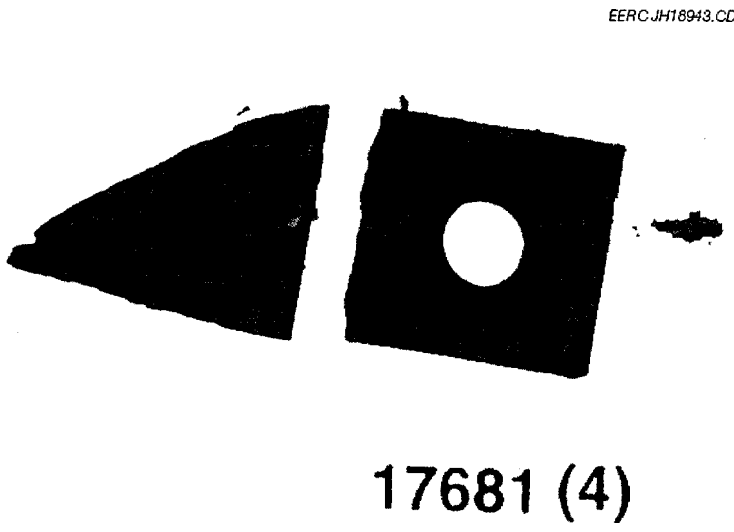


Figure 82. Metal Alloy ORNL #17681 (4) removed from the sample holder after the June test run.

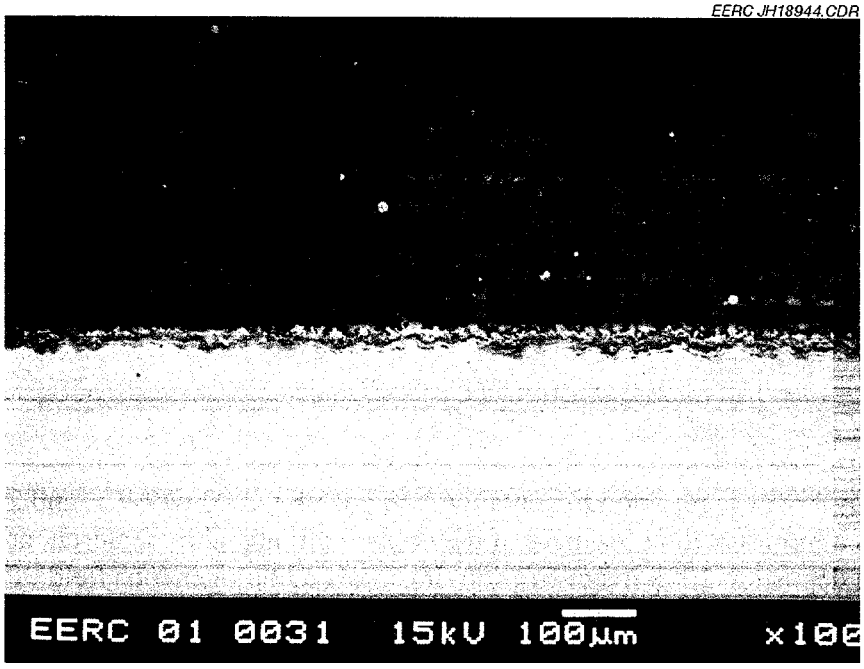


Figure 83. Example of cross-sectioned alloy material, corrosion product, and ash deposit at 100× magnification (ORNL #17681 [4]).

Subsurface corrosion in the sample cross section examined includes a few long pits extending 85 to 129 μm deep and 35 μm wide into the sample. Oxidation appears to be the major mode of corrosion in these areas, since the constituents of the corrosion product in these pits are Cr, Si, 0, and occasionally Fe. Trace S was present in the pits as well.

The surface of the sample exhibited almost no deep pitting, but it did show shallow pitting grading into a smoother surface recession as shown in Figure 84 at 1500× magnification. This figure shows the alloy in white covered by a layer of corrosion product in light and medium gray and topped by heterogeneous corrosion product-ash layer. The corrosion layers detached from the alloy and from each other during epoxy polymerization, indicating weak bonding to the alloy. The alloy-corrosion product interface contains mainly Cr (39-75 wt%), Si (5-28 wt%), and 0 (14-30 wt%). The outer surface of this corrosion layer contained less Cr (12-28 wt%) and more Si (45 wt%), possibly infusing from the ash. Fe concentration in the corrosion layer is generally less than 5 wt%. The layer ranges in thickness from 6, to 20 μm. The outer layer of corrosion contains several flue gas constituents, Ca, Si, Fe Al, Mg, and Ti (in order of decreasing proportion), and Cr at 1 l-57 wt%, suggesting that ash components in the flue gas assisted 0 in the corrosive degradation of the outer corrosion layer. No sulfidation or halide attack was indicated.

The ash deposit on the upstream face of the sample was originally up to 40 mm thick. A layer up to 1 mm thick remained on the sample after preparation, indicating more interaction with the alloy corrosion layer than most of the other samples, but was still relatively weak at the interface as indicated by separation during epoxy polymerization. SEM analysis indicated that the

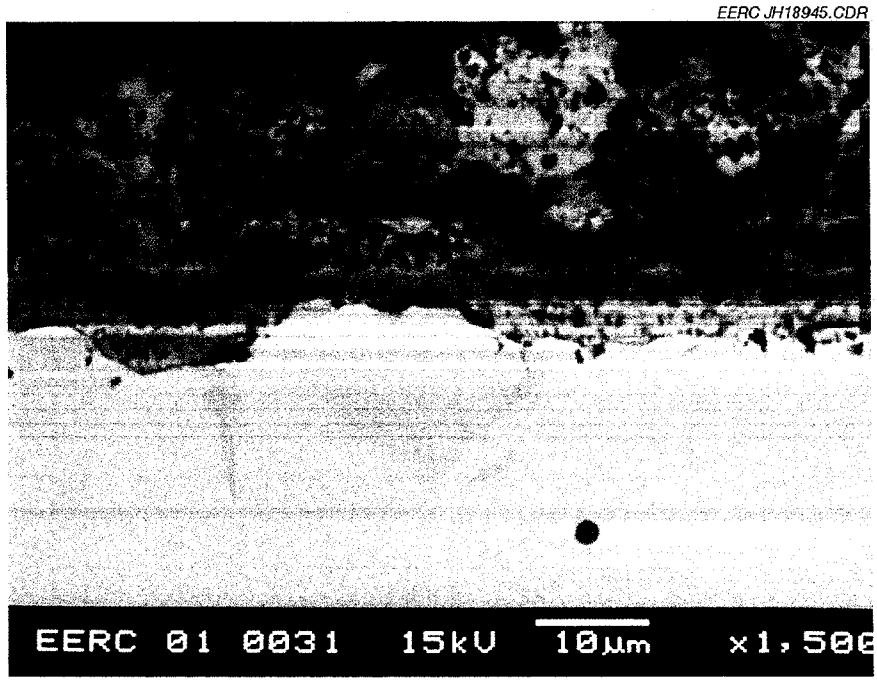


Figure 84. Example of cross-sectioned alloy material, corrosion product, and ash deposit at 1500× magnification (ORNL #17681 [4]).

ash 160 μm from the outer corrosion layer had higher Fe (12 wt%) and Cr (9 wt%) content and lower Ca (4 wt%) content than the CAH bulk ash analysis. The Cr in the layer indicates some dissolution of the corrosion product into the ash layer.

### *NMARL Sample 01-0032 Submitted by Vinod Sikka, ORNL #1 7433 (2)*

**Sample description:** 3 1.5 $mm^2$ x 13-mm alloy cuboid with 13-mm-diameter hole in the center of larger surface; stainless steel-colored. Previously exposed on the Cordero Rojo test.

**Postexposure appearance:** Figure 85 shows the sample removed from the sample holder after the June test run. The large mass of ash deposited on the sample separated easily from the sample. The surface is dullish gray and covered with patches of ash particles. Visual inspection suggests that the sample has been corroded.

SEA4 Morphology

The metal is reported to contain 44.25 wt% Fe; 31 wt% Ni; 20 wt% Cr; 2.0 wt% Mn; 1.5 wt% Mo; 0.40 wt% V; 0.25 wt% Ti, Nb, and Si; 0.09 wt% C; and 0.005 wt% B. Figure 86 shows a representative example of the cross-sectioned coupon, corrosion product, and ash deposit at 100× magnification. It reveals a homogeneous field of alloy, a typical corrosive intrusion into the sample, and the discontinuous oxide layer coating the sample. SEM analysis of the bulk material indicated 84 wt% Fe, 14 wt% Al, and 2 wt% Cr. This content is similar to that measured for Alloy #17433 exposed in the March test. However, the content of neither sample matches any of the alloy compositions supplied by ORNL.

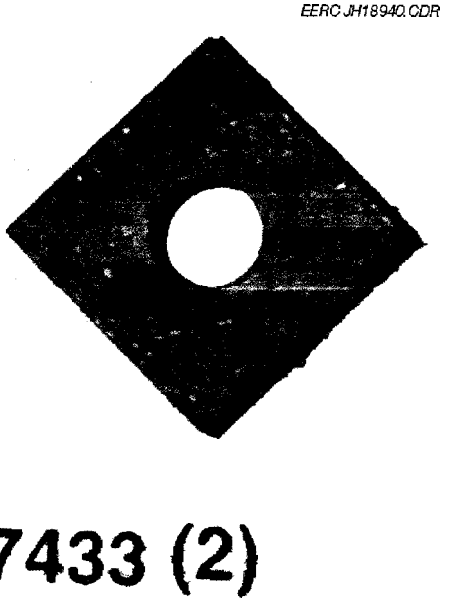


Figure 85. Metal Alloy ORNL #17433 (2) removed from the sample holder after the June test run.

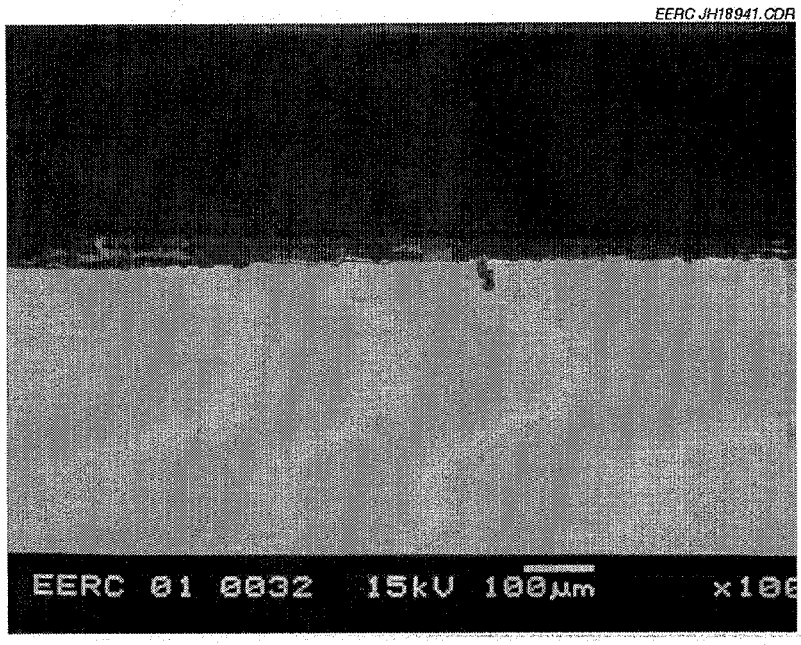


Figure 86. Example of cross-sectioned alloy material, corrosion product, and ash deposit at 100× magnification (ORNL #17433 [2]).

The sample underwent corrosion exhibited by both sporadic deep pitting of the surface and much shallower pitting grading into a relatively smooth oxidation. Figure 86 includes one of several deep pits in the sample, extending 52 µm into the metal alloy and 21 µm wide, as well as the shallow pitting which is more of a general, smoother, oxidation. Depth of shallow pitting was <10 µm. Figure 87 shows that same deep pit at 1500× magnification. Composition at the alloy-corrosion product interface of pits and recession areas was constant. Constituents of the dark gray areas of corrosion product included 62 wt% Al, 33 wt% O, 4 wt% Fe, and l-6 wt% S, with traces of Cr and, occasionally, Ti, P, Si, K, or Ca, suggesting the loss of Fe from the sample and formation of an Al-O skin resulting from oxidation by the flue gas constituents. Also visible in the alloy-corrosion product interface of the pit are a few light gray patches. These illustrate initiation of corrosive attack in progress, with decreasing Fe levels (63 wt%), increasing Al levels (30 wt%), and the presence of some 0 (3 wt%). At the surface, the transition areas include higher concentrations of 0 (18 wt%). These are present in Figure 87 as the white patches at the surface on either side of the pit. The deepest pit observed in the sample cross section extended 280 µm into the sample.

The corrosion product at the surface contains mostly areas with element proportions similar to those at the alloy interface (dark gray in the figures), but occasional spots of nearly pure Fe (83 wt%) 0 (14 wt%) are also present. At 67-83 wt%, Al remains the dominant element in the thin corrosion layer at the sample surface, likely having formed a partially oxidized layer with the 1 l-20 wt% 0 present. Minor constituents at the sample surface include 2-7 wt% Fe, l-2 wt% Cl, and 2 wt% S and Si.

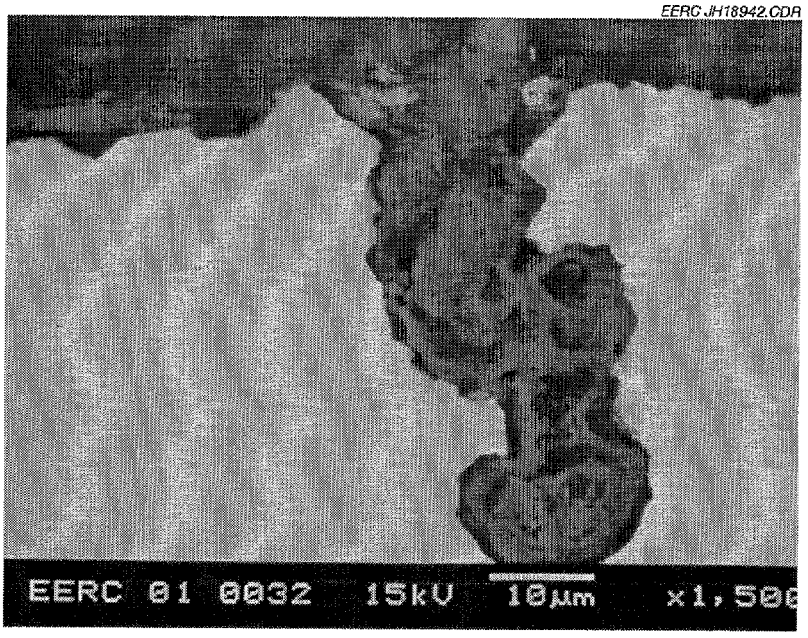


Figure 87. Example of cross-sectioned alloy material, corrosion product, and ash deposit at 1500× magnification (ORNL #17433 [2]).

The ash deposit on the upstream face of the sample was originally up to 40 mm thick. It was, however, not well bonded as it readily detached during removal of the sample from the stand. Very little ash remained on the sample after preparation. SEM analysis indicated that the ash had higher Fe (23 wt%) and Ca (22 wt%) content and lower 0 (26 wt%), Si (14 wt%), and Al (9 wt%) content than the ash analysis, indicating a predominance of Ca- and Fe-rich ash sticking to the surface or Ca-rich ash into which iron from the coupon had diffused.

Oxidation and sulfidation are the main forms of flue gas constituent attack on the sample. Ash constituent influence on sample corrosion was very minor. No erosive forces on alloy degradation were indicated.

### *NMARL Sample 01-0036 Submitted by Bob Swindeman, ORNL #310HCbN SS (HR3C Weld)-1*

**Sample description:** 32 square x 3.4-mm alloy cuboid, with an 1 l-mm-diameter hole in the center of larger surface; stainless steel-colored.

**Postexposure appearance:** The Swindeman samples were all exposed in an elbow following the process air-tube and-shell heat exchanger, which immediately follows the convective pass in which the previous samples were exposed. Average gas temperature for the Swindeman samples was 708°C. Figure 88 shows the sample removed from the sample holder after the June test run. The surface is coated with a thin brown layer of ash particle. The sample appears intact.

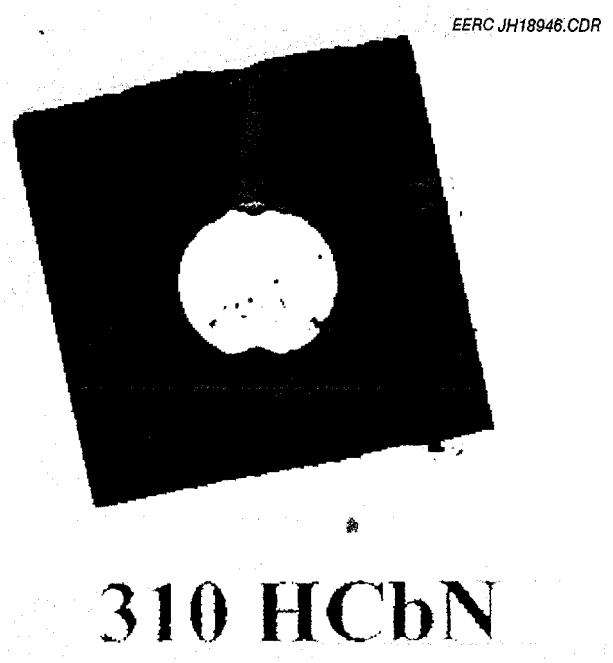


Figure 88. Alloy ORNL #310HCbN SS (HR3C Weld)-1 removed from the sample holder after the June test run.

SEA4 Morphology

The metal is reported to contain 51.54 wt% Fe, 25.65 wt% Cr, 20.15 wt% Ni, 1.22 wt% Mn, 0.64 wt% Si, 0.32 wt% Nb-Ta, and 0.2 wt% N. Figure 89 shows a representative example of the cross-sectioned alloy material, corrosion layer, and ash deposit at 100× magnification. The alloy material appears as a homogeneous white field. There are, however, fine white particles scattered throughout the alloy material. SEM analysis of the bulk material indicated a composition of 53 wt% Fe, 28 wt% Ni, 14 wt% Cr, and <2 wt% MO and 0. The fine particles include 44 wt% Fe, 34 wt% Cr, 18 wt% Ni, and <1 wt% 0, Si, Mn, and Nb.

Subsurface corrosion in the sample cross section examined was limited to a few thin intrusions extending less than 10 μm deep and 2 μm wide into the sample. Figure 90 shows the sample surface at 1500× magnification, including two such intrusions present as medium gray lines into the alloy. These intrusions are high in Cr (around 50 wt%), with some Mn (10–35 wt%), 0 (around 13 wt%), and Fe (9 wt%), and trace Ni, indicating limited oxidation into the near-subsurface.

The surface of the sample contains a very thin, continuous layer of corrosion product 2 μm thick. The concentration of corrosion product constituents varies across the sample, but generally includes 53 wt% Cr, 16 wt% 0, 13 wt% Fe, 7 wt% Mn, 5 wt% Ni, and trace Nb.

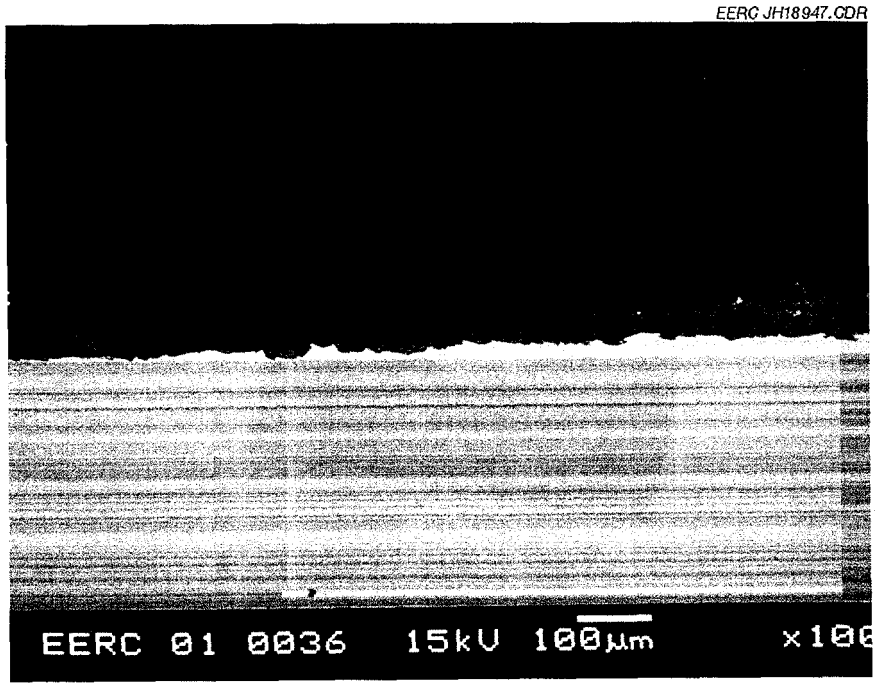


Figure 89. Example of cross-sectioned alloy material, corrosion layer, and ash deposit at 100× magnification (ORNL #310HCbN SS [HRC3 Weld]-1).

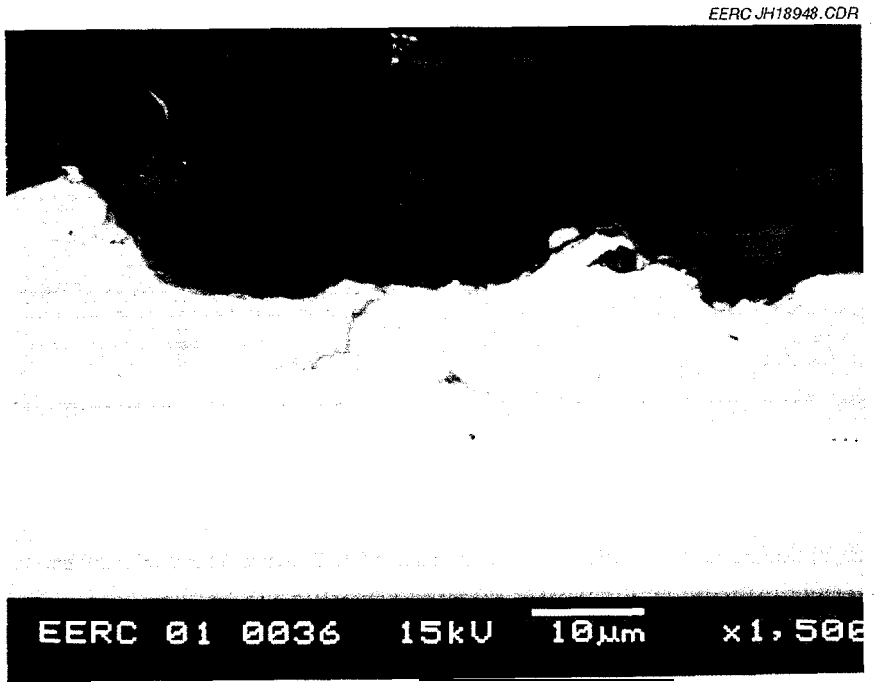


Figure 90. Sample surface at 1500× magnification (ORNL #310HCbN SS [HR3C Weld]-1).

The ash deposit on the sample was thin and uneven, ranging from 10 to 100 μm thick. SEM analysis of the material indicated that the content of the-ash deposited on samples in the elbow matched that of the ash deposited in the convective pass.

### *NMARL Sample 01-0037 Submitted by Bob' Swindeman, ORNL #625-1*

**Sample description: 33** x 3 1 x l-mm alloy cuboid with an 1 l-mm-diameter hole in the center of larger surface; stainless steel-colored.

**Postexposure appearance:** The Swindeman samples were all exposed in an elbow following the process air tube-and-shell heat exchanger, which immediately follows the convective pass in which the previous samples were exposed. Average gas temperature for the Swindeman samples was 708°C. Figure 91 shows the sample removed from the sample holder after the June test run. The surface looks dull gray through a thin coating of ash deposit. The sample appears intact. The color change suggests surface corrosion.

*SEM* Morphology

The metal is reported to contain 62.4 wt% Ni, 22.1 wt% Cr, 8.1 wt% MO, 3.57 wt% Nb-Ta, 3.2 wt% Fe, 0.28 wt% Si, and 0.23 wt% Ti. Figure 92 shows the cross-sectioned alloy material, corrosion layer, and ash deposit at 100× magnification. The alloy material appears as a homogeneous white field with fine white particles and occasional gray spots scattered throughout the alloy material. SEM analysis of the bulk material indicated a composition of 58.3 wt% Ni, 21.8 wt% Cr, 9 wt% MO, 4 wt% Nb, 3 wt% Fe, 2 wt% 0, 1 wt% Ta, and trace Ti and Si

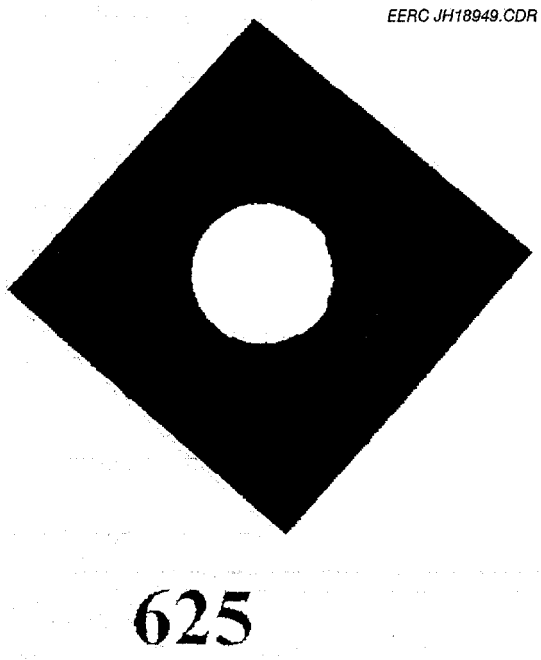


Figure 91. Alloy ORNL #625-1 removed from the sample holder after the June test run.

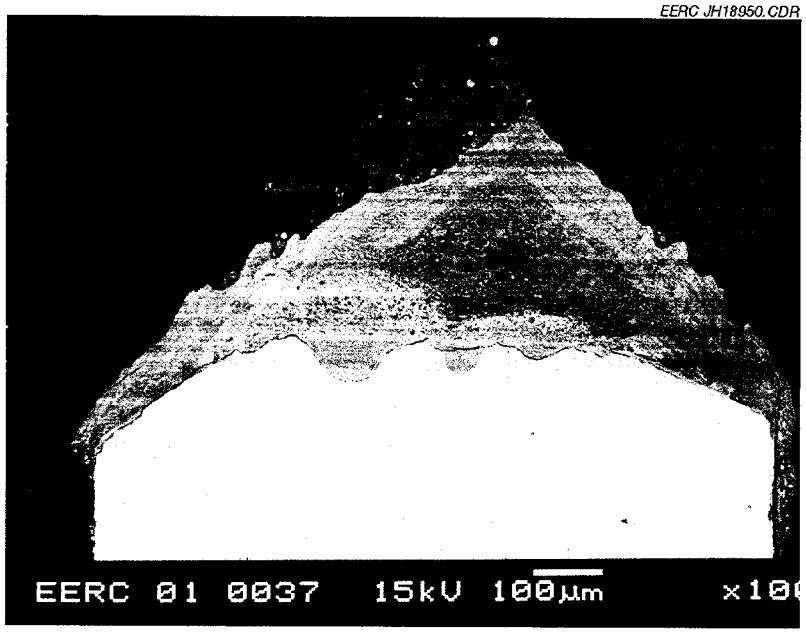


Figure 92. Example of cross-sectioned alloy material, corrosion layer, and ash deposit at 100× magnification (ORNL #625-1).

(cl wt%). The fine white particles include 64 wt% Ni, 10 wt% Cr, 8 wt% MO, 4 wt% Fe, 3 wt% Nb, and 2 wt% 0. The light grey spots are depressions in the cross-sectioned surface, representing voids in the material.

No subsurface corrosion was indicated in the sample cross section. Formation of broad, deep pits and an extensive corrosion layer at the surface are the dominant features of this sample. Figure 92 shows three large and two smaller areas of pitting that extend into the sample below an imaginary line of smooth recession. The homogeneous appearance of the corrosion product within these pitted areas is different than the look of the corrosion product projecting from the surface. The largest pit contains 66 µm of chromium oxide corrosion product (56 wt% Cr, 16 wt% O, 9 wt% Ni, 7 wt% Nb, 4 wt% MO, 3 wt% S, and trace Fe). Figure 93 shows the leftmost pit at 1500× magnification. The content of this corrosion pit matches that of the large pit. The submicron white spots and streaks in the corrosion product are rich in barium and sulfur. They most likely originated in the ash as barium sulfate (barite) particles that are still sticky at the exposure temperature (708 "C).

The surface of the sample is covered with a very thick, continuous layer of corrosion product ranging in thickness from 40 µm at the corners to 350 µm at the center point. Visual inspection and SEM analysis of this layer (visible in left corner of Figure 93 indicated a heterogeneous composition of entrained ash particles embedded in a nickel oxide matrix (55 wt% Ni, 15 wt% O, 8 wt% Fe and Cr, 2 wt% Si, and trace Al and Mg). The composition remains consistent to within 40 µm of the corrosion product-ash interface. In the outermost corrosion product layer, the embedded particle size and Ni content decrease, replaced by increasing Fe and

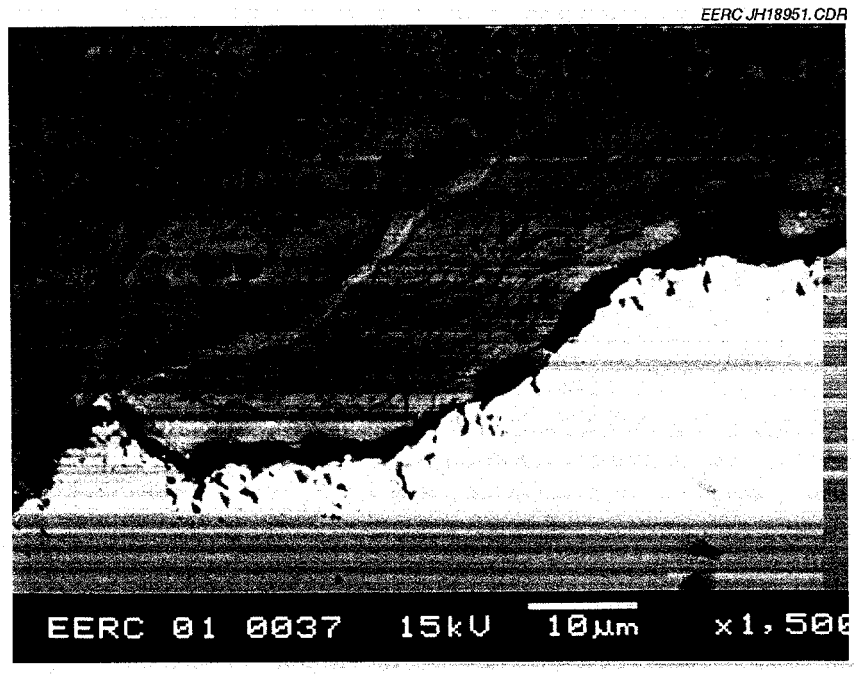


Figure 93. Sample surface at 1500× magnification (ORNL #625-1).

other ash constituents. The corrosion mechanisms throughout appear to be oxidation and sulfidation from the flue gas and interaction with ash constituents, especially Ca and Ba. No halide attack was indicated. No signs of erosive attack were indicated.

The ash deposit on the sample, visible in Figure 92, was limited to <200 µm thick. SEM analysis of the material indicated that the content of the ash deposited on samples in the elbow was similar to that of the ash deposited in the convective pass.

### *NMARL Sample 01-0038 Submitted by Bob Swindeman, ORNL #NF709-1*

**Sample description:** 31.76 x 23.68 x 31.91 x 32.12 x l.l-mm-thick alloy cuboid with 11 -mm-diameter hole in the center of larger surface; stainless steel-colored.

**Postexposure appearance:** The Swindeman samples were all exposed in an elbow following the process air tube-and-shell heat exchanger, which immediately follows the convective pass in which the previous samples were exposed. Average gas temperature for the Swindeman samples was 708°C. Figure 94 shows the sample removed from the sample holder after the June test run. The sample appears intact. The dull gray surface is partially obscured by the fine reddish brown layer of ash deposit. The color change suggests surface corrosion.

SEM Morphology

NF709 is reported to contain 51.114 wt% Fe, 24.88 wt% Ni, 20.52 wt% Cr, 1.48 wt% Mo, 1.03 wt% Mn, 0.41 wt% Si, 0.26 wt% Nb-Ta, .016 wt% N, and <0. 1 wt% C, Ti, P, B, S, and Ce.


Figure 94. Alloy ORNL #NF709-1 removed from sample holder after the June test run.

Figure 95 shows the cross-sectioned alloy material, corrosion layer, and ash deposit at 100× magnification. The alloy material appears as a homogeneous white field in the lower half of the figure. SEM analysis of the bulk material indicated a composition of 51 wt% Fe, 24 wt% Ni, 21 wt% Cr, 1 wt% Mn, and trace Si (<1 wt%).

No subsurface corrosion was indicated in the sample cross section examined. Shallow surface pitting and a thin, discontinuous corrosion layer at the surface are the features of this sample. Figure 96 illustrates these features at 1500× magnification. At the center is a small pit about 10 μm deep and 30 μm wide. The largest pit on the surface was 10 μm deep by 30 μm wide. The thickest corrosion layer above the sample surface was 7 μm high. The composition of the alloy material near sites of corrosive attack appears slightly enriched in Fe (53 wt%), Ni (27 wt%), MO (l-2 wt%), and Si (<1 wt%). One spot analyzed contained 4 wt% Ta. The Cr in these areas was reduced to 14 wt%. Most corrosion products in pits and attached to the surface contain mixtures of Fe (39-44 wt%) Ni (21-28 wt%) 0 (18 wt%) and Cr (32-63 wt%) Fe (14-27 wt%) 0 (11 wt%) with Ni (2-l 1 wt%). The average Si and Mn concentrations in the corrosion product were 1 and 2 wt%, respectively (ranging from <1 to 4 and 5 wt%). MO, Nb, and Ta were present in trace amounts in the corrosion product. Ti was not present. The composition suggests an absence of the chromium oxide layer that could protect the alloy from further attack by flue gas constituents such as 0. The irregular sample surface and discontinuity of the corrosion layer suggest a pattern of sequential pitting and scaling.

Ash constituents Ca and S were occasionally present at high concentrations (O-26 and 1-13 wt%, respectively), suggesting ash interaction in the development of the corrosion layer.

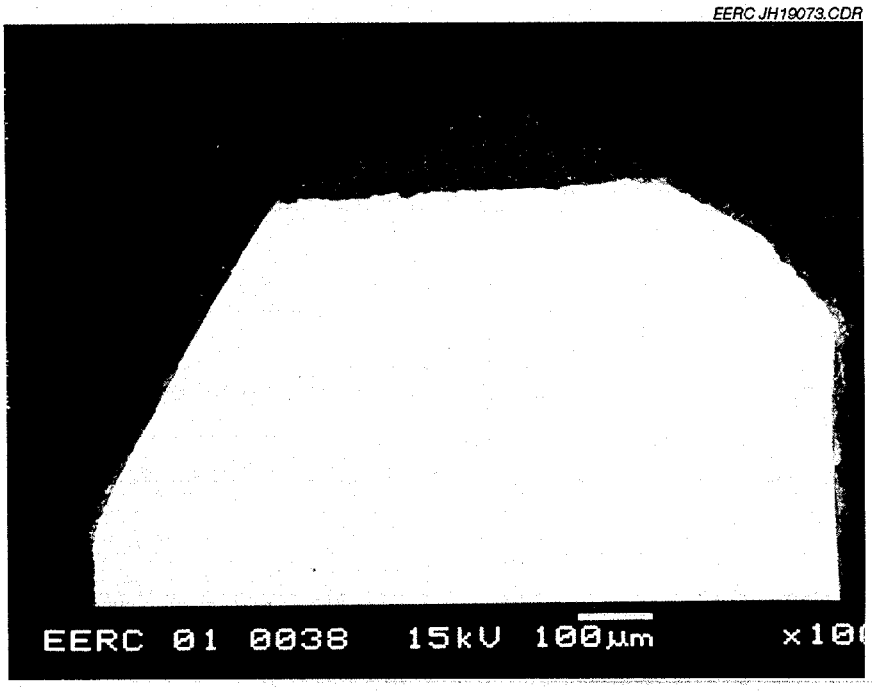


Figure 95. Cross-sectioned alloy material, corrosion layer, and ash deposit at 100× magnification (ORNL #NF709-1).

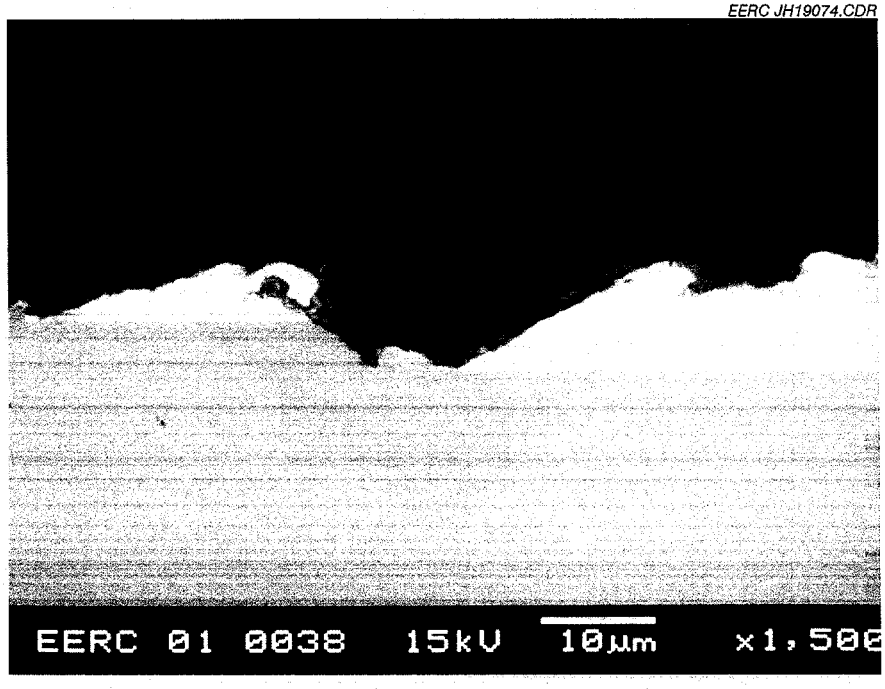


Figure 96. Sample surface at 1500× magnification (ORNL #NF709-1).

Other ash constituents-Al, K, Na, and P-were present at trace levels in the corrosion product. The corrosion mechanisms throughout appear to be oxidation and sulfidation. The irregular sample surface and discontinuity of the corrosion layer suggest a pattern of sequential pitting and scaling.

The amount of ash deposited on the sample, visible in Figure 95, was too limited to perform SEM analysis of the material.

### *NMARL Sample 01-0039 Submitted by Bob Swindeman, ORNL #RA253MA-1*

**Sample description:** 32 square x 3.04-mm alloy cuboid with an 1 l-mm-diameter hole in the center of larger surface; stainless steel-colored.

**Postexposure appearance:** The Swindeman samples were all exposed in an elbow following the process air tube-and-shell heat exchanger, which immediately follows the convective pass in which the previous samples were exposed. Average gas temperature for the Swindeman samples was 708°C. Figure 97 shows the sample removed from the sample holder after the June test run. The surface has hints of dark gray color under a thin brown coating of ash particle. The sample appears to be intact.

SEM Morphology

The metal is reported to contain 66.776 wt% Fe, 20.8 wt% Cr, 10.99 wt% Ni, 0.55 wt% Mn, 0.4 wt% Si, 0.18 wt% MO, and 0.15 wt% N. Figure 98 shows the cross-sectioned alloy material, corrosion layer, and ash deposit at 100× magnification. The alloy material appears as a

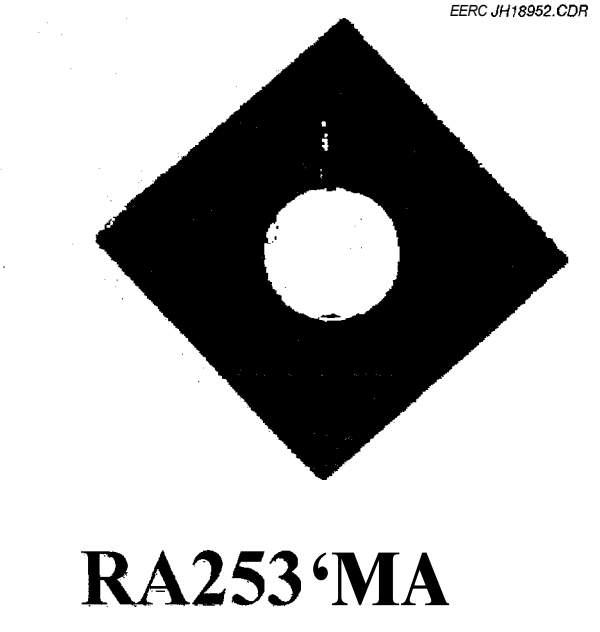


Figure 97. Alloy ORNL #RA253MA-1 removed from the sample holder after the June test run.

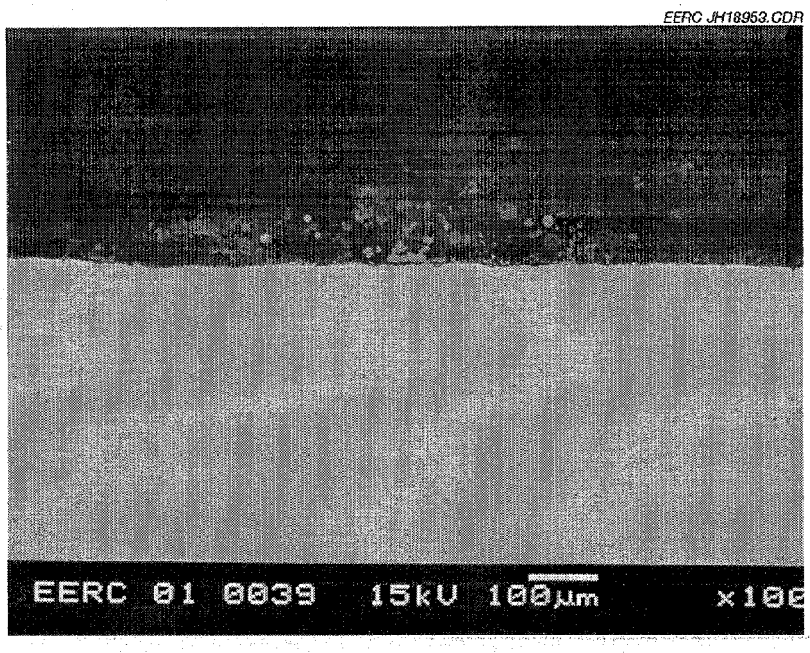


Figure 98. Example of cross-sectioned alloy material, corrosion layer, and ash deposit at 100× magnification (ORNL #RA253MA-1).

homogeneous white field in the lower half of the figure. SEM analysis of the bulk material indicated a composition of 61 wt% Fe, 21 wt% Cr, 11 wt% Ni, 1 wt% Si and Mn, and trace Nb, 0, and P (<1 wt%).

No subsurface corrosion was indicated in the sample cross section. Shallow surface pitting and a thin, discontinuous corrosion layer at the surface are the features of this sample. Figure 99 illustrates these features at 1500× magnification. To the left of center is a small pit, about 1 µm deep and 5 µm wide. The largest pit on the surface was 3 µm deep by 65 pm wide. The thickest corrosion layer above the sample surface was 24 µm high. Most above-surface layers, however, were <10 µm thick. The composition of the alloy material near sites of corrosive attack does not appear altered. Most corrosion products in pits and attached to the surface included a high percentage of Fe (37-58 wt%) with an average of 17 wt% Cr; 13 wt% Ni and 0; 4 wt% Si; 1 wt% S, K, and Al; and trace Ca and Mg. Even areas high in Cr (40 wt%) and 0 (19 wt%) contained 27 wt% Fe, suggesting the absence of the chromium oxide layer that could protect the alloy from further attack by flue gas constituents such as 0. The irregular sample surface and discontinuity of the corrosion layer suggest a pattern of sequential pitting and scaling. The corrosion mechanisms throughout appear to be oxidation and sulfidation. No halide attack or ash constituent interaction was indicated.

The ash deposit on the sample, visible in Figure 98, was very limited. SEM analysis of the material indicated a higher-than-average Fe content of the ash deposited on the sample. The Si and Al content were less than that of the ash deposited in the convective pass.

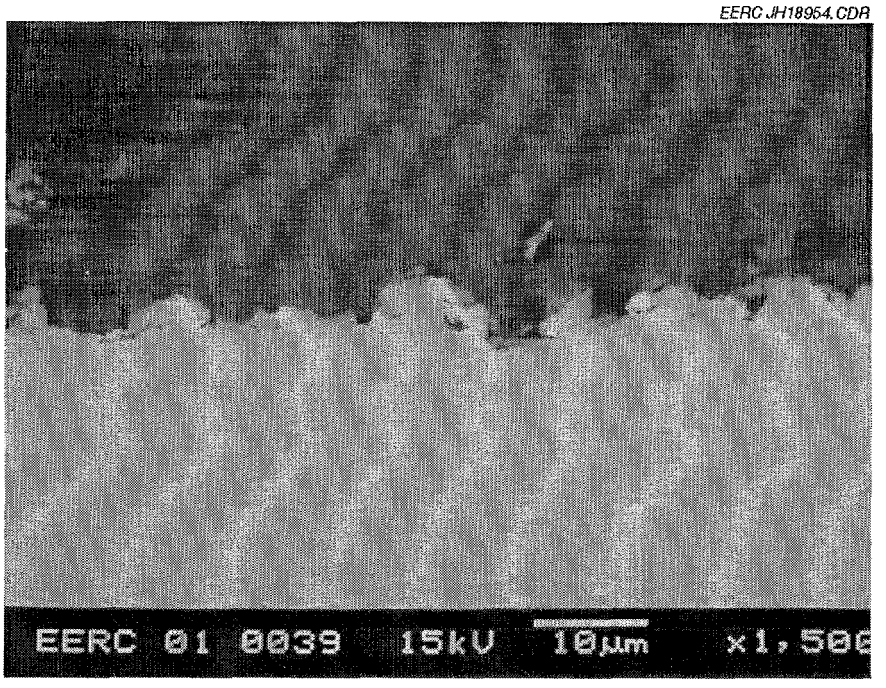


Figure 99. Sample surface at 1500× magnification (ORNL #RA253MA-1).

### *NMARL Sample 01-0040 Submitted by Bob Swindeman, ORNL #12RN72-1*

**Sample description:** 32.65 x 3 1.57 x 31.87 x 32.00 x 1.5-mm-thick alloy cuboid with 11-mm-diameter hole in the center of larger surface; stainless steel-colored.

**Postexposure appearance:** The Swindeman samples were all exposed in an elbow following the process air tube-and-shell heat exchanger, which immediately follows the convective pass in which the previous samples were exposed. Average gas temperature for the Swindeman samples was 708°C. Figure 100 shows the sample removed from the sample holder after the June test run. The surface is coated with a thin brown layer of ash particle. The sample appears intact.

SEM Morphology

Sample 12RN72 is reported to contain 51.608 wt% Fe, 25.01 wt% Ni, 19.13 wt% Cr, 1.76 wt% Mn, 1.37 wt% Mo, 0.54 wt% Ti, 0.45 wt% Si, and <0. 1 wt% C, N, P, B, and S. Figure 101 shows the cross-sectioned alloy material, corrosion layer, and ash deposit at 100× magnification. The alloy material appears in the lower half of the figure as bright white spots incorporated into a white field. SEM analysis of the bulk material indicated a composition of 49 wt% Fe, 25 wt% Cr, 21 wt% Ni, 2 wt% Mn, 1 wt% Si, and trace Ti and 0 (cl wt%). The composition of the white field is 53' wt% Fe, 23 wt% Ni, 2 1 wt% Cr, 2 wt% Mn, and trace Si and 0. The bright white spots comprise 40 wt% Fe, 32 wt% Cr, 12 wt% Ni, 8 wt% Si, 3 wt% Ti, 1 wt% Mn, and trace 0, Nb, and P.

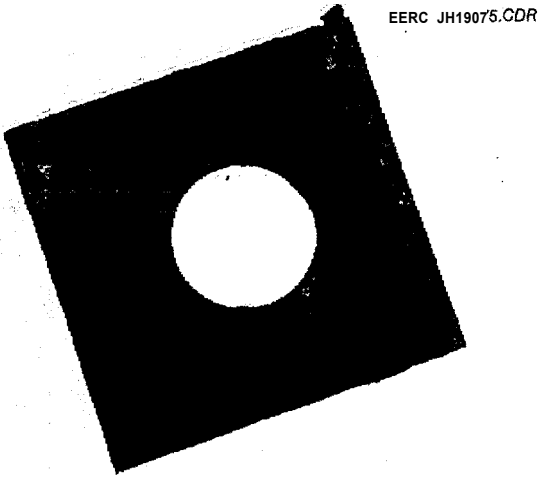


Figure 100. Alloy ORNL #12RN72-1 removed from sample holder after the June test run.

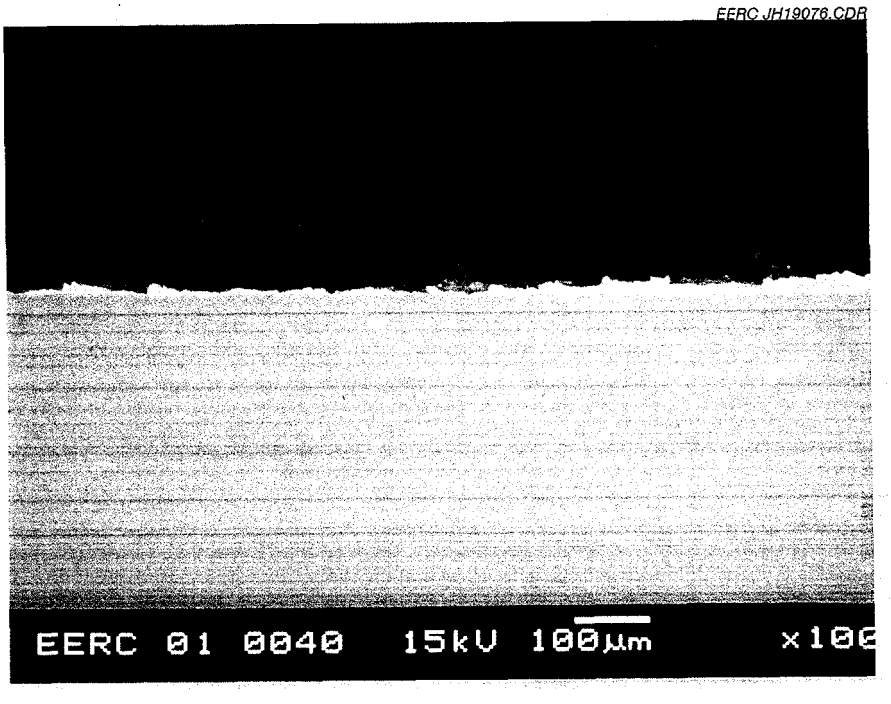


Figure 101. Cross-sectioned alloy material, corrosion layer, and ash deposit at 100× magnification (ORNL #12RN72-1).

No subsurface corrosion was indicated in the sample cross section examined. Surface corrosion consisted of a thin, discontinuous corrosion layer. Figure 101 includes the largest example of corrosion product at the center of the figure. Also illustrated in this figure is the typical irregular scaling observed throughout the sample surface in the cross section examined. Figure 102 is the large corrosion product at the center of Figure 101 at 1500× magnification. The mass is 45μm high and 80 pm wide. It includes large cracks and entrained ash particles and appears ready to separate from the sample surface. The composition of the alloy material near sites of corrosive attack was similar to the rest of the alloy material in the sample. The alloy-corrosion interface is mainly chromium (5 l-58 wt%) oxide (7-30 wt% 0) with some Fe (7-25 wt%), Ni (4-7 wt%), Mn (<5 wt%), Si (<4 wt%), and Ti (<2 wt%) and includes the band presented as bright white spots and adjacent light gray in Figure 102. The white spots contain more Si, Mn, and Ti; trace of Nb and P; and less Ni than the alloy-corrosion interface. Above this band, the corrosion layer is made up of entrained ash particles in a matrix comprising iron (41-61 wt%) nickel (9-29 wt%) oxide (15-21 wt% 0) with up to 20 wt% Cr and small amounts of Si and Mn and trace S. The entrained ash particles contain either Fe and aluminosilicates or Ca, S, and 0. The irregular sample surface and discontinuity of the corrosion layer suggest a pattern of sequential pitting and scaling. The layered nature of the corrosion layer and its composition suggest initial formation of an Fe0 layer followed by a CrO layer once the Fe content decreases. The underlying CrO layer does not remain attached to the alloy. The corrosion mechanism throughout appears to be oxidation.

The ash deposit on the sample, visible in Figure 101, was very limited. SEM analysis of the material indicated a composition unusually high in Nb-39 wt% 0; 15 wt% Si; 8 wt% Al and

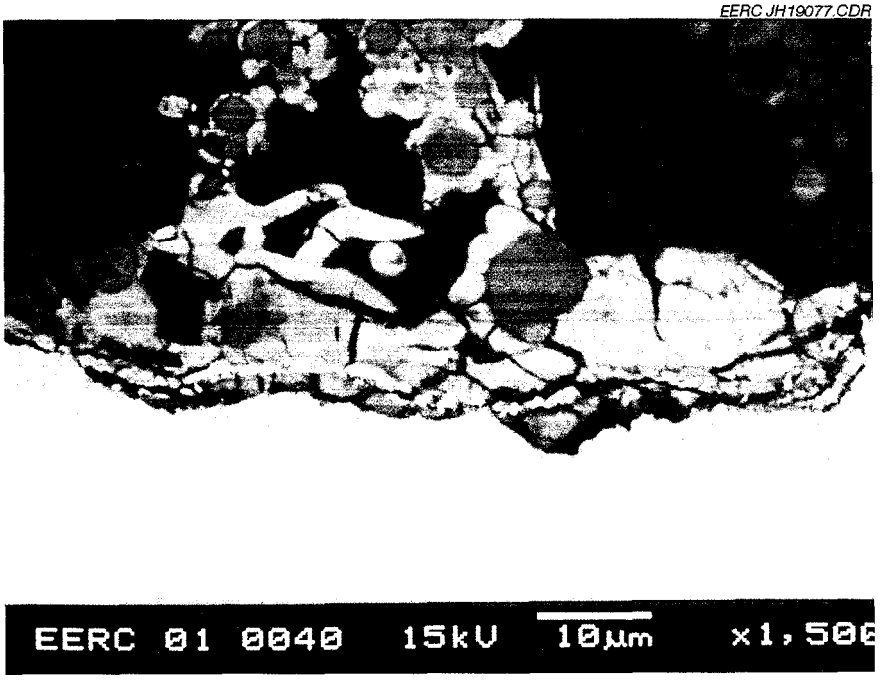


Figure 102. Sample surface at 1500× magnification (ORNL #12RN72-1).

Nb; 7 wt% S; 6 wt% Fe; 5 wt% Ca; 2 wt% K, P, Ba, and Ni; and trace Mg-probably resulting from the limited ash sample available.

### *NMARL Sample 01-0041 Submitted by Bob Swindeman, ORNL #310TaN-1*

**Sample description: 32.56** x 3 1.72 × 32.13 × 32.14-mm parameter x 1.5-mm-thick alloy cuboid, with an 1 l-mm-diameter hole in. the center of larger surface; stainless steel-colored.

**Postexposure appearance:** The Swindeman samples were all exposed in an elbow following the process air tube-and-shell heat exchanger, which immediately follows the convective pass in which the previous samples were exposed. Average gas temperature for the Swindeman samples was 708°C. Figure 103 shows the sample removed from the sample holder after the June test run. The surface is coated with a thin brown layer of ash particle. The sample appears intact.

SEM Morphology

The 310TaN alloy is reported to contain 51.176 wt% Fe, 24.9 wt% Cr, 20.2 wt% Ni, 1.6 wt% Nb-Ta, 1.53 wt% Mn, 0.33 wt% Si, 0.2 wt% N, and <0.1 wt% C, P, and S. Figure 104 shows a representative example of the cross-sectioned alloy material, corrosion layer, and ash deposit at 100× magnification. The alloy material appears as a homogeneous light gray field with fine white particles and occasional dark gray voids (depressions in the cross-section surface) scattered throughout the alloy material. SEM analysis of the bulk material indicated a composition of 48.8 wt% Fe, 23.9 wt% Cr, 19.4 wt% Ni, 3.5 wt% Nb, 2.2 wt% Mn, and cl wt%

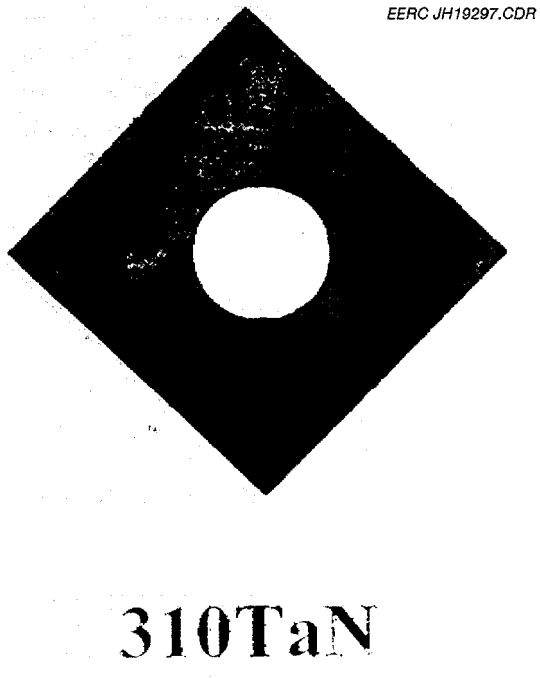


Figure 103. Alloy ORNL #310TaN-1 removed from the sample holder after the June test run.

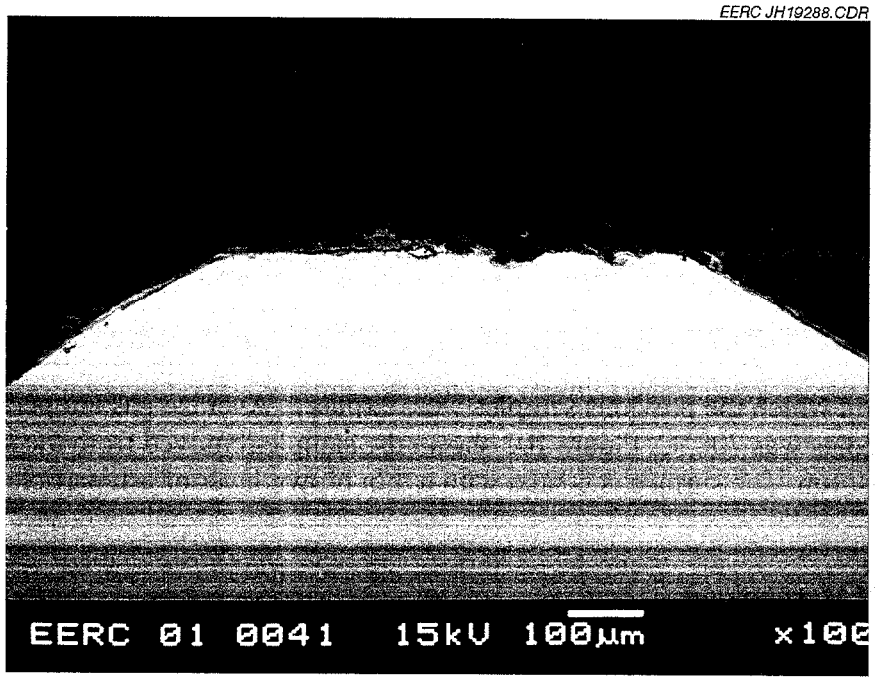


Figure 104. Example of cross-sectioned alloy material, corrosion layer, and ash deposit at 100× magnification (ORNL #310TaN-1).

Si and 0. The fine particles were high in Nb (54-66 wt%), Si (15-19 wt%), and Ti (6 wt%) and included low levels of Fe (3-l 1 wt%), Cr (O-9 wt%), Ni (2 wt%), Mo (1 wt%), and <1 wt% P, 0, and S.

Subsurface corrosion in the sample cross section examined was limited to a few thin intrusions extending less than 20 µm deep and 30-50 µm wide into the sample. Figure 104 includes two such intrusions and one pit 80 µm wide present on the upstream surface of the sample cross section. Figure 105 shows the sample surface at 1500× magnification, including the intrusion to the right of the pit in Figure 104. The alloy material adjacent to the intrusions shows loss of Cr and increased concentration of Fe (57-64 wt%) and Ni (25 wt%).

The Fe and Ni content of much of the corrosion product at the alloy interface is similar to that of the bulk alloy. Some of the Cr (now at 16 wt%) was replace by 0 (13 wt%) and trace K, S, and P. Mn and Nb are not present. The white corrosion product layer visible in Figure 105 in the intrusion and surface corrosion product is Cr and 0 with high Nb (5-24 wt%) and low Fe (5-15 wt%) content. The light gray material at the center of the corrosion product is Cr (61 wt%) 0 (21 wt%) with 6 wt% Mn, 5 wt% Fe, and trace Si, Ni, Al, S, P, and K.

The surface of the sample contains a very thin, continuous layer of corrosion product a few µm thick. The concentration of corrosion product beyond the white Nb-containing layer is 55 wt% Fe, 20 wt% Ni and O, 3 wt% Cr, and trace K, S, Mn, and Si. This FeNiO layer also contains entrained ash particles.

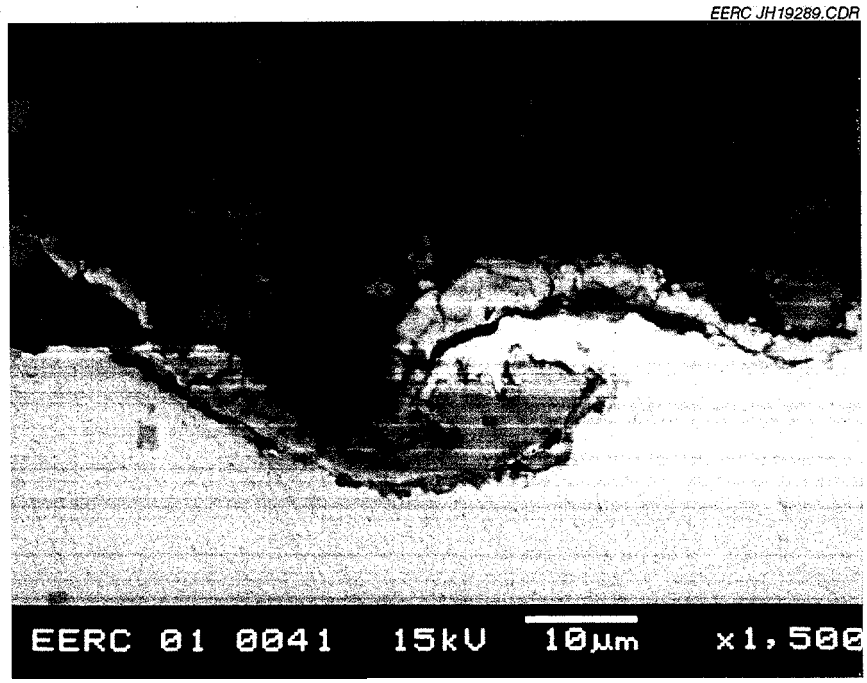


Figure 105. Sample surface at 1500× magnification (ORNL #310TaN-1).

The ash deposit on the sample was insufficient for bulk analysis.

***NMARL Sample 01-0042 Submitted by Bob Swindeman, ORNL #31 0HCbN-1***

**Sample description:** 32.84 x 31.21 x 31.68 x 31.17-mm perimeter x 3.18-mm-thick alloy cuboid, with an 1 l-mm-diameter hole in the center of larger surface; stainless steel-colored.

**Postexposure appearance:** The Swindeman samples were all exposed in an elbow following the process air tube-and-shell heat exchanger, which immediately follows the convective pass in which the previous samples were exposed. Average gas temperature for the Swindeman samples was 708°C. Figure 106 shows the sample removed from the sample holder after the June test run. The surface is coated with a thin brown layer of ash particle. The sample appears intact.

SEM Morphology

The 310HCbN alloy is reported to contain 54.243 wt% Fe, 24.23 wt% Cr, 18.68 wt% Ni, 1.61 wt% Mn, 0.64 wt% Si, 0.32 wt% Nb-Ta, 0.2 wt% N, and <0.1 wt% C, P, and S. Figure 107 shows a representative example of the cross-sectioned alloy material, corrosion layer, and ash deposit at 100× magnification. The alloy material appears as a homogeneous white field with occasional dark gray voids (depressions in the cross-section surface) scattered throughout the alloy material. Under high magnification (2000x), fine white particles become visible. SEM analysis of the bulk material indicated a composition of 49.8 wt% Fe, 25.1 wt% Cr, 20 wt% Ni,

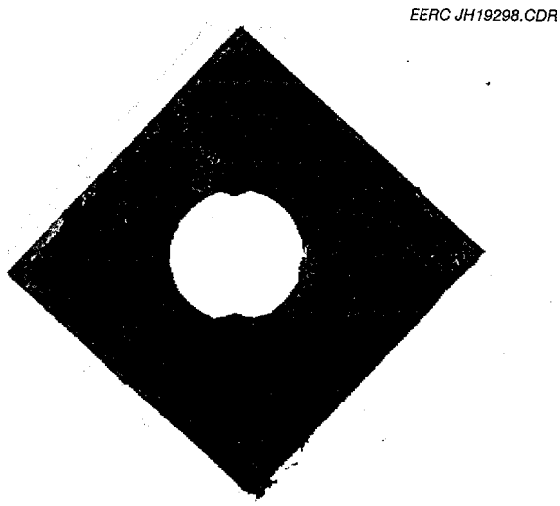


Figure 106. Alloy ORNL #310HCbN-1 removed from the sample holder after the June test run.

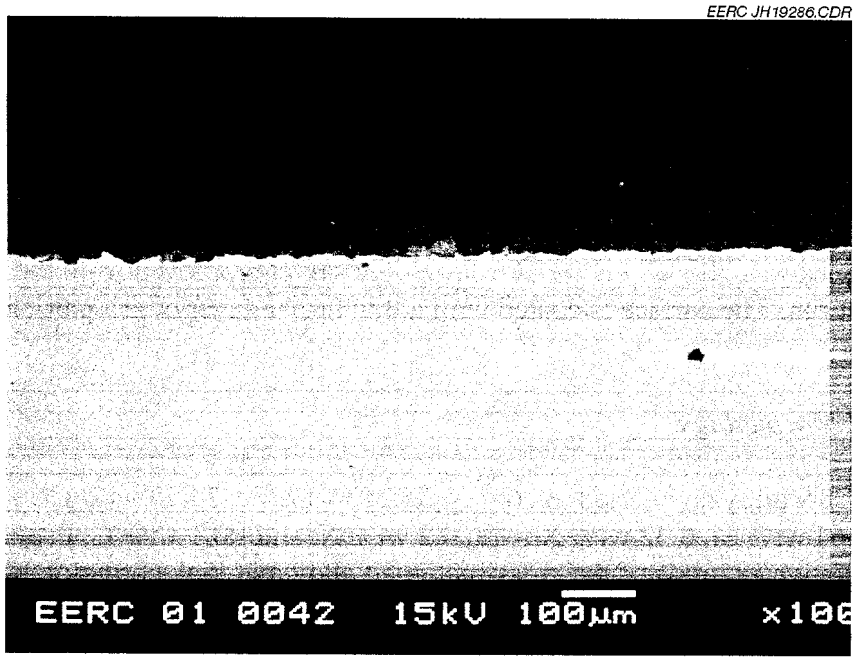


Figure 107. Example of cross-sectioned alloy material, corrosion layer, and ash deposit at 100× magnification (ORNL #310HCbN-1).

2 wt% Mn, 1 wt% Nb, and <1 wt% Si and 0. The fine particles were high in Nb (56.2 wt%) and Cr (3 1 wt%) and included low levels of Fe (7 wt%) and Ni and 0 (1 wt% each).

Subsurface corrosion in the sample cross section examined was limited to a few thin intrusions extending less than 20 μm deep and 40 μm wide into the sample. Figure 108 shows one such intrusion in the sample surface at 1500× magnification. The content of the corrosion product in the intrusion is mainly Cr, with the thickest mass comprising Cr (55 wt%) 0 (18 wt%), with some Mn (10 wt%), Fe (6 wt%), Ni (4 wt%), Nb and Si (2 wt%), and traces of S, Ca, K, and Al. Thinner sections of the subsurface corrosion product contain more Fe (28 wt%) and Ni (10 wt%) and less 0 (11 wt%), possibly due to inclusion of underlying alloy material in the SEM analysis of the corrosion product. In any case, the corrosion product content indicates loss of Fe and Ni, oxidation into the near-subsurface, and limited infiltration by other ash constituents.

The surface of the sample contains shallow pits extending 10 μm deep and up to 50 μm wide and is coated with a very thin, discontinuous layer of corrosion product l-5 μm thick. Figure 109 shows a typical pit at 2000× magnification. According to SEM analysis, Mn and Nb are absent from the alloy at the corrosion product interface, Cr content has decreased (20 wt%), and Fe and Ni content have increased (56 and 22 wt%, respectively). Traces of S and Ca are present in addition to Si. The corrosion product near the alloy interface is similar in content to but more oxidized than the corrosion product in the subsurface intrusion. In addition to Cr (5 1 wt%) and 0 (22 wt%), it contains 12 wt% Fe; 7 wt% Ni; 2 wt% Nb; 1 wt% K, Ca, Si; and S, and trace Mn. This layer appears medium gray in Figure 108. Moving away from the alloy, the next layer of corrosion product in Figure 108 is the white layer, which is also CrO, but contains more Mn

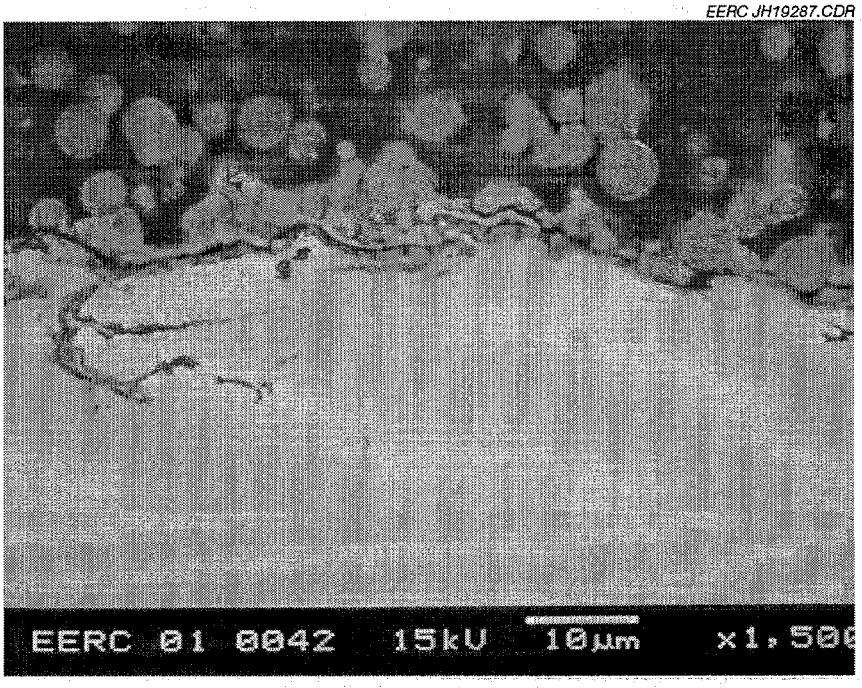


Figure 108. Sample surface at 1500× magnification (ORNL #3 10HCbN-1).

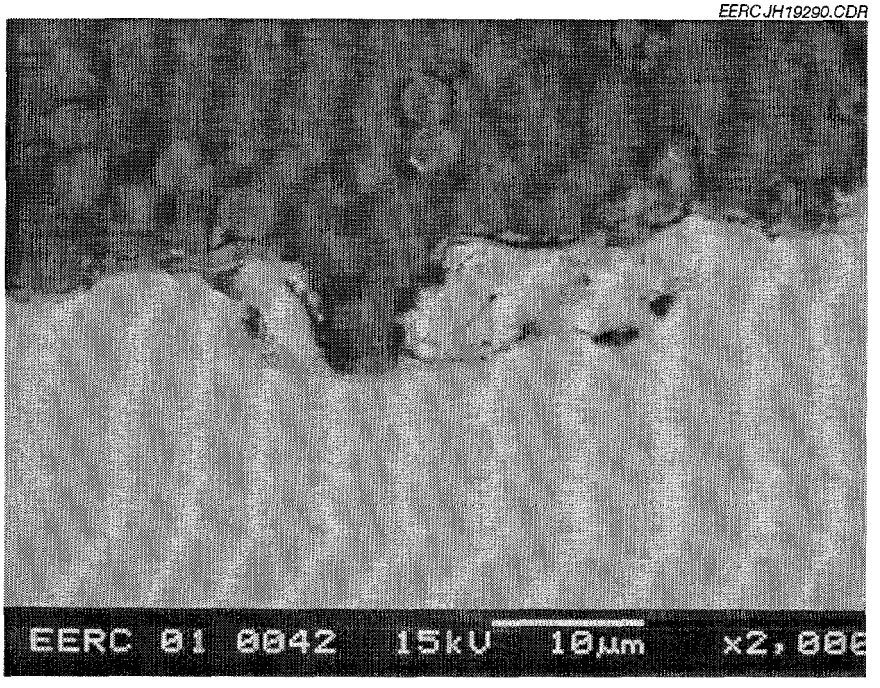


Figure 109. Typical surface pit at 2000× magnification (ORNL #310HCbN-1).

(8-15 wt%) and less Fe (8 wt%) and Ni (4 wt%). Trace Si, S, Nb, Ca, K, and Al are also present. This layer is detached from the medium gray CrO layer, possibly a result of sample preparation. Beyond this white layer, the corrosion product becomes a mixture containing Fe0 with Cr and Ni and entrained ash particles. Evidence of ash constituents incorporated into this layer includes the presence of Ti (8 wt%) and Mg (30 wt%) at two points in the matrix. The irregular sample surface and discontinuity of the corrosion layer suggest a pattern of sequential pitting and scaling. The corrosion mechanism throughout appears to be oxidation. Some sulfidation was indicated although the concentration of S was usually no more than 1 wt%. No halide attack was indicated.

The ash deposit on the sample as seen in Figure 107 was thin and uneven, ranging from 10 to 100 µm thick. SEM analysis of the thickest material indicated that the content of the ash deposited on samples in the elbow matched that of the ash deposited in the convective pass.

### *NMARL Tube Sample 01-0463 Alloy 956*

**Sample description:** 48-mm-outer-diameter tube x 30 mm long x 5.5-mm wall thickness; stainless steel-colored. This sample was taken from an uncooled pipe inserted in the CAH to set up the gas flow through the cooled CAH tubes. It was installed in the CAH in September 1998 and exposed in the system to approximately 2000 hours of combined gas and coal firing as part of the Combustion 2000 program. Its analysis is described here for comparison to the analyses of the other alloys exposed under the ORNL program.

**Postexposure appearance:** The surface is mostly coated with a thin brown layer, probably corrosion product. There are occasional spots where shiny metal is visible. The sample appears intact.

SEM Morphology

Metal Alloy 956 is reported to contain 73-75 wt% Fe, 19-21 wt% Cr, 4.5 wt% Al, 0.1-0.5 wt% Ti, and 0.5 wt% $Y_2O_3$. Figure 110 shows the cross-sectioned alloy material and corrosion layer at 100× magnification. The alloy material appears in the lower half of the figure as a homogeneous white field. Occasional dark spots in the material are depressions in the sample surface suggestive of voids inherent in the material. SEM analysis of the bulk material indicated a composition of 75.1 wt% Fe, 19.6 wt% Cr, 3.2 wt% Al, and trace 0 (<1 wt%).

No subsurface corrosion was indicated in the sample cross section examined. Surface corrosion consisted of a thin, mostly continuous corrosion layer. Figure 111 includes a typical example of corrosion product at 1500× magnification. The composition of the alloy material near the corrosion product interface was similar to the bulk material. The corrosion layer is <20 μm thick and is composed of two distinct layers. The inner, uniform layer of Al (63 wt%) 0 (33 wt%) with l-2 wt % Fe and Cr is l-7 μm thick. The outer layer comprises a heterogeneous mixture of regions composed of Fe (52 wt%), Al and 0 (each 18 wt%), and other regions composed of Al (38 wt%), 0 (28 wt%), Fe (15 wt%), both with small amounts (<6 wt%) of Mg, Ti, Na, Si, Ca, Cr, Ni, Mn, P, and Ba. The SEM analysis also indicated points comprising ash constituents and voids in the outer corrosion layer. The heterogeneous layer of corrosion product

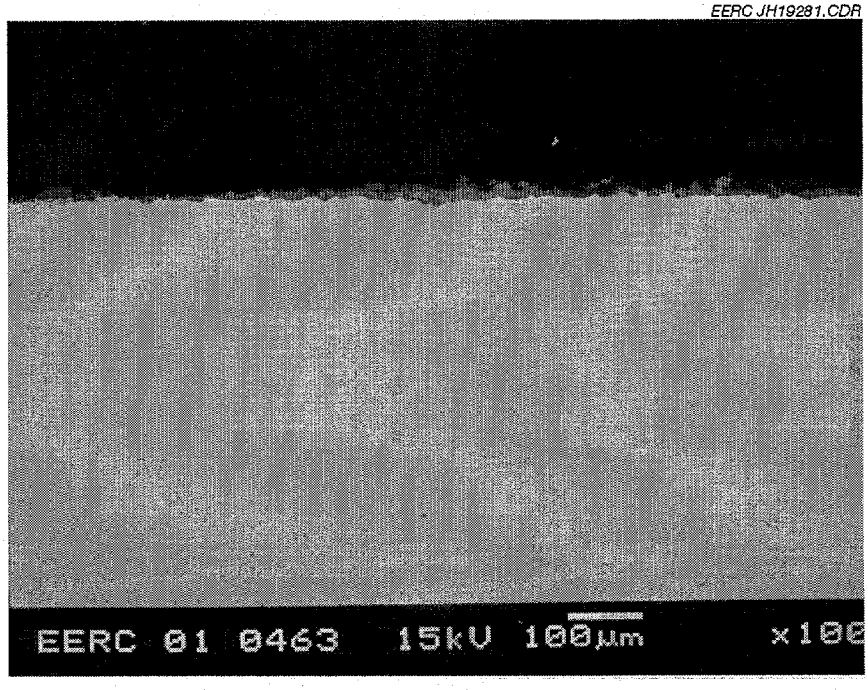


Figure 110. Cross-sectioned alloy material, corrosion layer, and ash deposit at 100× magnification (956).

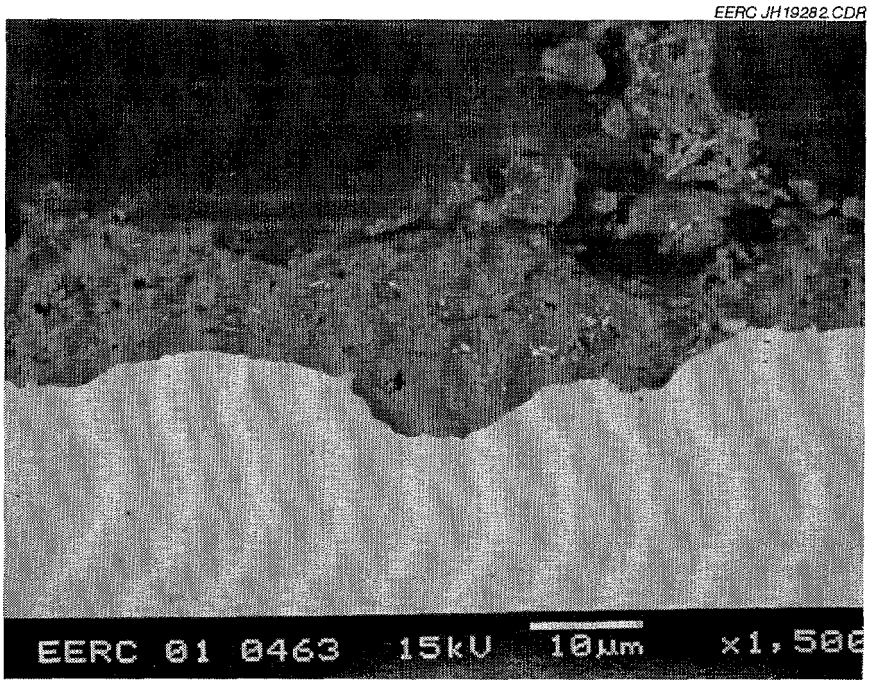


Figure 111. Typical example of corrosion product at 1500× magnification (956).

measured between 7 and 11 µm thick. At one section of the sample surface (approximately 20% of the perimeter included in the sample) the corrosion layer appeared to have separated from the alloy surface. There also appears to be damage to the alloy at the corrosion layer interface. Although the source of this damage is unknown, it may be associated with sample removal or preparation for analysis. Overall, the alloy appears to be well protected from the ash constituents by the alumina scale. The double layer of the corrosion product suggests two reaction pathways in the formation of the corrosion product, possibly. One interesting observation is the disappearance of Cr from the alloy. While the corrosion layer contains remains of the Fe from the alloy, no Cr was found beyond 2 wt%.

No ash deposit remained on the sample when it was submitted for analysis. Given its location in front of the CAH tubes and the presence of ash constituents in the outer corrosion layer, it is expected that the sample would have been coated with an ash deposit of composition similar to that previously reported during exposure in the SFS.

### *NMARL Tube Sample 01-0464 Alloy 956HT*

**Sample description:** 34-mm-outer-diameter tube x 30 mm long x 3-mm wall thickness; stainless steel-colored. This sample was taken from an uncooled pipe inserted in the CAH to set up the gas flow through the cooled CAH tubes. It was installed in the CAH in September 1998 and exposed in the system to approximately 2000 hours of combined gas and coal firing as part of the Combustion 2000 program. Its analysis is described here for comparison to the analyses of the other alloys exposed under the ORNL program.

**Postexposure appearance:** The surface is mostly coated with a thin brown corrosion and ash layer. There are occasional spots where shiny metal is visible.

SEM Morphology

Metal Alloy 956 is reported to contain 73-75 wt% Fe, 19-21 wt% Cr, 4.5 wt% Al, 0.1-0.5 wt% Ti, and 0.5 wt% $Y_2O_3$. Alloy 956HT is expected to have a similar content. Figure 112 shows the cross-sectioned alloy material and corrosion layer at 100× magnification. The alloy material appears in the lower half of the figure as a white field. At higher magnification (Figures 113 and 114), medium and dark gray spots become visible. SEM analysis of the bulk material indicated a composition of 7 1.7 wt% Fe, 22.3 wt% Cr, 4.2 wt% Al, and trace Ti and 0 (<1 wt%). The medium gray spots are Ti-rich (50 wt% Ti replacing half of all other constituents). Occasional dark spots in the material are depressions in the sample surface suggestive of voids inherent in the material.

No subsurface corrosion was indicated in the sample cross section examined. Surface corrosion consisted of a thin, mostly continuous corrosion layer. Figure 113 includes a typical example of corrosion product at 1500× magnification. The composition of the alloy material near the corrosion product interface was similar to the bulk material with the addition of <1 wt% Si. The corrosion layer is < 20 μm thick and is composed of two distinct layers. The inner layer of Al (63 wt%) 0 (34 wt%) with <3 wt% Cr, l-2 wt% Fe, and trace Ti and Ca is uniformly 3 μm thick. The outer layer comprises a heterogeneous mixture of Fe (50 wt%) 0 (22 wt%) and ash constituents. The SEM analysis also indicated voids in the outer corrosion layer. The

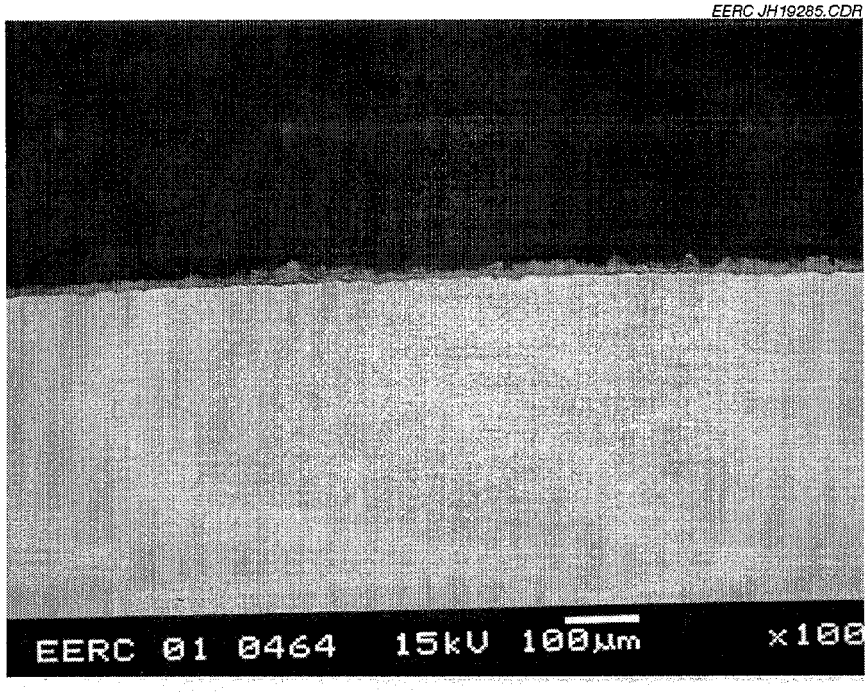


Figure 112. Cross-sectioned alloy material, corrosion layer, and ash deposit at 100× magnification (956HT).

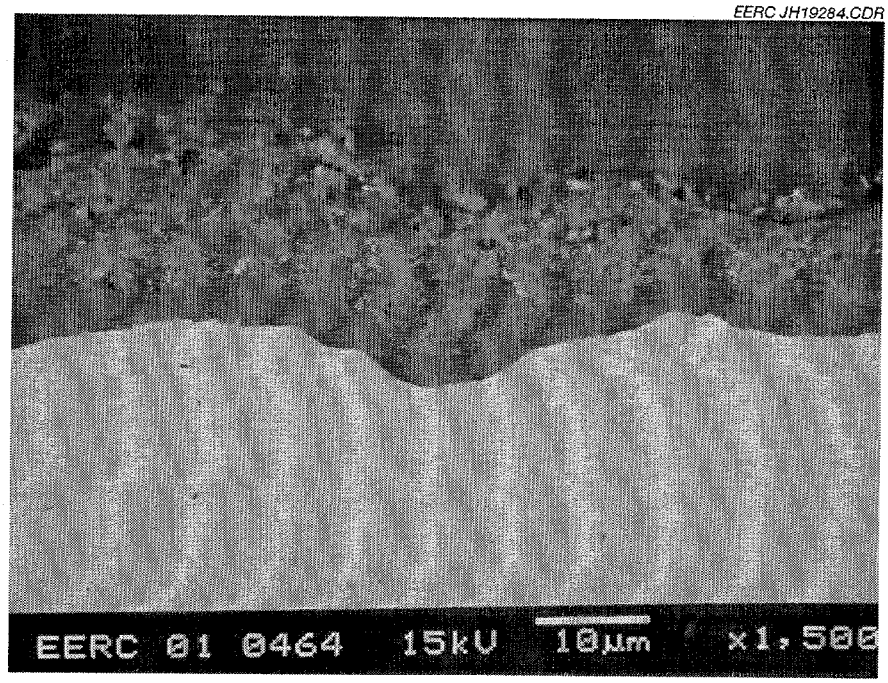


Figure 113. Typical example of corrosion product at 1500× magnification (956HT).

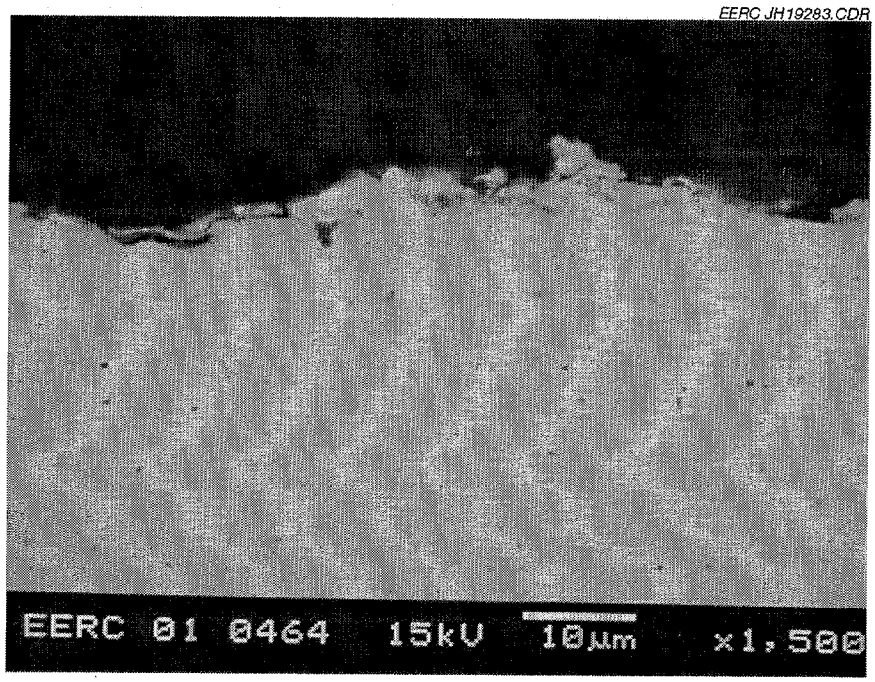


Figure 114. Sample surface without corrosion product at 1500× magnification (956HT).

heterogeneous layer of corrosion product measured <17 μm thick. The corrosion layer appeared well formed and well attached to the alloy surface except at one small section of the perimeter where the alloy surface was exposed. This area is shown at 1500× magnification in Figure 114. There appears to be damage to the alloy similar to the damage observed on NMARL sample 01-0463 at the corrosion layer interface. Although the source of this damage is unknown, it may be associated with sample removal or preparation for analysis. It is likely that the corrosion layer was separated and lost when this damage occurred. Overall, the alloy appears to be well protected from the ash constituents by the alumina scale. The doublelayer of the corrosion product suggests two reaction pathways in the formation of the corrosion product. One interesting observation is the disappearance of Cr from the alloy. While the corrosion layer contains remains of the Fe from the alloy, no Cr was found beyond 3 wt%.

No ash deposit remained on the sample when it was submitted for analysis. Given its location in front of the CAH tubes and the presence of ash constituents in the outer corrosion layer, it is expected that the sample would have been coated with an ash deposit of composition similar to that previously reported during exposure in the SFS.

It should be noted that comparison between 956 and 956HT reveals little difference in behavior during this test with either the visual inspection or the SEM analysis. The 956HT contained spots of Ti in the alloy and had a slightly more uniform alumina scale layer at the sample surface. It may have fewer voids at the alloy-corrosion product interface. However, both alloys performed very well during their 2000 hours of exposure.

## CONCLUSIONS

### Comparison of Material Performance During SFS Tests

#### *Effects of Coal Ash Composition on Corrosion Product Formation*

All sample types were examined for differences in corrosion behavior that could be traced to differences in composition between the coals fired in the two SFS tests. Of all of the alloy samples exposed, only two were available for exposure in each of the tests: ORNL 17681 and ORNL 17433. For each of the two alloys, one coupon of each was exposed in just the March test, and another coupon of each was exposed in both tests. For Alloy ORNL 1768 1, the sample exposed to both tests performed very similarly to that exposed to just the March test. For Alloy ORNL 17433, the sample exposed during both tests performed better than its duplicate, which was subject to breakout corrosion during the first exposure. Absence of significant differences in performance may indicate that either the protective barrier formed during the first test was sufficient to prevent further corrosion during the second exposure or that the second test introduced no new mode of attack despite different ash matrices. As with the metal alloys, the SiC/SiC ceramic composites, one of which was exposed during both tests, exhibited no evidence of reaction differences based on ash type. Unlike the SiC/SiC ceramics, each of the mullite ceramics was exposed only once. Jan 1 l-l and ORNL Ceramic B were exposed during the March test; ORNL 3-1, ORNL 3-2, ORNL 3-3, ORNL 3-4, ORNL 5-1, and ORNL 5-2 were exposed

during the June test. The major difference between exposed groups was the increased Fe content in the corrosion product of the June-tested samples. This is not surprising since the second ash deposited during that test was higher in Fe than previously deposited ashes. No significant differences were perceived on the mullite ceramic rings exposed during different tests.

A truer comparison of ash effects would result from duplicate samples, one of each being exposed during one test and the other during the other test. During these tests, however, the focus was on extending exposure time rather than exploring the effects of ash. Unfortunately, no coupons exposed in the SFS system were treated in a manner that such that coal-specific effects on the samples could be determined.

### *Scale Formation and Ash Interaction*

The 15 metal alloys and two ceramic composites were divided based on scale formation, and their performance was compared. Most samples exposed in the CAH pass and elbow formed one of four main types of scale: alumina, chromia, silica, and tantala. The Cr/Ta alloy sample exposed to high temperatures (15 10°C) and corrosive flue gas constituents just downstream of the slag screen dissolved into the slag. No scale formation occurred.

#### *Samples Exposed at 950 °C in the CAH Pass*

Ceramic and alloy samples exposed to flue gas and ash deposition in the CAH pass formed all four types of scale listed above and exhibited various general trends with respect to ash interaction and corrosion penetration.

Alumina: The mullite ceramic rings, Alloy 956, ORNL 17682, and ORNL 17433, formed alumina-rich or pure alumina scales. The alumina scales tended not to interact with ash constituents except Ca and Si. The low level of interaction was indicated by the fact that the ash layers tended to separate from the oxide scales upon sample cooling. Any ash constituents dissolved into the sample formed in a corrosion product separate from the alumina scale. Some alumina scales formed good barriers to subsurface corrosion, but some did not, most likely due to the differences in the concentration of aluminum in the alloy.

Chromia: ORNL 17681, Alloy 803, Alloy 020, and the Cr/Ta alloy formed chromia scales. The chromia scales were much more bonded to the ash deposits than were the alumina scales. SEM analyses showed that all chromia scales forming on the CAH pass alloys underwent some interaction with ash constituents. Most of these samples exhibited either shallow subsurface corrosion or hollow pores, indicating loss of alloy material.

Silica: The only samples that formed a relatively exclusive silica scale were the SiC/SiC rings. ORNL 1768 1, exposed during both tests, formed silica–chromia scale. In all cases, the scale interacted with ash constituents more than did the alumina scales, but less than the chromia scales. The most common interaction was incorporation of Ca, Al, and Fe into the scale. Neither composite sample examined exhibited signs of ash penetration into the sample. The alloy sample suffered some subsurface pitting that may have taken place during either or both tests. Silica was

also incorporated into the scale of the Cr/Ta alloy. The behavior of that sample differed substantially and is discussed in the Tantala section.

Tantala: In addition to an outer chromia scale, the Cr/Ta alloy formed a separate tantala scale, which incorporated some chrome and silica. The tantala scale underlying the chromia scale did not react with ash constituents. The sample exhibited limited surface pitting and no subsurface corrosion or alloy constituent loss.

Heterogeneous scales: Two samples in the CAH pass formed heterogeneous scales. Alloy 803 formed a uniform titania–chromia scale beneath the outer chromia scale. The scale, which included no ash constituents, did not appear sticky nor was it well attached to the sample. ORNL 17638 formed heterogeneous nickel oxide and nickel-chromia scales. This nonuniform scale was ineffective at maintaining a bond with the underlying sample surface.

*Samples Exposed at 708 °C in the Elbow*

The alloy samples exposed to flue gas and ash deposition in the elbow between process air heaters and the first set of shell-and-tube heat exchangers formed two types of scale and exhibited various general trends with respect to ash interaction and corrosion penetration.

Chromia: Five of the elbow samples-three 3 10 alloy mixtures, 12RN72, and 625—formed chromia scales. Chromia-scale-forming samples in the elbow tended less to incorporate ash constituents into their scale than at the higher temperature of the CAH pass. Ash particles, however, were seen enveloped by several of the chromia scale on these samples. Few of these samples exhibited subsurface corrosion. However, sequential pitting and scaling was common on several samples.

Heterogeneous scales: Three alloys in the elbow formed heterogeneous nickel oxide, nickel-chromia, and or iron nickel chromium oxide scales. They were 625, NF709, and RA253MA. Ca and Ba were the two ash constituents incorporated in the corrosion product of Alloy 625. Spherical ash particles, similar to those enveloped in some of the chromia scales on other samples in the elbow, were present in the corrosion product as well. The iron nickel chromium oxide scales were not consistent in their interaction with ash constituents. Although analysis of both scales suggests sulfidation, only one analysis included Ca and Al among the corrosion product components. Both scales were discontinuous; neither sample included signs of subsurface corrosion.

In general, for the elbow samples, no particular scale outperformed all others, but each produced characteristic ash constituent interactions. Temperature had a great effect on scale formation and ash interaction, and some samples withstood corrosive attack despite interaction with ash constituents.